T.C.
Uludağ Üniversitesi
Fen Bilimleri Enstitüsü

PERFORMANCE INVESTIGATION OF A MINI CYCLONE WITH VIRTUAL BODY

Ammar Mohammed Ali FDLELSEED

Yüksek Lisans Tezi

**PERFORMANCE INVESTIGATION OF A MINI
CYCLONE WITH VIRTUAL BODY**

Ammar Mohammed Ali FDLELSEED

T.C.
ULUDAĞ ÜNİVERSİTESİ
FEN BİLİMLERİ ENSTİTÜSÜ

PERFORMANCE INVESTIGATION OF A MINI CYCLONE WITH VIRTUAL BODY

Ammar Mohammed Ali FDLELSEED

Prof. Dr. Atakan AVCI
(Supervisor)

MASTER THESIS

MECHANICAL ENGINEERING DEPARTMENT

BURSA – 2018

TEZ ONAYI

Ammar Mohammed Ali EDLELSEED tarafından hazırlanan "PERFORMANCE INVESTIGATION OF A MINI CYCLONE WITH VIRTUAL BODY" adlı tez çalışması aşağıdaki jüri tarafından oy birliği ile Uludağ Üniversitesi Fen Bilimleri Enstitüsü Makina Mühendisliği Anabilim Dalı'nda **YÜKSEK LİSANS TEZİ** olarak kabul edilmiştir.

Supervisor : Prof. Dr. Atakan AVCI

Department Head : Prof. Dr. Recep Yemen Karadeniz   İmza
Uludağ University
Mechanical Engineering Department

Member : Prof. Dr. Atakan AVCI   İmza
Uludağ University
Mechanical Engineering Department

Member : Prof. Dr. İrfan Karagöz   İmza
Uludağ University
Mechanical Engineering Department

Member : Prof. Dr. Yusuf Ali kara   İmza
Bursa Technical University
Mechanical Engineering Deparment

Yukarıdaki sonucu onaylarım.

Prof. Dr. Ali Bayram
Enstitü Müdürü
03/09/2018

U.Ü. Fen Bilimleri Enstitüsü, tez yazım kurallarına uygun olarak hazırladığım bu tez çalışmasında;

- tez içindeki bütün bilgi ve belgeleri akademik kurullar çerçevesinde elde ettiğimi,

- görsel, işitsel ve yazılı tüm bilgi ve sonuçları bilimsel ahlak kurallarına uygun olarak sunduğumu,

- başkalarının eserlerinden yararlanılması durumunda ilgili eserlere bilimsel normlara uygun olarak atıfta bulunduğumu,

- atıfta bulunduğum eserlerin tümünü kaynak olarak gösterdiğimi,

- kullanılan verilerde herhangi bir tahrifat yapmadığımı,

- ve bu tezin herhangi bir bölümünü bu üniversite veya başka bir üniversitede başka bir tez çalışması olarak sunmadığımı

beyan ederim.

03/09/2018

Ammar Mohammed Ali FDLELS

ÖZET

Yüksek Lisans Tezi

SANAL GÖVDELİ MİNİ BİR SİKLON AYIRICININ PERFORMANSININ
İNCELENMESİ

Ammar Mohammed Ali FDLELSEED

Uludağ Üniversitesi
Fen Bilimleri Enstitüsü
Makina Mühendisliği Anabilim Dalı

Danışman: Prof. Dr. Atakan AVCI

Bu çalışmanın amacı; sanal gövdeli mini bir siklon ayırıcının performansının incelenmesi, farklı siklon uzunluklarının, siklon iç yüzey pürüzlülüğünüz farklı giriş hızlarının, siklon ayırıcının toplama verimi, kritik partikül çapı, teğetsel hız profilleri ve basınç kaybı üzerindeki etkisini incelemektir. Sayısal analizlerde ticari CFD yazılımı olan Fluent kullanılmıştır. Hesaplanan sonuçlar deneyesel sonuçlar ile karşılaştırılarak doğrulanmıştır. Teğetsel hız profilleri, siklon verimliligi, kritik partikül çapı ve basınç kayiplari 10 cm'den 20 cm'ye kadar farklı siklon uzunluklarında ve 18.5, 27.8, 37.04, 46.3, 55.5 ve 64.8 m / s giriş hızlarında, 0.004131 Kg / sn kutlesel debide incelendi. CFD tahminleri ve analiz sonuçları , siklon uzunluğundaki artışla beraber siklon verimini ve basınç kaybını azaltacağını gösterdi. Ayrıca siklon uzunluğu arttığı takdirde teğestel hızda azalma meydana gelmiştir. Buna neden olan şey, daha uzun siklonlarda gözlenen düşük savurma veriminden kaynaklanmaktadır. Siklon uzunluğu arttığında, siklon toplama veriminde düşüş meydana gelmektedir, çünkü artan siklon uzunluğuyla beraber, siklonun teğetsel giriş hızı azalmaktadır ve havanın daha az bir kısmı, azalan kesit alanı nedeniyle daha fazla hızlanabileceği siklonun alt kısmına ilerlemektedir, Öte yandan, CFD tahminleri, havanın siklonun giriş hızındaki artışıyla ve siklona giren partikül çapının artmasıyla beraber, siklon verimliliğinin yükselmesine aynı zamanda basınç kaybının düşüşüne ve Teğetsel hız artışına neden olduğunu göstermiştir. Deneyler, uzunluğu 10 cm ve 20 cm olarak değişebilen bir siklon üzerinde gerçekleştirilmiştir ve böylece siklon uzunluğunun diğer parametreler üzerindeki etkisi incelenmiştir. Deneysel çalışmanın sonuçları sayısal çözümden elde edilen verilerle karşılaştırılmıştır. Verilen sonuçlar birbiriyle iyi bir uyum göstermektedir.

Anahtar kelimler: Siklon ayırıcı, Siklon toplama verimliliği, Sasınç kaybı, Hesaplamalı akışkanlar mekaniği**.**

2018, XIII + 108 sayfa.

ABSTRACT

MSc Thesis

PERFORMANCE INVESTIGATION OF A MINI CYCLONE WITH VIRTUAL BODY

Ammar Mohammed Ali FDLELSEED

Uludağ University
Graduate School of Natural and Applied Sciences
Department of Mechanical Engineering

Supervisor: Prof. Dr. Atakan AVCI

The aim of this study is design and experimental investigation performance of a mini cyclone separator with virtual body and to carry out and investigate the cyclone efficiency, cut-off diameter, tangential velocity profiles and pressure losses under the influence and effect of different cyclone length, roughness and inlet velocity of a cyclone separator. The governing equations for this flow were solved by using Fluent CFD code First and Second numerical analyses were run to verify numerical solution and were compared with experimental results. Tangential velocity profiles, cyclone efficiency, cut-off diameter and pressure drops were calculated by define the height of cyclone from 10 cm to 20 cm, inlet velocity 18.5, 27.8, 37.04 , 46.3 , 55.5 and 64.8 m/s , 0.004131 Kg/s has been added as mass flow rate. Analyses of results and CFD predictions has shown that an increase in cyclone length lead to decrease of cyclone efficiency and pressure drop in addition to tangential velocity decreases with increasing cyclone height, so that should be responsible for the lower separation efficiency observed in long cyclones. The higher tangential velocity will not give rise to the higher cyclone efficiency, in order to explain that the cyclone efficiency decreases when the cyclone height is increased, less gas will migrate down to the bottom section where it can be accelerated due to the decreased cross-section area, in contract CFD predictions showed an increase in cyclone inlet velocity and particles diameter lead to increase of cyclone efficiency, pressure drop and Tangential velocity increasing with cyclone inlet velocity increase. An experiments have been carried out on a cyclone with a 10cm length and 20 cm, the effect of changing cyclone length were studied . The results of experimental measurements are compared with data obtained from numerical solution. The given results show qualitative agreement with each other.

Key word: Cyclone separator, Cyclone collection efficiency, Pressure drop, Computational fluid dynamic.

2018, XIII + 108 pages.

ACKNOWLEDGEMENTS

TABLE OF CONTENTS

Pages

LIST OF SYMBOLS AND ABBREVIATIONS

Symbols	Explanation
a	Cyclone inlet height [m]
b	Cyclone inlet width [m]
B	Particle outlet diameter [m]
D	Cyclone body diameter [m]
de	Gas outlet diameter [m]
h	cyclone cylinder height [m]
H	Cyclone height [m]
L	natural length of cyclone [m]
P	Pressure [Pa]
Q	Volumetric gas flow rate [m3/s]
R_w	Cyclone radius body [m]
Re	Vortex finder radius [m]
d	Cyclone body
g	Gas
f_r	Friction in inlet cyclone
V_f	Vortex flow
Ө	Tangential coordinate directions
R	Radial coordinate directions
S	Gas outlet duct deep length [m]
ΔP	Width of filter [m]
ΔP	Cyclone pressure drop [N/m2]
$ΔP_X$	Vortex finder pressure drop [N/m2]
u	Velocity parallel the wall
u_T	Shear velocity
y	Distance from the wall
k	Von Karman constant (0.4187)
$\emptyset_{ij}$	Pressure-strain term

Gb	Generation of turbulence kinetic energy due to buoyancy,
G_k	Turbulence kinetic energy generation depending on the mean velocity gradients,
YM	Compressible turbulence fluctuating dilatation contribution in to the overall rate
σ_ϵ and σ_k	The turbulent Prandtl numbers for ϵ and k
δ_{ij}	Kronecker delta
k	Turbulent kinetic
τ_p	Particle relaxation time
ρ	Gas density [kg/m3]
v	Kinematic viscosity ($v = \mu/\rho$) [m^2/s]
v_T	Turbulent (eddy) kinematic viscosity ($v_T = \mu_t/\rho$) [m^2/s]
μ	Dynamic viscosity [kg/(m s)]
μ_t	Turbulent viscosity [kg/(m s)]
ϵ	Turbulence dissipation rate [m2/s3]
α	Inlet gas moment-of-momentum ratio[-]
β	Inlet width and the cyclone radius ratio [-]

Abbreviations	Explanation
CFD	Computational Fluid Dynamics
DNS	Direct Numerical Simulation
DOE	Design Of Experiment
DPM	Discrete Phase Modeling
(EVM)	Eddy viscosity models
GCI	Grid Convergence Index
GEC	Grade Efficiency Curve
LES	Large Eddy Simulation
MM	Muschelknautz Method of modeling
PIV	Particle Image Velocimetry
RANS	Reynolds Averaged Navier-Stokes
RBFNN	Radial Basis Function Neural Network
RNG	Renormalization Group
RSM	Reynolds Stress turbulence Mode

Rep   Reynolds number of the particle

SGS   Sub grid Scale Model

VOF   Volume of Fluid.

LIST OF FIGURES

Page

LIST OF TABLES

Page

XIII

1. INTRODUCTION

1.1. Overview of Dust Separator

There are mainly four types of industrial dust separator which is fabric separator, inertial separators, electrostatic separator and wet collector scrubbers (Stein., A. C., Hoffmann., L. E., 2008). The purpose selection of any type depends on the size of particle. The type of inertial cyclone separator is used to separate dusty air from gas streams due to a integration of forces, such as gravitational, centrifugal, and inertial. The dust forces to area where the forces act on the gas stream are minimal. The dust that is separated eliminated by the gravity inside a hopper, where it stored for a time. Three other primary types of inertial collector are , settling chambers, baffle chambers and centrifugal collectors (e.g., cyclone separator). Settling separator chamber   can be simply designed and can be manufactured from any kind of material on the other hand, the dust collectors that is used as primary is seldom because of low efficiency and need space requirements larger than others (Elsayed, 2011). A settling separator chamber compose of a little bit big box initiated inside the ductwork. Speed of dust-filled airstream decreases due to a sudden expansion at the chamber and heavier particles settle down. For more efficient collectors. A practical use is as pre cleaners. Baffle chamber separator is used such as pre cleaners for most collectors with high efficient. Fabric separator are generally known as bughouses. Separate dust particulates from dusty gases can be used in Fabric collectors filtration, fixed baffle that use in Baffle chambers causes the conveying gas stream which cause a sudden change of direction. Large diameter, heavy density particles move to a dead air stream and settle and do not follow the gas stream. The most dust separator efficient types can accomplish separation efficiency of not less than 99% for small dust. Wet separator scrubbers is dust collectors that use in liquid. For such kind of separator, the cleaning liquid (commonly water) moves into direct contact with gas that have particles dust. When the gas contact is greater in the liquid streams, then the dust efficiency for removal dust is higher. Electrostatic forces use electrostatic collector use to remove particles of dust from gases exhaust. A number of direct current high voltage, discharge electrodes is located in collecting electrodes ground. These particles charged are drawn to positive or a ground

or electrode charged to it. The particles of air-borne has a negative charge as they move into the ionized field of electrodes. The dusty gases go through the stream formed by the collecting electrodes and discharge (Stein., A. C., Hoffmann., L. E., 2008).

Cyclonic separator device use to remove particulate from gas, air or liquid, without need to use filters, by exert of separation vortex. if particulates are removing dust from liquids so a hydro cyclone should be used. Gravity and rotational force are used to separate of fluids fluid-solids mixture. The same method use to eliminate drop of liquid from a stream gaseous. The parameters performance of a gas cyclone, cyclone efficiency, cut-off diameter and pressure drop are so sensitive to the geometry of cyclone. The cyclone length has high affects the collection efficiency same as the pressure drop.

A high rotating air flow is formed within a cylindrical container (cyclone). Flowing air in inside helical pattern, moving from the wide end top of a cyclone ending at the narrow bottom end before moving out from the cyclone through the center in a straight stream and out to the top. Particles with heavy (denser) have much inertia to go through the curve of the stream, in the rotating stream and strike the wall, then trap to the bottom of cyclone where it can be extracted. However the conical system, the rotating flow moves towards the narrow end of the cyclone as the rotational radius of the stream is reduced, so its separate small particles then smaller one. The geometry of cyclone with flow rate, together is called the *cut point* of the cyclone. It defines as the particle size that removed from the stream by a 50% efficiency. a greater efficiency is removed with larger Particles than the cut point, and smaller particles efficiency will be removed with a lower efficiency.

The present study work in different field. First, the effecting of cyclone length variation in the cyclone performance parameters compare to the experiments has been done on the same cyclone model. Second, comparison is given among the geometrical variables for similar increase particles diameter, inlet velocity with increase cyclone lengths. In addition to that the aim of this experiment is to carry out investigate cyclone tangential velocity profiles, cyclone efficiency, and cyclone pressure losses under the influence

and effect of different height and velocity inlet of a cyclone separator. It has been investigated that while the cyclone length increasing the collection efficiency decrease and also the pressure loss. It was shown that by optimizing the cyclone length, the velocity inlet of the cyclone designed must be taken into consideration. This study shows how cyclone length effects on performance parameters. Two cyclone with different models and increasing their velocity inlet and length of the cylindrical was carried out and successfully simulated by using (RSM) and the RNG k-ε and Standard k-ε turbulence models together with first and higher order algorithms schemes. RSM turbulence model has successfully secured the physical flow in the gas cyclones and showed very proper predictions of the pressure losses, grade cyclone efficiency, concerning to the experiment on cyclone model.

1.2. Cyclone Separators Types and Principals

A gas cyclone is a device utilize centrifugal force to separate liquid or solid particulates from a contaminated gas. The cyclonic gas refer to the centrifugal separators. The flow enters through the tangential inlet near to the top of cyclone, that accelerate the axial gas spiral and gives a centrifugal force which allow the particles coming to settle along, and move down, to inner wall of cyclone. The separated particles exit out of the cyclone body while the reverses gas phase flows axial direction and moves out through the gas outlet tube (finder vortex). A typical cyclone separator shows in figure 1.1. Moreover, cyclones are well Centrifugal separator use cyclonic centrifugal action to separate dusty particles from the gas stream. In a such cyclone, the gas-dust mixture enters tangentially that force the stream into a spiral movement. suited for high pressure and temperature applications. the circular flow create centrifugal force the dust particles to strike toward the wall of the cyclone. the particles trap into a hopper located bottom.

According to many, the cyclone separator has the most efficient dust separator, cyclones are well Centrifugal. Its robustness results from the ability to withstand harsh operating environments and lack of moving parts. The simple types of inertial, centrifugal, separator use generally are single cyclone and multi clone (multiple-cyclone) separators.

3

Cyclone is the device most widely used gas-solid separators in the industry application. They can be produced from a wide different of materials as there is no rotating parts. for this reason it has low production and low maintenance costs due to the simple design of the cyclones. Sufficient level of particulate collection efficiency and low pressure losses make the cyclones suitable for the gas-solid separation process.

Cyclone is designed as axial and tangential entrances, the tangential cyclone are the most commonly used in the industry. In tangential cyclones type, the particles are separated from the gas stream by exert of centrifugal forces. The air with dust entering from the tangential inlet that creates swirl motion in the cyclone. Particles subjected to the centrifugal force effect are blasted into the cyclone wall and travel downward along with the exert of vortex to the dust box. The outer vortex, that moves downward from the conical section, creates a secondary vortex movement in the middle region. Due to this secondary vortex formed, the air is eventually separated from the particles that leaves the cyclone from the outlet pipe at top of cyclone. The formation of two inverted two-sided interstices in the stream and the presence of air-moving particles in the flow medium which is extremely hard to solve the cyclones flow field (TEKE, 2010).

1.2.1. Cyclones advantages and disadvantages

Such as other devices, cyclone separators advantages are (Stein., A. C., Hoffmann., L. E., 2008) :
• very compact in the most applications.
• some processes can handle tacky solids with liquid irrigation.
• can be made from most suitable material for the service including plastics, ate steel, alloys, casting iron metals, aluminum.
ceramics, etc.
• it can construct from metal sheet or in smaller units.
• use to separate solids or liquid particles; sometimes mix with integrated design.
• the separated product remains dry and can be useful.
• low capital maintenance and investment costs in applications.

• its used under tough processing conditions, especially at high pressures, temperatures and with aggressive chemically feeds.

• no rotating moving parts.

• very durable.

• can be coated with corrosion or erosion resistant.

Some disadvantages of cyclones are (Stein., A. C., Hoffmann., L. E., 2008) **:**

• fouling or erosive wear can effect if solids are abrasive .

• below their 'cut-off diameter the particle sizes has low efficiency when operate under low solids conditions.

• generally higher pressure drop than other separator types.

• can be worked below expectations if not operated and properly designed. Despite this problem, such as the fouling and erosion problem reported above, is cannot be unique to the cyclones.

1.2.2. Cyclone applications

cyclones devices have many application in virtually every industry that is require to separate particles from each other. some cyclones use in industrial applications with different range and sizes, varying according to applications and locations. Nowadays, cyclone separators can be found in:

• electric power stations

• vacuum cleaning machines

• crushing, separation and grinding in the chemical and mineral industry

• ship unloading installations

• bed fluidized and systems like reactor riser or catalytic crackers and cockers

• production units for synthetic detergent

• food plants process

• wood-waste and fossil fire combustion units (commonly in upstream of a wet scrubber, fabric filter or electrostatic precipitator)

• dust equipment sampling

• spray dryers

Cyclones are used to analyze solids due to their characteristic like density, size, mass, or shape. As a consequence of high reliability and simple design, cyclone is used adequately to separate mixtures of two phase gas liquid, like remove water droplets from steam and cooler, also use to separate oil-moisture from the air compressors discharge, another examples that cyclone use to the entrained droplets that exiting from venture scrubber. As well, they are applied in machine process to separate hydrocarbon droplets and entrained oil generated from injection, distillation, spraying, or other process which is result in the entrained droplets production for two phase mixture.

1.2.3. The cyclonic separation performance

Generally the dust gas is sent to swirling motion due to centrifugal forces. The dusty particle is raise toward the wall, then moved downward to the outlet of dust due to the downwardly directed the gas flow near to the wall, for the common type of flow reverse cyclone, swirling motion is carried to design inlet in a way which will draft the gas to pass through tangent to the inner wall body. The gas is forced slowly into the inner cyclone region, in a conical part of cyclone, which lead axial movement to direct upward. This pattern flow is referred to a double vortex: outer vortex with a downward direct axial flow and inner one with an upward direct flow (Elsayed, 2011). In the cross section inlet rectangular the gas moves axially and swirls downwards in the outer separation part space. Particles in gas inlet are thrown outwards to the wall in centrifugal field, and moved downwardly to the dust exit by the gas flow directed near the wall. through finder vortex gas move outside the cyclone, which expand downward from the roof center. This pipe outlet has different names, vortex tube and dip-tube are the most common, particularly from the finder vortex.

There are two most important issues have to be known when investigating the performance of cyclones which is the cyclone particle collection efficiency and pressure loss (TEKE, 2010). Estimation of these values are very difficult because of the complexity of the flow in the cyclone. There are many studies, researches about

cyclones in the literature. Cyclone studies are depend on the calculation of the critical diameter and fractional of the particles with 50% efficiency. This kind of study was conducted by (Lapple ,1951), (Shepperd and Lapple ,1939), (Leineweber ,1964), (Liden and Kenny ,1991), (Barth ,1956), (Barth and Muschelknautz ,1970), (Leith and Licht ,1972), (Chan and Lippmann ,1977) , (Mothers and Löffler , 1988), (Ioza and Leith , 1990), (Avcı and Karagöz , 2000, 2001 and 2003), and (Karagoz and Avcı , 2005). Part of these models, it is easy to use, some of this parameters and if we use more parameters it will be difficult to solve. But the results are quite sufficient to give a general idea as far as it is difficult to solve the system completely due to the complex structure of the flow. There are various studies on calculation of pressure loss in cyclones. The simplest models are derived from geometric parameters, and (Shepperd and Lapple, 1939), (Casal and Martinez, 1983), (Dirgo, 1988) and (Coker, 1993). (Barth, 1956) developed a model that takes into account the cyclone friction surface. Pressure drops and the effect of the dust charge was also taken up by different researchers (Gil et al., 2002). Made a result of the experiments, the amount of dust in the gas increases and the pressure decreases . It was observed the reason for this is the decrease in tangential velocity. Also various mathematical models have been proposed which express the dependence of the amount of dust on the amount of dust (Muschelknautz 1970, Gil et al., 2002). (Leith and Litch (1972) used theoretical calculations to calculate particle collection efficiencies in cyclones They worked. The coefficient of drag and the particles not retained by the cyclone again cycling occurrences were taken into account. they have developed a theory to calculate the particle collection efficiency which gives good results for input tangential cyclones. (Dirgo and Leith , 1985) investigated the efficiency of cyclone particle collection experimentally and theoretically studied. The work was done on Stairmand cyclone. Experiments 860 kg / m3 density and particles with diameters of 1-7 μm and with velocities inlet of 5, 12, 16, and 26 m / s.. According to the results of Experimental Lapple, Barth, Dietz and Leith-Licth theoretical models, Bart and Leith-Licth theorems are accepted.

1.2.4. Cyclone performance affecting Factors

There are different parameters that affecting the flow pattern and cyclone performance. These factors can be classified as follows:

1. The dimensions of cyclone
• Diameter of cyclone
• Cone tip diameter
Finder vortex diameter
• Cylinder height
• Inlet height
• Inlet width
• Finder vortex length
• Cyclone total height
2. Gas properties
• Velocity
• Pressure
• Viscosity
• Density
• Temperature
3. Particle properties
• Diameter and distribution
• Density
• Mass loading
• Shape
4. Other parameters
• Roughness of wall
• Eccentricity of finder vortex
• Shape of finder vortex.

1.2.5. Cyclone separators types

The common types of inertial or centrifugal separator use are single-cyclone separators and multiple cyclone separators(multi cyclone). Single cyclone generate dual vortex to eliminate the dust from the gas. The main vortex helix downward and carry most of heavier particles. on the other hand near the bottom of the cyclone create inner vortex, spirals upwardly and carry smaller dust particles For multiple-cyclone separator which is consist of number of small cyclones diameter. Which are operate in the parallel and they have a common inlet gas and outlet. Multi cyclones operation on the same process of cyclones–create main downward vortex and an rising inner vortex.

The geometry of a cyclone with a slot type inlet is determined by the following eight dimensions as shown in Figure 1.1.
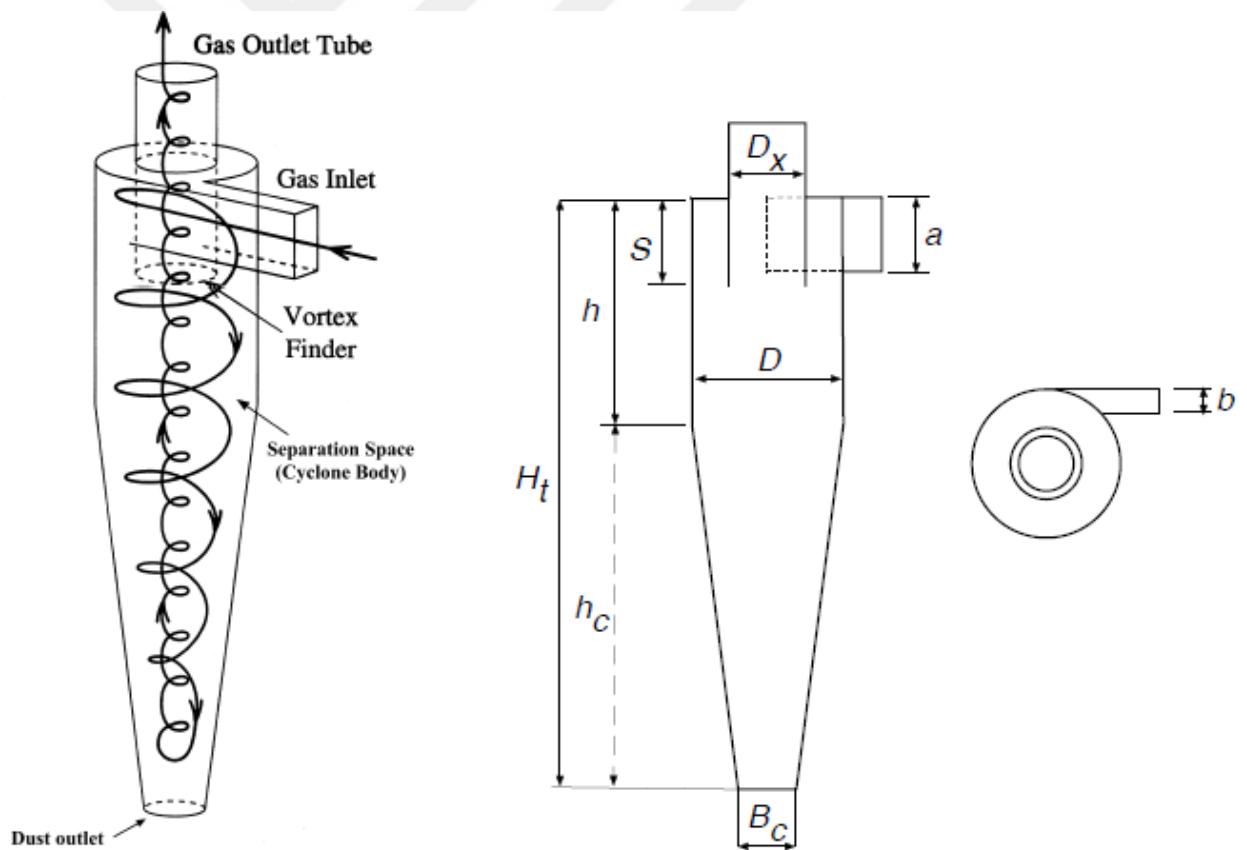
Figure 1.1. Sketches of a cylinder-on-cone cyclone with a tangential inlet, reverse-flow.

The geometrical notation is indicated in the right sketch:

1. the body diameter (barrel diameter) D
2. the vortex finder diameter Dx
3. the total height of the cyclone (from roof to dust exit) Ht
4. the height of the conical section hc or the height of the cylindrical
5. the inlet height a
6. the inlet width b
7. 7., the vortex finder length (from the roof of the separation space) S
8. section h
9. the cone-tip diameter (dust exit diameter) Bc.

1.2.5.1. Centrifugal (inertial) single-cyclone separators

Centrifugal separator as well as sedimentation, but some of its forces and parameter is added in order to give an efficient separation. In a device work due to the centrifugal force, is created to increase the acting force on the particles. Due to the centrifugal affecting on the separation of dust for different phases and densities, may be built in rotary and stationary equipment types. The relative centrifugal force defined as the force act on a particle in centrifugal field in terms of multiple of its own weight in the gravitational field. In this type of collectors, centrifugal forces exert on particles are several times much greater than gravity since it enters to the separator cylinder. This results for short time can be solved by gravity. It is been mainly used to separate fluids for different phases. The equation that centrifugal force effecting on the particle is :
$\left(C_f\right) = m\,w^2\,r$ which, m – represent particle mass; w – particle angular velocity ; r – distance radially from axis of the rotation.

$$(C_f)_r = \frac{w2\,r}{g} \qquad (1.1)$$

$$W = 2\ \pi\,N/60$$

N revolution per minute

$$(C_f)r = 1.11 \times 10^{-5} \ N^2 \ r$$

r is radius of axis rotation, effective mass of particle = V ($\rho_P - \rho_f$) V – particle volume ;
ρ_P – particle density; ρ_f – fluid density

$$u = \frac{d_p^2 p(\rho_p - \rho_f)w^2 r}{18\mu} \qquad (1.2)$$

If the particle density is greater than fluid density, the particles move outward from the rotation axis (acceleration is +ve), if the particle density is less than fluid density, the particles move in ward direct to the axis (retardation is +ve).Terminal velocity (u) is proportional to the radius (r). True terminal velocity, u_s can be reached after short initial interval time. For the centrifuges having thin layers of liquid, the particles velocity is considered constant across as a layer.

1.2.5.2. Multiple-cyclone separator

The construction employs each of these principles through the use of carefully designed stages of separation regions. The achievement of the Multi-Cyclone Separator lies between the principals of physics: Centrifugal force, impingement, and gravity. The cyclone in parallel tubes are constructed between a bottom and a top plate and inlet compartment is separated completely from the bottom and top compartment of the vessel. The gas is saturated then enters the first stage inlet plenum of the cyclone separator, that contains the cyclone support risers constructed in a parallel construction. The gas stream velocity is significantly decreased in this chamber, the bulk solids and liquids quickly fall to the bottom of the tube containing the cyclones. Moreover separation occurs as a result of the riser support tubes. As the liquid negotiates this maze of tubes, affecting upon the risers, the 5-10 micron particles sheet and coalesce into the risers, draining down towards the cyclone sheet tube. The gas then enters parallel of multiple cyclone tubes suited on the bottom sheet tube. Each cyclone has two tangential inlet points that drive the gas into a counter-clockwise downwards

direction, increasing the velocity flow and transmitting a small radiuses centrifugal force upon the solid and liquid particulate. The particles are then thrown downwards past the vortex of the cyclone tube into the collection sump, the scrubbed gas then rises upwards through a precisely engineered riser tube to the vessel outlet. For Efficiency Multi-Cyclone Scrubbers remove 100% of solid particles and large, 100% of all liquid particles 8.0 microns and larger, and 99% of all 5 to 8 micron and liquid particles when operating at design conditions. The multi-cyclones are a simplistic design separator for demisting and dedusting services targeting the applications with slight characteristics fouling at gas high densities. It has ability to extract particles sand and to separate liquid droplets.

1.3. Cyclone Classification

In the cyclone separators Classification;, the separate of different dense phase in the cyclone (in this case the air is the less dense phase while the calcite dust is the dense phase) in a certain parts of the cyclone diffuses due to the particle size. in this study Calcite dust, used in experiments, is available on the market at a different average particle size. In addition, within this calcite powder, dust particles in different sizes are present in different percentages. The dust particles contained in these different calcite powders used in the experiments were given in detail.

a different average particle size. In addition, within this calcite powder, dust particles in different sizes are present in different percentages. The dust particles contained in these different calcite powders used in the experiments were given in detail.

1.3.1 General concerns on particle classification

Classifications are characterized by cut size d50. A perfect classifier separates the particle which is larger than *d50* into the dusty product and maintain the rest into fine product. Classification efficiency could be given either in distribution efficiency or mass efficiency. Mass efficiency compares the mass of small and coarse products but it couldn't give detailed information about each size class behavior.

So after classification, particles size handling of the coarse or fine fractions more or less overlap. one of the parameters in classifier evaluating performance is the efficiency classification. Other factors such as sharpness of separation and energy consumption can considered in classifier design.

1.3.1.1 Vortex air classifier

The Vortex air classifiers are belong to the type of centrifugal classifiers. Rumphf firstly systematically studied this type of classifiers (Nied, R., 1996). In Alpine Commercial vortex air classifiers are available , as shown in Figure 1.8., the first industrial design that separates particles at size cut 10 μm. A main advantage of the air vortex classifiers is that de-agglomeration happens during classification which leads to dispersion of the raw materials in air flow. The disadvantage , that is the product to air ratio has significant effect on the cut size. A vane is installed in the classifier to create a forced vortex to solve this problem, where the   rotor speed determined the circumferential velocity component. However, most of them based on either free vortex model or the combination of forced and free vortex models. The balances between centrifugal forces and air drag forces are the basic principle of determining cut sizes .

1.3.1.2. Cross-flow classifier

The design of Cross-flow classifiers that the direction of airflows are in perpendicular to the gravity. As can be shown in Figure 1.9., the gas injecte to the classifier horizontally from the inlet left wall. the powder is fed downwardly into the classifier and the material inlet is nearby the gas nozzle. . The particles are separate since the coarse powders and the fine powders have different trajectories in the separation zone due to the fluid drag forces and gravitational forces. The particles are send to fan-shape in the chamber The dusty powders trap quicker than the fines. Several plates are inserting at the certain distances to the inlet gas, the classified particles are collected into fractions.

The efficiency and operation of these device is strongly affected by gas velocities. Wang et al has studied the affecting of gas velocity on cut size and the separation sharpness. They were found that with increasing velocity gas the cut size increases linearly. Simulations by Fluent were also performed, which employed Euler-Largrangian approach.

1.3.1.3. Rotating wheel classifier

The classifiers of Rotating wheel use rotating blades to create centrifugal field or air vortex (Kolacz, 2002). The main advantage of rotating wheel classifier as in a vortex air classifier is the discarding any external compressor to send air. However, the volumetric flow rate of air needed for classification is less in the rotating wheel classifier. The blades on the rotor swirl the air so that the centrifugal zone separation is formed. Large particles are thrown off the blades and fall down at the wall. The small particles, however being not able to escape from the airflow, are taken by air into the top outlet.

several rotating wheel classifiers are developed by Hosokawa. The mixture of air and particles in such classifier, enter the bottom inlet classifier and move upwards directly into a conical vessel. The particles come to the rotor where the classification takes place. Varying the speed of rotation of the rotator is controlled by cut size. These device up to 1.5 tons per hour is used to separate the ground limestone, fine quartz powder, cement. In the cut sizes range from 20 to 100 μm and product coarse recovery of 70 to 80% .

1.3.1.4. Hydrocyclone

A l hydrocyclone consists of lower conical section and top cylindrical section . The raw material is fed into the body through the tangential inlet on the top wall. The liquid-solid mixture followed a downwards in helical pathway. Hydrocyclones may be connected in serial in order to produce several size fractions. There has been increasing number of designs of hydrocylones. The centrifugal pushed dusty particles away from

the fluid stream to the wall where the coarse particles dropped and were collected below. The small particles remained in the stream of fluid and discharged above.

The hydrocyclones applications could be found in carbonaceous material removal from upgrading gypsum which is produced to make phosphoric acid, classifying pigment, classification of crystal magma and so on. There are a number of parameters effect on a hydrocyclone separation efficiency including geometry, pressure, flow rate and temperature. (Yoshida, HU., Takashina, TA., Fukui, KL., 2004) studied the affecting of slurry temperature and inlet shape of the performance classification. It was reported that cut size of spiral inlet is smaller than that of the inlet tangential when the flow rate of liquid was constant. The movable guide plate using further reduced cut size.

1.3.1.5. Cyclone separator

Cyclone separators work like a centrifuge, with the continuous sending dirty air. In the cyclone separator, dirty gas is injected into the chamber. meanwhile The chamber inside creates spiral vortex, same as a tornado. The lighter particles of the gas have less inertia, so it is influenced by the vortex and go up it. On the other hand, larger density particles have much inertia and are not easily influenced by the vortex.

1.3.1.6 Other wet classification methods

A number of new classification methods is developed in past a few decades. (Meier, J., Klein, G.M., Crossflow, K.V. 2002.) by using a cross flow filtration device investigated a wet classification method.. to control flow conditions and enable ease of removal of the particles deposited on the filtration membranes a flat duct modules have been developed. The working system deposition processes is particle size dependent. The operations mainly consisted of two steps. Firstly, the flowing mixture over the membranes. The fine particles are brought into the membranes surfaces, while the coarse particles were cleaned. On the other hand the second step is to wash the membranes and send the fine particles. The system were tested under both laminar and turbulent flows at different flow rates. The effect of concentrations of the particles were

also carried out. The system was constructed to a pilot-plant scale and found to be practically successful. The main advantages of the design is that ultra-fine particles (<1µm) could be classified with a very sharp particles size distribution.

1.4. Cyclone Separator Characteristic

1.4.1. Forces in vortex flow

The swirling motion through a vortex flow occurs in many equipment like cyclones, spray dryers ,hydro cyclones and vortex burners. The distribution of tangential velocity can exhibit two types of perfect swirling flows :
• free vortex flow
• forced vortex flow
The free flow vortex behaves as way a fluid frictionless does, and the swirl tangential velocity is such the moment- of the fluid elements can be same above all radii. While the forced vortex flow is define as swirling flow that has tangential velocity distribution same to body rotating solid (Stein., A. C., Hoffmann., L. E., 2008). If the fluid swirling has infinite viscosity, that means it has behavior same to solid body, obviously there is no shearing motion exist in the fluid layers at different radii. The tangential velocity distribution is between these two swirling flows in real swirling flows. The fluid element is forced to have same angular velocity. A forced vortex flow is Swirl with a constant angular velocity.

$$v_\theta = \Omega r \tag{1.3}$$

This equation refer to the first ideal swirl flow, where v_θ represent the tangential velocity & r is the coordinate radial.

1.4.2. Centrifugal force

The important force in a cyclone characteristic is centrifugal force on cyclones the Separation particles is caused by centrifugal forces, which is a result of the swirling

motion of the gas. The particles that are denser than the gas before moving downward to the bottom are forced to move towards the wall cyclone (Hoffmann, A. C., Stein, L. E., 2008). This force is corresponding to the diameter cubed (Pisarev, G. I., Gjerde, V. I., Hoffmann, A. C., Peng, W., Balakin, B. V., Dijkstra, H. A., 2011), the centrifugal force of fluid elements are balanced by the force that generate a gradient in static pressure. The force is acting on the rotation axis, and that will make sure the element stays in its path. The centrifugal force that is a force acting on system, under consideration has to turn with particle. In a stationary coordinate system   it is actually a centralizing acceleration that will led the particle undergoes continually to remain in orbit.

1.4.3. Axial velocity

The flow with axial velocity is upward in inner region near to the axis and downward with an outer position close to the wall. The upward direction generally referred to the inner vortex and downward direction as outer vortex.

The axial velocity is supposed to be zero at the bottom of cyclone before flow reverses itself (Peng, W., Hoffmann, A. C., Boot, P. J. A. J., Udding, A., Dries, H.W. A., Ekker, A., Kater, J., 2002). An axial inlet in the cyclone tends to a high axial symmetry degree in the flow. This can be considered advantages like eliminating the region prone for clogging on a back side of the finder vortex. Around the centerline, the velocity in axial direction usually makes a dip. This happens due to the flow is directed downwardly.

1.4.4 Tangential velocity

The important velocity profile is tangential velocity, since the centrifugal force exert on the particles encircling. The flow can be consider as Rankin vortex, and combination of quasi-free vortex flow with surrounding the quasi-forced vortex flow (Peng, W., Hoffmann, A. C., Boot, P. J. A. J., Udding, A., Dries, H.W. A., Ekker, A., Kater, J., 2002). Refer to Chen (Chen, 1999), the increasing radius will increase the tangential velocity and reaches a maximum at about 60-70% of the diameter before it tends to decrease towards the wall.

The tangential velocity profile velocity is approached to zero along centerline and in the wall. The maximum velocity value is located at a certain distance from the centerline represented by a radius, R1 . This radius is generally lower than the vortex finder radius.

1.4.5. Cyclone pressure drop

It is need to know the difference between dynamic and static pressure in cyclones. Measuring the wall static pressure in the downstream & upstream piping is the most common way to measure the cyclone pressure drop. Dynamic & static pressure can be defined from the Bernoulli equation for a steady flow of frictional fluid. In Equation (1.4) the static pressure is referred to p, and the dynamic pressure is $\frac{1}{2}\rho v^2$

$$\frac{p}{\rho} + \frac{1}{2}v^2 + gh = constant\ along\ a\ streamline \qquad (1.4)$$

From this equation, v is represent the gas velocity, ρ is fluid density, g is gravity, and h is the cyclone height. The static and pressure is shown on the left side as the first and second term. The dynamic pressure is generally called a velocity head. Both of are divided by fluid density. The overall pressure drop involve the dynamic and static pressure, this could be divided into three parts In cyclones,:
• loss in the finder vortex
• loss in the inlet vanes
• loss in the separator body

The vortex finder is part of a cyclone which has the greatest loss of pressure. There is one exception which is highly loaded cyclones. For such case, losses of wall associated with frictional drag become a significant contribution to pressure drop due to expense of losses in a vortex core, and the finder vortex. The pressure drop in the inlet vanes are less than for the separator body. The most important pressures role is to limit intensity of the swirl in separation space. That means less intensive vortex will give more frictional loss at the wall gives. This wall losses cannot act on the overall pressure losses. In the cyclone pattern, the gas transports inward from the outer part to the inner part,is being accelerated with the basis of conservation of vortex moment-of-

momentum. That will lead the static pressure to decreases and it can be stated the vortex convert static pressure into dynamic pressure. Mechanical Dissipation energy is dependent on the friction of the wall and in the vortex core this dissipation gives a permanent pressure drop over the cyclone. it has been clearly note that fact about pressure drop in cyclones is decreasing with increasing wall roughness or body length of cyclone. These three factors affect the increase in the wall friction (Hoffmann, A. C., Stein, L. E., 2008).

1.4.6. Overall separation efficiency

During the cyclone operations there are three fractions particles have to be concerned. These are the captured or underflow, the feed, and the lost/emitted particles in the overflow. Their masses are presented with the symbols M_c, M_f and M_e give the balance for solids mass over a cyclone:

$$M_f = M_c + M_e \tag{1.5}$$

The equation represents the total efficiency, η can be found a mass fraction captured by the cyclone:

$$\eta = \frac{M_c}{M_f} \tag{1.6}$$

The efficiency of the cyclone is calculated by collecting samples trapped from the cyclone and balancing two fractions. An overall separation is generally what counts most in industrial process. However, it doesn't the ideal way to carry out the actual separation performance of a certain cyclone.

1.4.7 Cut-off size

The equilibrium of the forces can be used to determine the pressure loss, separation efficiency & operational parameters. The cut-off size is determined by balancing the centrifugal force and the drag force. In cyclones, The particles that have a diameter size lower than the cut size are carried out through the dust hopper. While the particles with a diameter larger than the cut size are transported outward and separated. This is true

only in theory. In real, the separation efficiency curve depends on operation conditions and the geometrical dimensions in the cyclone.

1.5 The Study Plan

As it was reported below the current study carried out and investigated the effects of different cyclone length, inlet velocity, and wall roughness in addition to the different particle diameter on the cyclone performance parameters. The characteristics of the flow field have been studied in the cyclones under the effect of varying cyclone length and inlet velocity are specified so result has been given by define the height of cyclone from 10 cm to 20 cm, inlet velocity 18.5, 27.8, 37.04 , 46.3 , 55.5 and 64.8 m/s and 0.004131 Kg/s has been added as working fluid flow rate. The cyclone model were simulated and assessed successfully using RSM turbulence model with higher advection schemes. The Reynolds Stress Model turbulence has successfully captured the flow physics inside the gas cyclones and show accurate predictions of the grade separation efficiency pressure drop, and cut-off diameter. In addition to that many experiment has been held on a mini cyclone with aid of different auxiliary equipment using carbon calcite as working fluid, air at ambient condition is supplied from a centrifugal pump to the experimental. The centrifugal compressor is drawn the air to the system from blower to the outlet. In order to adjust the flow rate, a control valves are used to change the flow according to a desirable velocity.

Finally the result given by CFD and experimental result was compared, a good agreement is observed between two results in term of cyclone efficiency, pressure drop, cut-off size and tangential velocity profile values.

2. THEORETICAL AND FUNDAMENTAL OF GOVERNING EQUATION

2.1. Turbulence Governing Equation

This chapter give theory about the turbulences model that is used in CFD for different possible solution of multi type of cyclones.

2.1.1. Introduction

Turbulent flow is defined by fluctuating velocity field. This fluctuation is high frequency, small scale so it's too high computationally to simulate by engineering calculation. So the instantaneously ideal governing equation can be ensemble averaged, time-averaged or in another way manipulated to eliminate the solutions of small scales which give result of new set of equations with further unknown quantities but turbulences model have to change this variables into known parameters.

ANSYS FLUENT has a different options of turbulence models (Swanson, April 2009)**:**

- Reynolds stress models (RSM)
- ➢ Linear pressure-strain RSM model
- ➢ Quadratic pressure-strain RSM model
- ➢ Low-Re stress-omega RSM model
- Spalart-Allmaras model
- k-ε models
- ➢ Standard k-ε model
- ➢ Renormalization-group (RNG) k-ε model
- ➢ Realizable k-ε model
- Large eddy simulation (LES) model, which includes one of the following sub-scale models.
- ➢ Smagorinsky-Lilly subgrid-scale model.
- ➢ WALE subgrid-scale model

➢ Dynamic Smagorinsky model

➢ Kinetic-energy transport subgrid-scale model

2.1.2. Choosing the turbulence model

The choice of specific turbulence model depends mainly on parameters such the physics factor in the flow, established solution for specific type of problem, the grade of solution required, an available computational parameters and the spending time for the simulation. It is obviously fact that there is no single turbulence model is common accepted like being Standard for all of problems. To identify the most proper model application, we should know the limitations and capabilities of the different options. The Spalart- Allmaras model needs less computational effort rather than the standard k-ε model when we solve alternative transport equation. If we Compare the k- ε and k-w models, that mean the RSM model requires CPU time and more memory this because of the increasing number of transport equations for Reynolds stresses model. However, ideal program in ANSYS FLUENT is decreased the CPU time to iteration. The realizable k-ε model needs slightly more computational attempts than standard k-ε model.

However, according to the other functions and terms in such governing equations and for higher degree of non-linearity, computations with the RNG k-ε model need 10–15% more CPU time than that with standard k-ε model. same the k-ε models, k-ε models are two-equation models, and need the amount same of computational effort mean, the RSM in ANSYS FLUENT requires about 50–60% CPU time more per iteration with respect to the k-ε and k-w models. In addition, more15–20% memory is needed. So if we look to the time per iteration, choosing the specific turbulence model can act on ANSYS FLUENT's ability in order to give a converged solution. For example, RNG k-ε model is designed, while the standard, k-w models known as flexible over-diffusive in a certain situations so that a turbulent viscosity decrease in response to high strain rates. As far as diffusion has stabilizing influences on a numeric, RNG model is accepted to Capable to instability in solutions of steady-state. Moreover, this would not necessarily consider as a disadvantage of RNG model, so these properties make it more

positively and responding quickly for physical instabilities like time-dependent turbulent shedding vortex. Similarly, the k-w and k-ε need less iterations to converge than the RSM models.

General parameters are given to help you choose the perfect turbulence model for the flow that is required to model.

The following Information is presented in sections:

• Reynolds-Averaged Approach vs. LES

• Reynolds Stress Transport Models vs. Boussinesq Approach

• Reynolds,Ensemble Averaging

2.1.3. Wall Boundary conditions

IF its fine enough mesh to solve the viscosity-dominated sub layer, kinematic viscosity v is set to zero at walls the modified turbulent kinematic viscosity v is set to zero (Swanson, April 2009), the wall shear stresses are obtained from the relationship of laminar stress-strain:

$$\frac{u}{u_\tau} = \frac{\rho u_\tau y}{\mu}$$
(2.1)

If the mesh is bad to solve a viscous sub layer, so it is suggested the centered of the wall-adjacent cell drop within the boundary of logarithmic region layer, and the law-of-the-wall can be employed:

$$\frac{u}{u_\tau} = \frac{1}{k} \ln E \left(\frac{\rho u_\tau y}{\mu} \right)$$
(2.2)

Hrere u represents parallel velocity to the wall u_T is shear velocity, y is distance from the wall, E = 9.793. and k for von Karman constant (0.4187).

2.2. Reynolds Stress Model (RSM)

2.2.1. Overview

Discarding the hypothesis of the isotropic eddy-viscosity, by solving transport equations for the Reynolds stresses RSM closes the Reynolds-averaged Navier-Stokes equations, together with the equation and for the dissipation rate. The Reynolds stress model (RSM) can be considered as the most complicate type of turbulence model which provided by ANSYS FLUENT. Since the RSM explain the streamline curvature effects rotation, swirl, and strain rate rapid changes in a more strict manner than other one-equation and two-equation models, for complex flows it has a potential to give an accurate predictions. This means another five transport additional equations are needed for 2D flows, in comparison to seven additional transport equations solved by 3DHowever, the RSM fidelity predictions are still limited to closure assumptions employed to various model terms in exact transport equations for Reynolds stresses. Modeling the dissipation-rate terms and pressure-strain is in particular challenging, and usually considered responsible for accuracy compromising the RSM predictions. However, RSM can be used when the features of interest flow are the result of Reynolds stresses anisotropy. For examples cyclone flows, rotating flow passages, highly swirling flows in combustors and stress-induced secondary ducts flows. RSM may not always produce result that is so net superior to a simple models in all classes of the flows to the additional computational expense (Swanson, April 2009).

The identical Reynolds stress transport equations form might be initiated by taking moments of exact momentum equation. Such kind of process where the exact momentum equation is multiplied by a fluctuating property, Unfortunately the product being Reynolds averaged, many of terms in the definite equation is modeling assumption is required and unknown that is to close the equations.

2.2.2. Reynolds stress transport equations

The Reynolds stresses transport equations, $\overline{\dot{u_\iota} \; \acute{u_j}}$ may be written as follows:

$$\underbrace{\frac{\partial}{\partial t}\left(\overline{\acute{u_\iota}\acute{u_j}}\right)}_{Local\ time\ derivative} + \underbrace{\frac{\partial}{\partial x_k}\left(U_k\ \overline{\acute{u_\iota}\acute{u_j}}\right)}_{C_{ij}=convection} = \underbrace{-\frac{\partial}{\partial x_k}(\overline{\acute{u_\iota}\acute{u_j}\acute{u_k}} + \frac{\overline{P\acute{u_j}}}{\rho}\delta_{ik} + \frac{\overline{P\acute{u_\iota}}}{\rho}\delta_{jk})}_{D_{T,ij}=Turbulent\ diffusion} +$$

$$\underbrace{\frac{\partial}{\partial x_k}\left[v\frac{\partial}{\partial x_k}\ \overline{\acute{u_\iota}\acute{u_j}}\right]}_{D_{L,ij}=Molecular\ diffusion} - \underbrace{(\overline{\acute{u_\iota}\acute{u_k}}\frac{\partial U_j}{\partial x_k} + \overline{\acute{u_j}\acute{u_k}}\frac{\partial U_i}{\partial x_k})}_{P_{ij}=Stress\ production} +$$

$$\underbrace{\overline{\frac{\acute{p}}{\rho}\left(\frac{\partial\acute{u_\iota}}{\partial x_j} + \frac{\partial\acute{u_j}}{\partial x_\iota}\right)}}_{\varphi_{\iota j}=Pressure\ strain} - \underbrace{2v\overline{\frac{\partial\acute{u_\iota}}{\partial x_k} + \frac{\partial\acute{u_j}}{\partial x_k}}}_{\varepsilon_{ij}=Dissipation}$$

$$(2.3)$$

The various terms in these equations , $D_{T,ij}$, C_{ij} , φ_{ij} and ε_{ij} should be modeled to close these equations. However C_{ij} , $D_{L,ij}$ ad P_{ij} do not require any modeling. these sections describe the assumptions modeling required for equation set closing.

2.2.3 Pressure-Strain term modeling

Model The Linear Pressure-Strain:

In (Swanson, April 2009), By default the term pressure-strain $\emptyset_{ij}$ in Equation 2.3., is modeled depending on the proposals of Gibson and Launder , Fu et al, and Launder. The approach is classical to modeling $\emptyset_{ij}$ using the following equations:

$$\emptyset_{ij} = \underbrace{\emptyset_{ij,1}}_{Slow\ pressure\ strain} + \underbrace{\emptyset_{ij,2}}_{Rapid\ pressure\ strain} + \underbrace{\emptyset_{ij,w}}_{Wall\ reflection\ term} \qquad (2.4)$$

Here $\emptyset_{ij},1$ represents pressure-strain slow term, known also as the return-to-isotropy term, $\emptyset_{ij},2$ represents rapid pressure-strain term, and $\emptyset_{ij}w$ is called wall-reflection term. The slow pressure-strain term, $\emptyset_{ij},1$, is modeled as

$$\phi_{ij,1 =} -c_1\frac{\varepsilon}{k}[\overline{\acute{u_\iota}\acute{u_j}} - \frac{2}{3}\delta_{ij}k] \qquad (2.5)$$

with C1 = 1.8.

The rapid pressure-strain term $\emptyset_{ij,2}$, is formed as

$$\phi_{ij,2 =} - c_2[(\left(P_{ij} - c_{ij}\right) - \frac{2}{3}\delta_{ij}(P-C)$$ (2.6)

where C2 = 0.60 is constants, $P=\frac{1}{2}P_{kk}$ and , $c=\frac{1}{2}c_{kk}$

Where P_{ij} and c_{ij} are defined as in;

$$\underbrace{\frac{\partial}{\partial t}\left(\overline{\acute{u_\iota}\acute{u_j}}\right)}_{Local\ time\ derivative} + \underbrace{\frac{\partial}{\partial x_k}\left(U_k\,\overline{\acute{u_\iota}\acute{u_j}}\right)}_{C_{ij}=convection}$$

$$= \underbrace{-\frac{\partial}{\partial x_k}(\overline{\acute{u_\iota}\acute{u_j}\acute{u_k}} + \frac{\overline{P\acute{u_j}}}{\rho}\delta_{ik} + \frac{\overline{P\acute{u_\iota}}}{\rho}\delta_{jk}) }_{D_{T,ij}=Turbulent\ diffusion} + \underbrace{\frac{\partial}{\partial x_k}\left[v\frac{\partial}{\partial x_k}\overline{\acute{u_\iota}\acute{u_j}}\right]}_{D_{L,ij}=Molecular\ diffusion}$$

$$\underbrace{-(\overline{\acute{u_\iota}\acute{u_k}}\frac{\partial U_j}{\partial x_k} + \overline{\acute{u_j}\acute{u_k}}\frac{\partial U_i}{\partial x_k})}_{P_{ij}=Stress\ production} + \underbrace{\overline{\frac{\acute{p}}{\rho}(\frac{\partial\acute{u_\iota}}{\partial x_j} + \frac{\partial\acute{u_j}}{\partial x_\iota})}}_{\varphi_{\iota J}=Pressure\ strain} \underbrace{-2v\overline{\frac{\partial\acute{u_\iota}}{\partial x_k} + \frac{\partial\acute{u_j}}{\partial x_k}}}_{\varepsilon_{ij}=Dissipation}$$

$$\phi_{ij,w =} \acute{c_1}\frac{\varepsilon}{k}(\overline{\acute{u_k}\acute{u_m}}\,n_k\,n_m\,\delta_{ij} - \frac{3}{2}\overline{\acute{u_\iota}\acute{u_k}}\,n_j\,n_k - \frac{3}{2}\overline{\acute{u_j}\acute{u_k}}\,n_j\,n_k)\frac{c_\mu^{3/4}k^{2/3}}{K\varepsilon d}$$ (2.7)

In Eq 2.7., this n_k is the x_k component of unit normal to wall, d represent normal distance to the wall K, is the von Karman constant (=0.4187); and $\acute{c_1} = 0.50$, $\acute{c_2} = 0.30$ and $\acute{c_\mu} = 0.09$ are conants.

$\boldsymbol{\phi_{ij,w =}}$ is included by default in the Reynolds stress model.

2.3. Standard, RNG, and Realizable k-ϵ Models

This section introduce the standard, RNG, and realizable k-ϵ models. All models have a same forms and with transport equations for k and ϵ. The main differences in the models are follows below:

• the turbulent Prandtl numbers governing turbulent diffusion of k and ϵ

• the method of turbulent viscosity calculating

• destruction and generation terms in the ϵ equation

Methods of calculating transport equations, turbulent viscosity and constants model are presented independently to each model. The feature which is essentially common to all type of models follow, including generation of turbulent because of shear buoyancy, due to the effects of modeling heat, compressibility, and mass transfer.

2.3.1. Standard k-ϵ Model

Overview

Economy, robustness and reasonable accuracy for a different range for the turbulent flows show its common use in industrial flow and simulations of heat transfer. The simplest models complete of turbulence are two-equation models which the solutions of two transport equations separately allows the length scales and velocity turbulent to be independently found. Standard k-ϵ model in the ANSYS FLUENT vary within this class of models and become the workhorse of the practical engineering flow calculations in time since it has been proposed by Spalding and Launder. It can be considered a semi empirical model, and relies of the model derivation equations on empiricism and phenomenological considerations . As the weaknesses and strengths of standard the k-ϵ model become known, many developments was made made to the model to enhance its performance. Two of theis variants are available in the ANSYS FLUENT: the realizable the k-ϵ model and the RNG k-ϵ model. The standard k-ϵ model is treat as a semi-empirical model depend on transport equations model for turbulence kinetic energy (k) and its dissipation rate (ϵ). Transport equation model for k is derived from exact equation, while the transport equation model for ϵ was obtained by using bears little resemblance and physical reasoning to its exact mathematically counterpart. The derivation of the model k-ϵ, the hypothesis that flow is fully turbulent, and the molecular viscosity effects are negligible. Standard k-ϵ model is valid only for fully turbulent flows.

Standard k- ϵ Model Transport Equations

Turbulence kinetic energy, k, with its dissipation rate of, ϵ, are obtained from the transport equations below (Swanson, April 2009):

$$\frac{\partial}{\partial t}(\rho k) + \frac{\partial}{\partial x_i}(\rho k u_i) = \frac{\partial}{\partial x_i}\left[\left(\mu + \frac{\mu_t}{\sigma_k}\right)\frac{\partial k}{\partial x_i}\right] + G_k + G_b - \rho\epsilon - Y_M + S_K \qquad (2.8)$$

And

$$\frac{\partial}{\partial t}(\rho\epsilon) + \frac{\partial}{\partial x_i}(\rho\epsilon u_i) = \frac{\partial}{\partial x_i}\left[\left(\mu + \frac{\mu_t}{\sigma_k}\right)\frac{\partial\epsilon}{\partial x_j}\right] + C_{1\epsilon}\frac{\epsilon}{k}(G_k + G_{3\epsilon}G_b) - C_{2\epsilon}\rho\frac{\epsilon^2}{k} + S_\epsilon \quad (2.9)$$

Where, Gb is the turbulence kinetic energy generation due to buoyancy, G_k is the turbulence kinetic energy generation due to the mean velocity gradients, can be calculated as mentioned in Turbulent Production Modeling in the k- ϵ, Models, YM is the contribution of the dilatation fluctuation in compressible turbulence for the overall dissipation rate, σk and σ_ϵ are the Prandtl numbers turbulent for k and ϵ, respectively, $C_{1\epsilon}$, $C_{2\epsilon}$, and $C_{3\epsilon}$ are constants. Sk and S_ϵ are user-defined source terms.

2.3.2. RNG k-ϵ model

The RNG k-ϵ turbulence model is obtained from instantaneous Navier-Stokes equations, using the mathematical technique called "renormalization group" (RNG) methods. The analysis derivation results in model with different constants from those in standard k-ϵ model, additional functions and terms in transport equations for k and ϵ model. RNG k-ϵ model was derived by using an accurate statistical technique (called renormalization group theory). It is similar in term of the standard k-ϵ model, but also includes the following enhancement:

• RNG theory gives an analytical formula to turbulent Prandtl numbers, while the standard k-ϵ model is using user-specified, constant values.

• RNG model provides additional term in its dissipation rate equation that improves the accurate rapidly strained flows.

• Standard k-ϵ model has a high-Reynolds-number model, RNG theory analytically-derived for effective viscosity differential formula which is consider for low-Reynolds-

number effects. Effectively use of this feature does, depend on a suitable treatment of the near-wall region.

• The swirl effect on the turbulence is included in RNG model, improving swirling flows accuracy.

According to the features mentioned above make the RNG k-ϵ model more reliable and accurate for wider class of the flows than standard k- ϵ model.

Transport Equations for the RNG k-ϵ Model

The RNG k- ϵ model has a similar form to the standard k- ϵ model: EQN2.9

$$\frac{\partial}{\partial t}(\rho k) + \frac{\partial}{\partial x_i}(\rho k u_i) = \frac{\partial}{\partial x_i}\left(\alpha_k \mu_{eff} \frac{\partial k}{\partial x_i}\right) + G_k + G_{kb} - \rho \epsilon - Y_M + S_K \qquad (2.10)$$

And

$$\frac{\partial}{\partial t}(\rho \epsilon) + \frac{\partial}{\partial x_i}(\rho \epsilon u_i) = \frac{\partial}{\partial x_i}\left(\alpha_\epsilon \mu_{eff} \frac{\partial \epsilon}{\partial x_i}\right) + C_{1\epsilon}\frac{\epsilon}{k}(G_k + G_{3\epsilon}G_b) - C_{2\epsilon}\rho \frac{\epsilon^2}{k} - R_\epsilon + S_\epsilon \qquad (2.11)$$

Where, Gb is the turbulence kinetic energy generation due to buoyancy, G_k is the turbulence kinetic energy generation due to the mean velocity gradients, can be calculated as mentioned in Turbulent Production Modeling in the k- ϵ, Models, YM is the contribution of the dilatation fluctuation in compressible turbulence for the overall dissipation rate, σk and σ ϵ are the inverse effective of turbulent Prandtl numbers for k and ϵ, respectively, $C_{1\epsilon}$, $C_{2\epsilon}$, and $C_{3\epsilon}$ are constants. Sk and S_ϵ are user-defined source terms.

2.3.3 Realizable k-ϵ mode

The realizable k- ϵ model is improved recently (Shih, T.-H., Liou, W. W., Shabbir, A., Yang, Z., Zhu, A. k., 1995) differs from the standard k- ϵ model in two important ways:
• The dissipation rate ϵ new transport equation was derived from exact equation for transport of the fluctuation for mean-square vortices. On the Reynolds stresses the term "realizable" means that the model satisfies certain mathematical constraints uniform to the physical turbulent flows.

29

• The realizable k- ϵ contains has new formulation for the turbulent viscosity. Neither the RNG k- ϵ nor standard k- ϵ model the model is realizable. An instant benefit for the realizable k- ϵ model is more accurate in predictions the spreading rate for both round jets planar and. It is provide superior performance too, for flows that involve rotation, boundary layers under the effects of strong adverse pressure gradients, recirculation and separation. realizable k-ϵ model, is combining of Boussinesq relationship and eddy viscosity to understand the mathematics definition that obtain the following expression to the normal Reynolds stress in strained mean incompressible flow:

$$\bar{u}^2 = \frac{2}{3}k - 2v_t \, \partial U / \partial x \tag{2.12}$$

using Equation $v_t = \mu_t / \rho$ one gives the result of the normal stress $\overrightarrow{u2}$ due to the definition is a positive quantity, becomes negative, for example., "non-realizable", when the strain is enough large to satisfy

$$\frac{K}{\epsilon} \frac{\partial U}{\partial x} > \frac{1}{3C_\mu} \approx 3.7 \tag{2.13}$$

It can similarly, also shows that shear stresses for Schwarz inequality is ($\overline{u_\alpha \; \dot{u_\beta}} \, 2 \; <$ $\overline{\dot{u_\alpha} \, 2 \; \dot{u_\beta} \, 2}$ no summation over β and α) can be broken at large mean strain rate. Most straight forward way to secure the realizability (positivity of the normal stresses and Schwarz inequality for shear stresses) is to make Cμ variable sensitizing it to the mean deformation and the turbulence (k, ϵ). The notion of variable Cμ is given by many models including Reynolds, and well substantiated by evidence of experimental. For example, Cμ is determined to be around 0.09 in the inertial sub layer of boundary layers equilibrium, and 0.05 in a strong homogeneous for shear flow.

2.3.4 Reynolds averaged Navier Stokes (RANS)

It is acceptable to analyze the flow through two parts, when flow is turbulent, a fluctuating component and a mean (time-averaged) component 0

$$u_i = \overline{u_i} + \acute{u}_\iota \tag{2.14}$$

$$P = \overline{P} + \acute{p} \tag{2.15}$$

$$T_{ij} = \overline{T_{ij}} + \tau'_{\iota J} \tag{2.16}$$

Over line is a shorthand for *time average* and for case of RANS $U_i \equiv Uj$, and $\overline{\overline{u}}=0$. *Reynolds Decomposition* is belong technique of decomposing. Including this decomposition into instantaneous equations and time averaging results in the *Reynolds averaged Navier-Stokes* equations (RANS).

$$\frac{\partial U_i}{\partial x_j} = 0 \tag{2.17}$$

$$\frac{\partial(U_i)}{\partial t} + U_j \frac{\partial U_i}{\partial x_j} = -\frac{1}{\rho} \frac{\partial P}{\partial x_i} + \frac{\partial}{\partial x_j} [v \frac{\partial U_i}{\partial x_j} - \overline{\acute{u}_\iota \quad \acute{u}_J}]$$

$\overline{\acute{u}_\iota \quad \acute{u}_J}$ called the Reynolds stress tensor represents the correlation between fluctuating velocities. All the influence of turbulent fluid motion on the mean flow is bulged to this single term as averaging process. This will let huge savings in terms of computational requirements. However, the averaging process generates another six new unknown variables. So, in total ten unknowns are derived (1-pressure, 3-velocity, 6 Reynolds stresses) and four equations (1-continuity ,3 components of momentum equation). Thus, we need six equations to close the problem. This is referred to the *Closure problem*.

There are two main categories depending on the way the Reynolds stress tensor is closed, namely model the eddy viscosity models and the Reynolds stress. The Reynolds stress tensor derived from time averaging of Navier- Stokes equations are closed by substitute it with the eddy viscosity then multiplied by the velocity gradients. This can be referred to as the *Boussinesq assumption*.

$$\overline{u_i' u_j'} = -v_t \left(\frac{\partial \overline{U_i}}{\partial x_j} + \frac{\partial \overline{U_j}}{\partial x_i} \right) \tag{2.18}$$

where v_t is the turbulent eddy kinematic viscosity. that make Eq. 2.18 valid for contraction as result of Eq. 2.18, it should be rewritten as,

$$\overline{u_i' u_j'} = -v_t \left(\frac{\partial \overline{U_i}}{\partial x_j} + \frac{\partial \overline{U_j}}{\partial x_i} \right) + \frac{2}{3} \rho \delta_{ij} k \tag{2.19}$$

where δ_{ij} represents Kronecker delta, $\delta_{ij} = 1$ if $i = j$ and $\delta_{ij} = 0$ if $i \neq j$. k represents turbulent kinetic energy given by,

$$k = \frac{1}{2} \overline{u_i' u_j'}$$

The eddy viscosity can be handled as scalar quantity and is found using a length scale l and the turbulent velocity scale v depend on the dimensional analysis.

$$v_t \sim \ v_L \tag{2.20}$$

There is various kind of eddy viscosity models (EVM) depending on the eddy viscosity is closed. In Reynolds stress models (RSM), the equations are solved for each single Reynolds stress component such as determining equation for one length scale. However, RSM is computationally more demanding when compared to other EVM's.

In EVM's equation, one turbulence quantity was solved and the second turbulent quantity is derived from algebraic expression. Algebraic equation EVM's normally using geometric relation to compute the other eddy viscosity. These two quantities are used to characterize the eddy viscosity. For two equation EVM models for two turbulent quantities can be solved by describing the eddy viscosity.

2.4 Discrete Phase Modeling

2.4.1 Governing equations for the particles

There is definite reasonable assumptions was made to characterize the particles fluid medium transport . Based on the physical properties of dust particles partly and to the mathematical modeling required, The major simplifying assumptions are as follows,

• The large ratio of particle to fluid density : density of the dust particles are higher if compared to the fluid medium (air)

• The particles are suggest to be spherical.

• Dominant force is the drag force: This is a direct result for the assumption above. So when density of the particles are higher than the fluid medium density, several forces such as buoyancy, the lift force, and Basset force are readily discarded negligible act on the particles transport.

• One-way coupling: A phenomenon of mutual mass, energy transfer and momentum between phases are termed as coupling. Elghobashi presented map of regimes of interactions between fluid turbulence and particles. For dispersed-phase volume fraction values less than $10-6$, particles are supposed to be negligible which is effects on turbulence and this is termed called one-way coupling.

the particles existence can raise the turbulence if the ratio of particle response time to turnover time of the large eddy is greater than unity, or can decline turbulence if the ratio is less than unity. This is called interaction of two-way coupling. For the third regime that volume fractions are greater than $10-3$, to the other two-way coupling between turbulence and particle collisions will take place and there is regime termed as four-way coupling. All the above incorporating assumptions, Lagrangian equations governing particle motion is written as :

$$\frac{dx}{dt} = u_p \tag{2.21}$$

$$\frac{du_p}{dt} = F_d(u - u_p) + g_x \frac{(\rho_p - \rho)}{\rho_p} \tag{2.22}$$

Xp represents particle position, g_x represents gravitational force, p and ρ, are the particle and density respectively of the fluid. Usually, at each given point the particle moves with a different velocity than fluid. The fluid velocity difference (u) and the particle velocity (u_p), termed as the *slip velocity* ($u - u_p$), will cause unbalanced pressure distribution in addition to viscous stresses on the particle surface that presents a resulting force called *drag force*. In Eq. 2.22, the term F_d ($u - u_p$) is drag force per unit mass particle. F_d is given by :

$$F_d = \frac{1}{\tau_p} \frac{C_d Re_p}{24} \tag{2.23}$$

where τ_p is particle relaxation time given by,

$$\tau_p = \frac{d_p^2 \rho_p}{18\mu}$$

Laws of drag coefficient :

Different experimentally based on empirical correlations for drag coefficient depend on Rep shpuld be available in the literature. The drag coefficient Cd is a function of Reynolds number particle (Rep). The particle Reynolds number is defined as:

$$Re_p = \rho \, d_p \left| \frac{(u - u_p)}{\mu} \right| \tag{2.24}$$

In the Fluent, for spherical particles the drag coefficient tcan be calculated by using the correlations developed by Morsi and Alexander . It is given by:

$$C_d = a_1 + \frac{a_2}{Re_p} + \frac{a_3}{Re_p^2} \tag{2.25}$$

where a1, a2 and a3 are constants which apply to smooth spherical particles inthe stipulated range of Rep.

2.4.2. Modeling the particle phase

Coming to the fundamental mathematical modeling of two-phase flow, the two most widely used approaches are the Lagrangian trajectory approach and Eulerian continuum approach.

2.4.2.1. Lagrangian trajectory approach

The Lagrangian approach can be used if the phase particle is so diluted which the particles characterization behavior by continuum models is not feasible. An advantage of the Lagrangian vusing is the ability to fluctuate easily physical properties combined with individual particles like diameter, density, etc. The particles motion are expressed by an ordinary differential equations in the Lagrangian coordinates are directly obtained to give individual tracks for the particles . To make a solution of the Lagrangian-equation for the particular moving the particle, the gas phase dynamic behavior (generally obtained by an Eulerian approach) and another particles surrounding the moving particle could be pre-determined. However the corresponding particle trajectory and particle velocity are calculated for each single particle, the approach can be applicable to given a discrete nature of particles motion. Thus, to obtain averages statistical with accurate acceptable, large number of particles have to be tracked. Thus, phenomena of local physical related to the flow particle behavior can be easily examined. Hence, Lagrangian models are used for testing, development, t and validation of continuum models.

Lagrangian approach can be classified into two types namely, Stochastic trajectory methods and deterministic trajectory methods due to the effect of turbulence. In a deterministic method, all turbulent transport processes of the particle phase is neglected while the stochastic method takes into consideration the effect of the fluid turbulence on the motion of particle depending on instantaneous fluid velocity in formulation of the particle motion equation.

2.4.2.2. Eulerian continuum approach

The approach is suitable when one need the macroscopic field description properties of dispersed phase such as pressure, mass flux, velocity, temperature, and concentration. Eulerian approach is suitable for simulating large-scale with particle flow processes. In the Eulerian approach, the particle is used as second fluid which behaves such as continuum and the equation is developed for the particles average properties. For example, the particle velocity is average velocity over the averaging volume. Thus, this approach require refined modeling to describe the key phenomena and effects are found in the industrial processes.

2.4.3. Stochastic trajectory approach

Generally this models are used in eddy interaction model (EIM) firstly is introduced by Hutchinson et al. and further improved by Ioannides and Gosman. The instantaneous particles motion is governed by Equations 2.26 and 2.27 are written in the general form below.

$$\frac{dx}{dt} = u_p \qquad\qquad (2.26)$$

$$\frac{du_p}{dt} = \frac{1}{\tau_p}(u - u_p) + g \qquad\qquad (2.27)$$
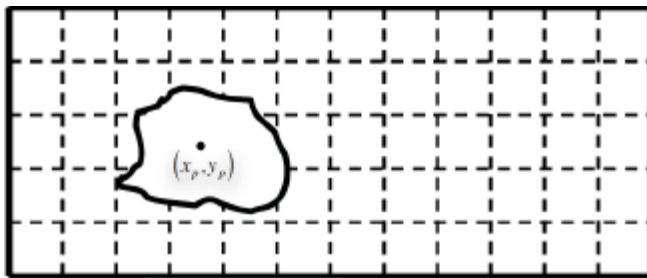
Figure 2. 1. 2-D illustration the particle within eddy

Figure 2.1 indicates a 2-D schematic representation of the eddy inside the rectangular domain for any given position of particle (x_p, y_p), It is acceptable that eddy has own

fluctuation $\acute{u}$, which stay constant until particle leaves this eddy. this eddy factors are first calculated depend on the dissipation rate and local fluid kinetic energy. The particle position (x_p, y_p), is supposed to be located at center of this hypothetical eddy. A particles leave an eddy are depend on a specific *interaction time* of the particles with the eddy. Since this interaction time is reached while the particle equations time integrated, the particles are supposed to have left present eddy. So, due to the new particle position, new eddy parameters have been determined and new fluctuations $\acute{u}$ are assigned to the eddy.

The process may repeat many interaction times required for particle to get the required distance. If numerically significant particle number is tracked in this way, assembling averaged behavior is represent turbulent dispersion is induced by the current fluid field . This interaction time can be defined as the minimum of the two time scales, one is the being the crossing-time of particle in eddy and the other a typical turbulent eddy lifetime, $t_{int} = min(t_e, t_c)$. In the LES simulations, the resolved velocity fluctuations effect on the particles is considered so there is nothing need for interaction model eddy like in RANS .The above eddy interaction model is required only for RANS simulation to take into consideration the turbulence effecting on the particle. Figure 2.2 represent the flow chart explains the steps included in the tracking one particle injected.
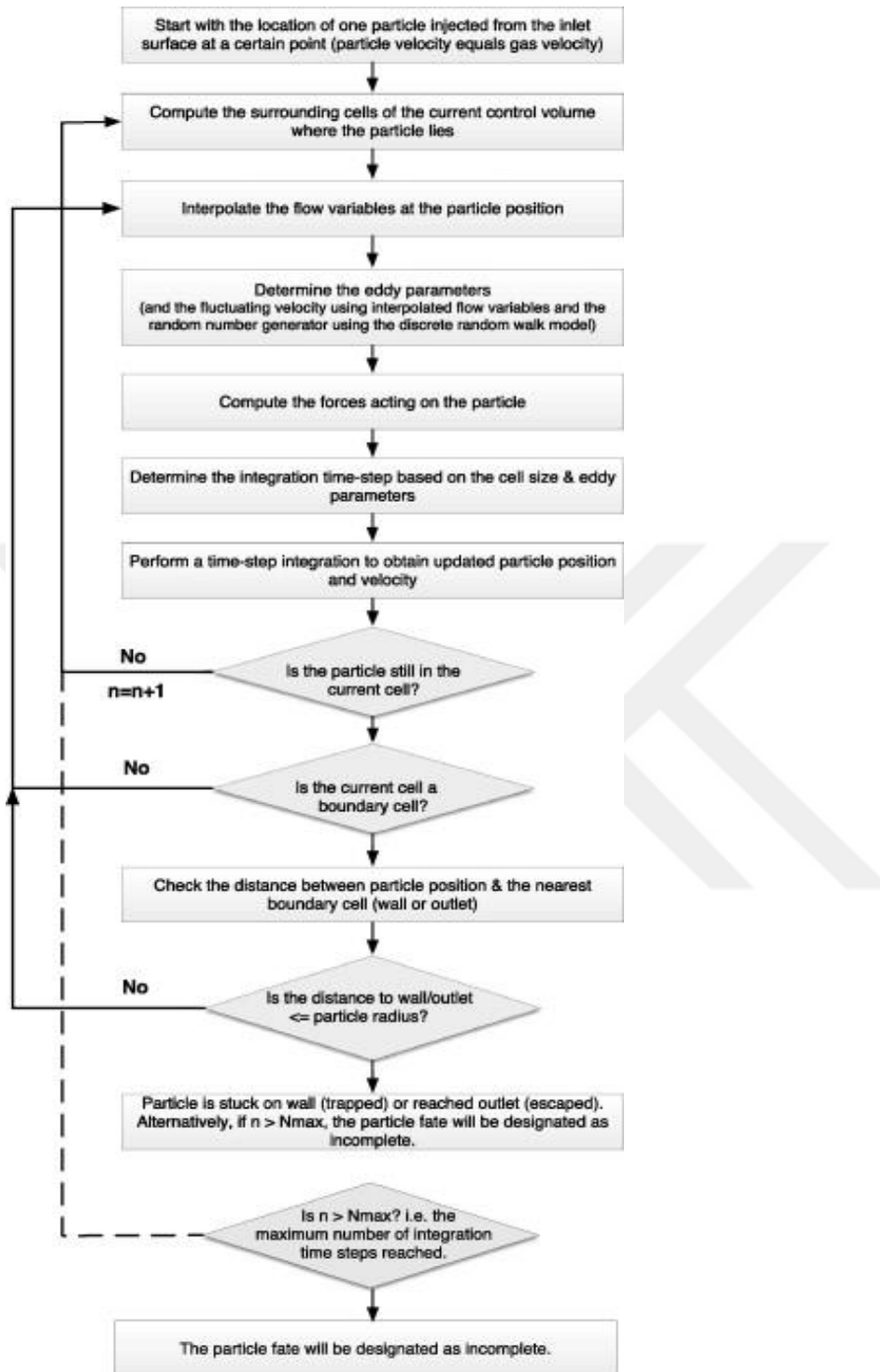
Figure 2. 2. Chart explaining the steps included in tracking one particle injected.

2.5. Multi-Phase Flows

Multiple fluids can mix with each other as they move together in the same environment or can be divided. The gravitational force and centrifugal forces acting on separation are only very high can be examined when flow models are used. In multiphase flows, each fluid has its own physical properties that can present itself Today, there are 5 types used in commercial CFD software we can talk about multi-phase model (TEKE, 2010).

2.5.1. Volume of fluid model

VOF, the initials of "Volume of Fluid", analyzes the non-interfering fluids Used in meat. In this model, the fluids do not interfere with each other and a cell it is completely filled with a single fluid. Thus, a free surface area between the fluids has. Used in VOF model free surface flows and large bubble column.

2.5.2. Eulerian model

The Eulerian multi-phase flow model analyzes at least two fluids used. Fluid gas can be in liquid and solid phases. For Eulerian multi-phase flow model there is no constraint on the volumetric fraction of the fluid in the mixture. In this model the mass conservation and the momentum equation for the fluid is solved separately. Phases is solved by the momentum transfer equation, mass and heat transfer For the solution, continuity and energy equations are used. Single pressure for all fluids field is resolved. In addition, the turbulence equations are solved separately for each phase.

2.5.3. Mixture model

Mixture model is preferred when there are intermixing fluids It should be. Momentum, continuity and energy equation for N fluid or particles are solved the volumetric fraction equations are solved for the secondary phase. Typical applications sedimentation, cyclone separators and bubble flow modeling.

3. EXPERIMENTAL METHOD & MATERIAL SETUP

3.1. Description of Cyclone Separator Experiments

The experiments were investigated using an experimental test equipment. The overall layout sketch in Figure 3.1. Fresh air at ambient condition is supplied from a centrifugal pump to the experimental. The centrifugal compressor is located in a downstream of the separator and air is drawn to the system from blower to the outlet. In order to adjust the flow rate, a control valves are used to change the flow according to a desirable velocity.

Separator body design is cylindrical and due to Pisarev et al (Pisarev, G. I., Gjerde, V. I., Hoffmann, A. C., Peng, W., Balakin, B. V., Dijkstra, H. A., 2011). This shape can reduce the uncertainty that caused by the geometry. The Figure 3.1. below shows the gas flows horizontally into the tube then changes its direction to the vertical.

.
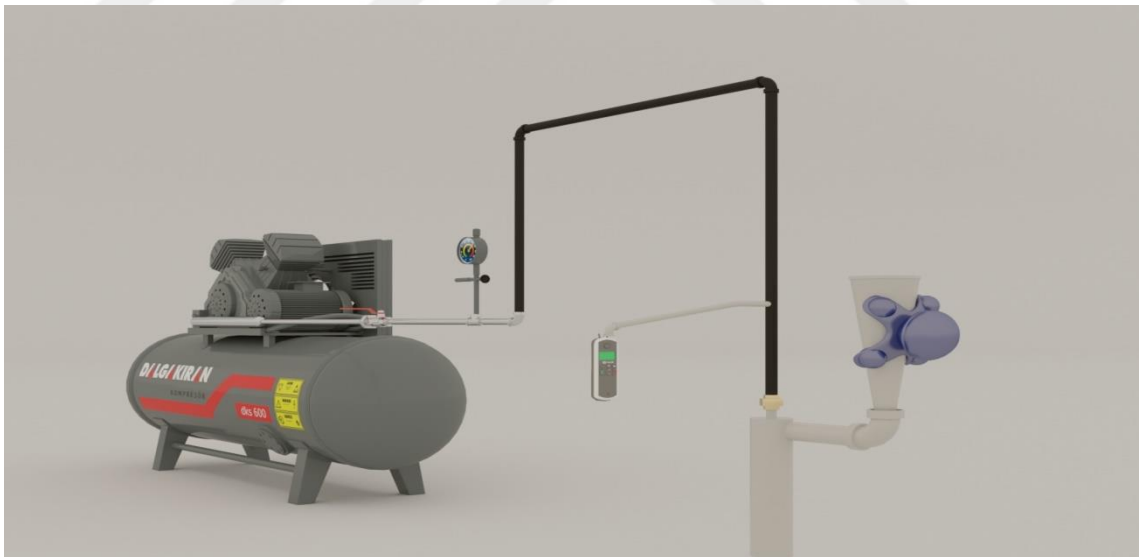
Figure 3. 1. The experimental setup of the cyclone equipment.

Three baffles were installed to reduce the flow before reaching the swirl vanes, so that the flow could be distributed better over the annular cross-section. The swirl tube consists of three distinct constructions:

- ❖ separator body
- ❖ vortex finder
- ❖ swirl vanes

The experiment was carried out under normal conditions (at atmospheric temperature and pressure) in a laboratory environment. In order to ensure that the measurements are accurate, the laboratory is set up in a lab environment, away from humidity, high temperature and variable air currents. The simple schematic for this experimental setup is given in Figure 3.1. When this mechanism is being used, the pipe, connection elements, should be tight well to prevent leak-proof. For both cyclones (Cyclone 1 , Cyclone 2), the test scheme shown in Figure 3.1 is used.

The air-powder mixture moves in the direction of the arrow as shown on the diagram . The air pressure is provided by the ' 2.2 KW' blower which is required for vacuuming. A flow meter and a valve are connected to the pipe and blower inlet, the pipe connected to this flow rate is connected to the outlet of the cyclone. According to that, the flow rate is measured through the cyclone with a sensitive of 0.1 m3 / h and the desired flow rate is adjusted by using a ball valve. Thus the dust air entering the cyclones can easily be adjusted to the desired values. The outlet pipe of the cyclone separator is connected to the hose, a hole was opened about 100 mm at the cyclone outlet. The pressure difference between the cyclone outlet and the external environment was measured by means of a hose from this hole. The 'Testo 521 pressure difference meter' shown in Figure 3.2 (a) has 2 different inlet air holes. This device measures a static pressure difference between the two points either by ejecting from two points coming into these two holes or by vacuuming air. Therefore, the pressure loss at the cyclone separator outlet point can be measured, from the pipe of cyclone outlet which is connected to a hole in the Testo device, while the other hole is left open to allow the exhalation through this way static pressure was measured for different flow rate. This pressure difference can be seen on the unit screen in various units, depending on the desirable unit, a specific unit can be defined from setting menu of the unit, Pascal unit was set to measure static pressure between inlet and out let of the cyclone separator (ÇALIŞKAN, 2017).

Before starting the experiment the powder air mixture in the experiments are taken by certain amount in a strainer which is connected to vibration device that is used to maintain the dust interring the cyclone separator properly at constant concentration. When the vibration device is turned on, the dust contain in the strainer moves through the strainer. Thus, the dusts that are clumpy or damp are separated from each other and mixed with air in the particle size that they have, and entered through the inlet section of the cyclone separator. It is also aimed to simulate the behavior of dusts in real environment conditions while feeding the powder at constant concentration. The powder-air mixture automatically supplied throughout the test helps to ensure that the test results are more accurate. Each of the experiments was carried out for 30-60 minutes for both cyclones. This is the minimum time that cyclone performance values, collection efficiency, and other classification performance give stable results. If the experiments carried out below this duration it would give a different results, from the flow rate point of view when we increase the flow rate the experiment will take much time to carry out .

the powder-air mixture entering the cyclone separator in the experiments was used as dust is calcium carbonate $CaCo_3$, which has a density of 2,7 gr / cm^3, the properties of this Calcium Carbonate, are given in Table 3.1.

Table 3. 1. The properties of the Calcium Carbonate

Component	CaCO3
Molecular Weight	100.0869 g/mol
Crystal System	Hexagonal
PH	8-9 (25 °C)
Hardness	3
Melting point	1340 °C
Resolution(g/L)	0,014 (20 °C, in water)
Density	2,7 gr/cm3

The reasons for using calcite powder in experiments are; due to the density of the air it is mixed with the air properly and spreading in a proportional manner, not to hold too much moisture, to offer a wide scale as a particle size, to be suitable for room conditions, to be low cost and not to be combustible, can also be shown in Figure 3.2.

Ground Calcium Carbonate

(a)   (b)   (c)
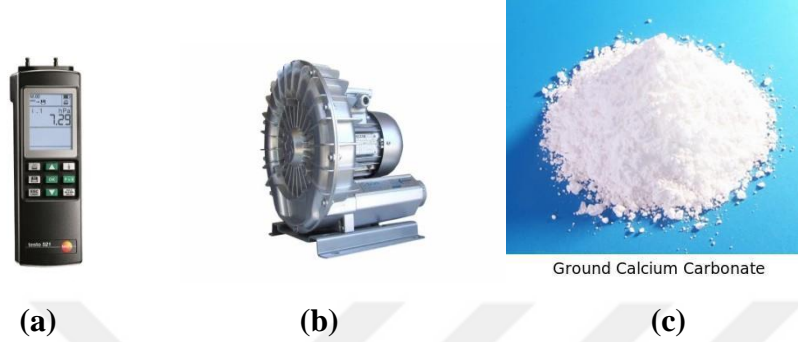
Figure 3. 2 The equipment used in experiment**.**

3.1.1. Cyclone separator experiment

Experiments have been carried out for a mini cyclone, with an inlet cross section of 3 * 20 mm. In these experiments, the valve was opened at certain stages to send dusty air at defined flows through the cyclone during the experiments. According to these experiments, the values (Q) that was used for experiments were determined as 4, 6, 8, 10,12,14 m3 / h. According to this theory, the velocities of the air entering Cyclone was calculated due to the Equation 3.1 (A: Cyclone inlet cross-sectional area): V_{inlet}: 18.5, 27.78, 37,04, 46,3, 55.5, 64.8 m / s has been identified respectively.

$$V_{inlet}\ (m/s) = \frac{Q*10^6}{A*3600}.$$
(3.1)

Carbon calcite powder was used in each experiment in an amount of 50 gr and the average particle size is 15 µm , the particle size distribution was shown in Figure 3.3.
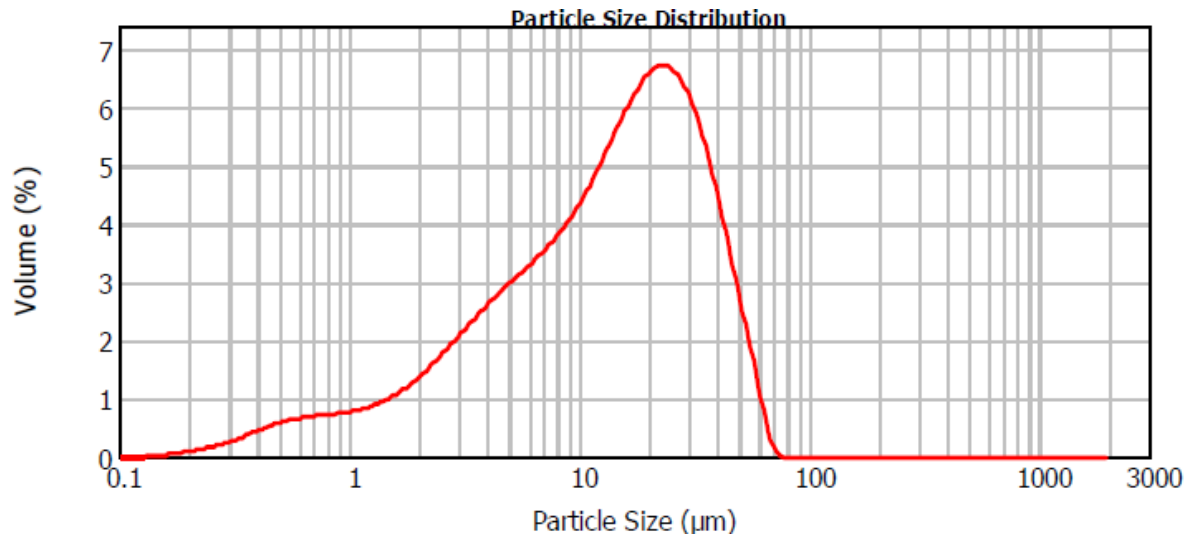
Figure 3. 3. Particle size analysis of calcite powder sample.

The working principle of the Mastersizer 2000 device for measuring the grain size inside the material is based on vacuuming and removing small particles by using Mie Theory to measure the dimensions of small particles, Particle size measurements were done by the Mastersizer 2000 analyzer of particle size as shown in Figure 3.4.

Figure 3. 4. Malvern Mastersizer 2000

The Mie Theorem takes into account both the fracture and the permeability around the powder size in the medium. In order to use the Mie model, its necessary to know the fracture indices of both sample and the environment. The experiments with both cyclone separators (Cyclone 1 and Cyclone 2), the rate of air entering the cyclone was taken as the basic variable parameter. Another configuration of the experiments, the arrangement of the dust collectors in their position in the cyclone separator, has been tested at each determined point. The results obtained from each experiment were analyzed in detail and results were formed. These results are two variable parameters; the result of the combination of flows and configuration.

Experiments carried out in the laboratory are carried out with a slightly shorter experiment time at high flow rates so that the calcite powder can be mixed with air at the same concentration in each experiment and it takes a long time in low flow rates. As a result, each experiment took between 45-60 min. As a result of each experiment, the calcite powders in the dust collectors contained in the cyclone separator were carefully weighed and then sampled from each of other for particle size analysis. The collection efficiency of a cyclone separator is then calculated according to Equation 3.2.

To find cyclone separation efficiency of particles the equation below as used.

$$\text{fractional collection efficiency} = \frac{\eta p \ trapped}{\eta p \ injeceted} \qquad (3.2)$$

fractional collection efficiency for 10cm length, 18.5 m/s for 15 $(\mu m)dim = \frac{46}{50} = 92\%$

fractional collection efficiency for 20cm length &18.5 m/s for 15 $(\mu m)di = \frac{42.5}{50} = 85\%$

for 10 cm cyclone length the same procedures have done by define the length using closed disks inside cyclone body. 50 gr of powder was carefully weighted and added to cyclone by exerting the force of vibration device to insure the flowing of powder inside cyclone, according to specific flow rate that is needed for experiment. The trapped powder was re weighted and using the   same Equation 3.2. to measure cyclone collection efficiency, pressure drop for instantaneous flow rate can be measured by using The 'Testo 521 pressure difference meter' shown in Figure 3.2 (a) it's used by

measuring a static pressure difference between the two points either by ejecting from two points coming into these two holes or by vacuuming air.

3.1.2. Classification efficiency

The powder with a mean particle size of 29.7 µm (Fig. 3.5) and the powder with an average particle size of 14 µm (Fig. 3.6) were used in the Cyclone 1 experiments. It is possible to examine all of the particulate dusts contained in these dusts in Figure 3.5 and Figure 3.6.
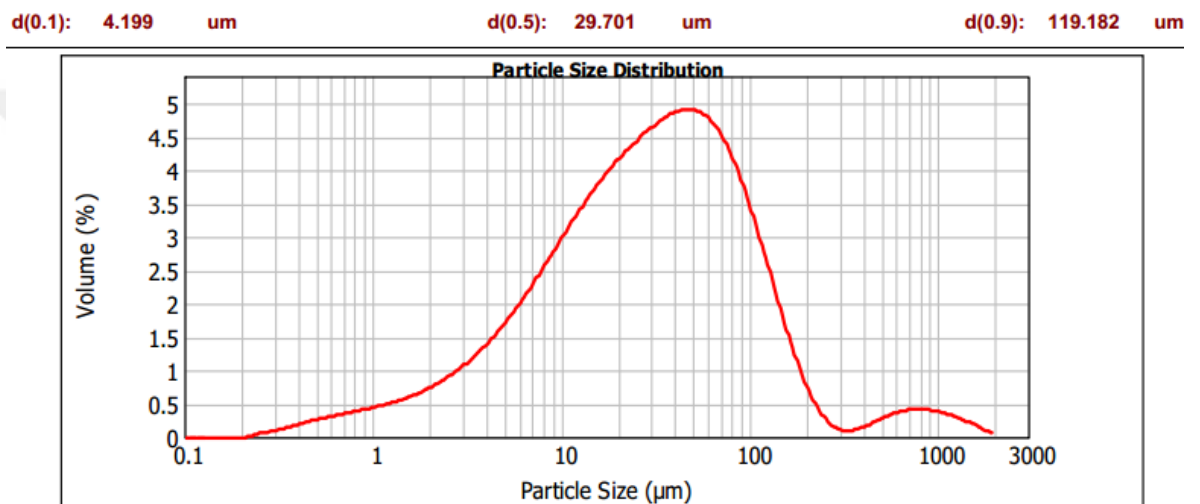
Figure 3. 5. The calcite powder used for cyclone 1 contains dust particles
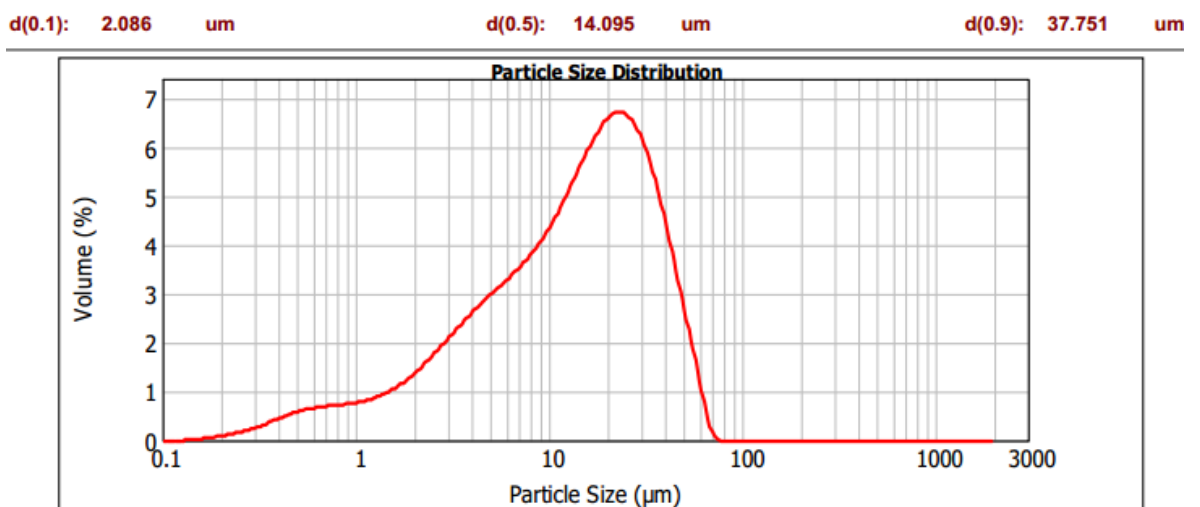
Figure 3. 6. The calcite powder used for cyclone 2 contains dust particles

For example; For calcite powder with an average particle size of 14 μm for Fig. 4.5, the proportion of powders with dust particles between 1 μm and 2 μm is 4,31%. (ÇALIŞKAN, 2017). According to these analyzes, the performance of classification of dusts cyclone separators can be better examined. As these dusts contain many different dust particles, a large number of configurations are tested and many experiments should be carried out while the classification performance is examined. In this way, the performance of the cyclone separators to classify to the minimum and maximum dust particle sizes can be analyzed. A number of configurations have been tested in Cyclone 2 experiments, especially designed for high classification performance.

3.1.3 Cyclone classification performance

Experiments on Cyclone, the configurations for examining the classification performance are given in Figure 3.7. In these configurations, an examination was carried out according to the cases of 2, 3 and 4 dust collectors in the cyclone separator. For Cyclone the amount of calcite powder collected and the particle size of the calcite powder collected in the experiment were also examined

Conf. 1   Conf. 2   Conf. 3
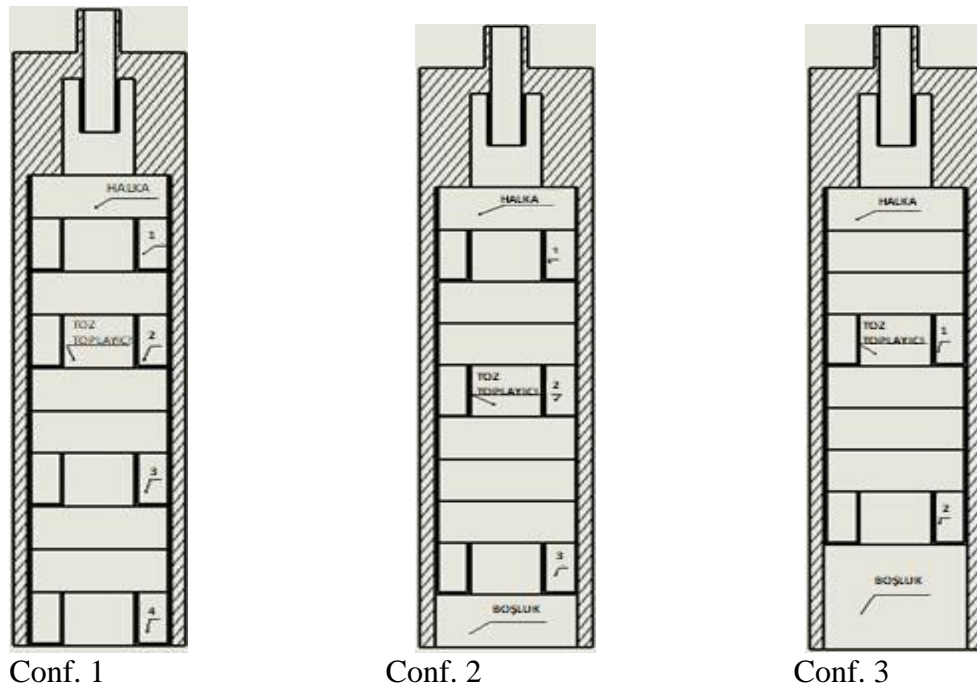
Figure 3. 7. Configurations investigate the classification performance for Cyclone

In these given configurations; the names of the dust collectors are numbered starting from the top dust collector. In Conf.1 there are 4 dust collectors , in Conf. 2 there are 3 dust collectors, in Conf.3 there are 2 dust collectors. The results of these three different configurations are given in Table 3.2 to give a distribution in terms of amount of dust and size (ÇALIŞKAN, 2017).

Table 3. 2. Results of experiments was done on different configurations for Cyclone

Flow Rate: 10 m3 / h Average Particle Size: 29,7 μm								
configurations	**Dust Collector 1**		**Dust Collector 2**		**Dust Collector 3**		**Dust Collector 4**	
	Sample collected	Particle size	Sample collected	Particle size	Sample collected	Particle size	Sample collected	Particle size
Conf. 1 (Containing 4 dust collectors)	24,9 gr	50,41 μm	18,1 gr	26,41 μm	2,85 gr	22,74 μm	1,7 gr	9,61 μm
Conf. 2 (Containing 3 dust collectors)	20,6 gr	48,814 μm	21,9 gr	20,41 μm	4,3 gr	6,38 μm		
Conf. 3 (Containing 2 dust collectors)	29,6 gr	50,16 μm	18,65 gr	12,25 μm				

These results, given in Table 3.2 for 10 m3 / h flow rate and 29.7 μm average particle size calcite dust. According to the results given at Conf .1 dusts of particle size 50,407-26,411-22,743-9,61 μm, respectively, were collected in the dust collector.

It can be seen that partial classification can be made in 4 different particle sizes. However, considering the dust particle sizes in the dust collector 2 and dust collector 3 are close to each other (26,411-22,743 μm), the most net classification is made clear in

Konf.2. As a result, when looking at the results of cyclone experiments, Cyclone has the ability to clearly classify the powders in 3 different particle sizes.

In configuration 2; the dust particles (calcite) in the dusty air entering the cyclone separator are clearly separated into 3 separate classes. In these 3 classifications, dust particles were collected in the dust collectors at sizes of 48,814, 20,406 and 6,383 μm, respectively. As can be seen from the results, the larger size particles are collected in the upper dust collectors in the cyclone, while the smaller size particles are collected in the lower dust collectors. This is because of ; the large particles in the dust entering the cyclone separator from the top dust collector, due to the exerts of centrifugal forces there. they fall further into the reservoirs of the dust collectors above. Subsequently, the remaining small particulate powders, with the centrifugal force dropping downward in the cyclone separator, are blown into the cyclone walls and fall into the dust collectors below. (Fuping Qian et al.,2009) in their work; the cyclone separator wall moves due to the high axial velocity resulting from the centrifugal force of the particles. At the same time, they noticed that the flow rate closest to the inner wall of the cyclone showed better separation performance of cyclone. The classification performance of Cyclone 1 was investigated based on the variation of the constant flow rate configuration in the results given in Table 3.2. Experimental studies on the results in Figure 3.8., use variable flow rate and fixed configuration (CONF.2) at 4 and 8 m3 / h. This experimental investigation is to carry out how the effect of flow rate changing in the cyclone, cycling performance , lead to the change in velocity of the air entering the cyclone.

If we look at the experimental results in Figure 3. 9., it has been understood that the flow rate change has no effect on the classification performance of the Cyclone 1 separator. However, the values obtained from the test results at 8 m3 / h are; the effect of the increase in flow rate has shown that the dust collected in the dust collectors makes the particle size larger. When the mass of the collected dust in the cyclone collectors is taken into consideration, it has been seen that a more proportional distribution is obtained in the high flow rates. This has shown that the larger centrifugal

49

forces generated by the high-flow rate cause a more proportional change of dusts in the dust collector in the cyclone separator as can be shown in Figure 3.8., below .
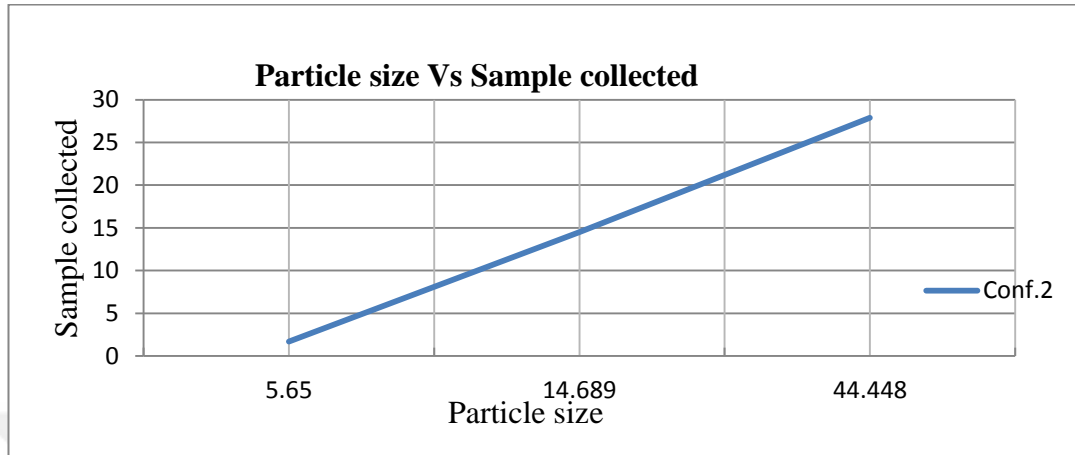
Figure 3. 8. Classification according to flow variation in fixed configuration for cyclone.

When the amount of dust collected in a dust collector 1 at the uppermost portion of the cyclone separator is also taken into consideration, It was determined that according to the flow rate 8 m3 / h and 4 m3 / h larger particles were collected. The reason for this is also thought to be that the higher centrifugal forces give more force to the powders and cause larger particle sizes to throws the particles dust toward the top of the wall cyclone. In their study in (Tetsuya et al, 2009), they observed that the dust particles remained in the cyclone separator due to the low flow rate. The more particles remaining in the cyclone separator, the greater the susceptibility to centrifugal forces (ÇALIŞKAN, 2017).

The dimensions of the dust particles collected in the dust collectors, as given in Table 3.2., and Figure 3.8., were measured with a Mastersizer 2000 particle size meter. This measurements, a particle size analysis curve was obtained in detail from the samples. For example; In Conf.2 the experiment carried out at 8 m3 / h flow arte , particle analyzes of powders in dust collectors are given in Figure 3.9.
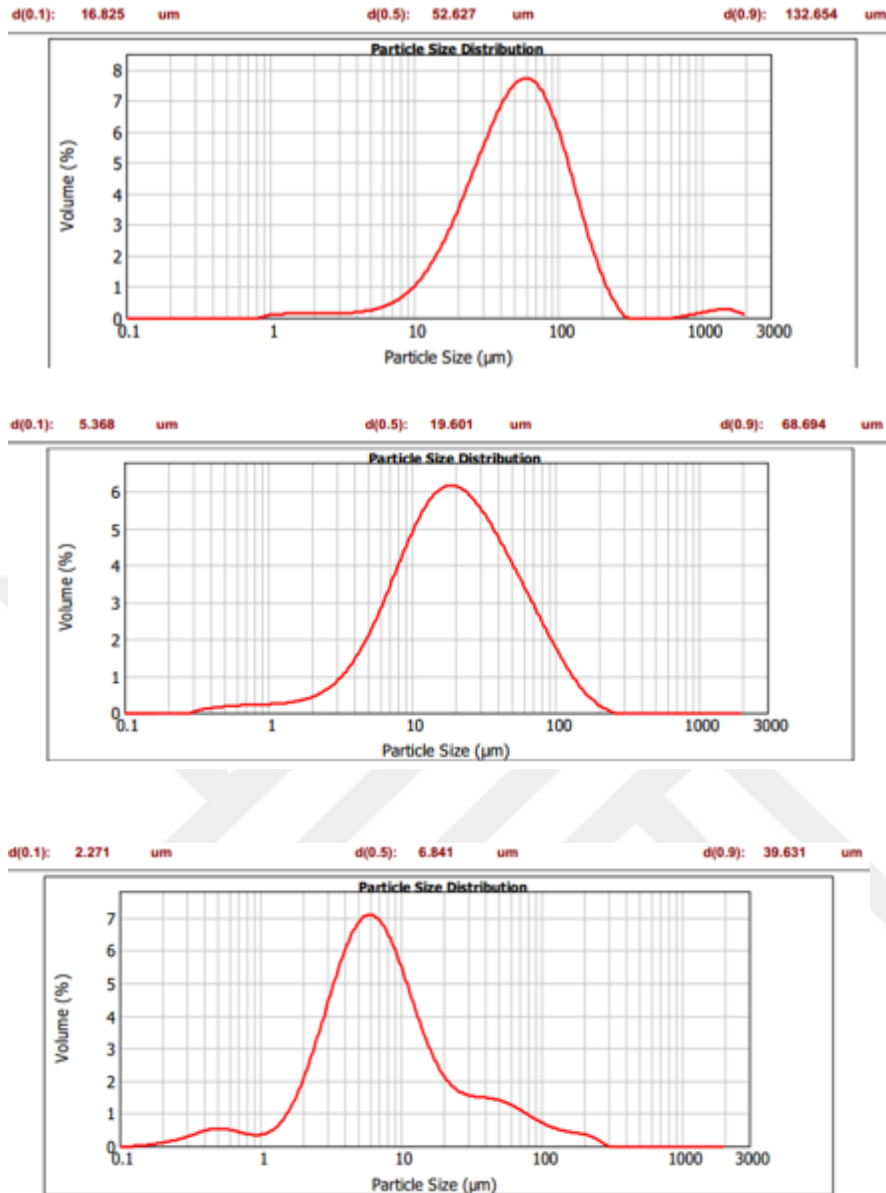
Figure 3. 9. Particle analysis of powders in dust collectors for 8 m3 / h .

3.2. Computational Fluid Dynamic Solution

3.2.1. Description of the numerical simulations

The collection efficiency and pressure loss performance test of cyclone separator are the result of the patterns flow gas, solid and pressure field inside the cyclone. Once the fluid flow field is well established using the gas flow analysis, discrete phase model (DPM) is used to investigate particle trajectories for a range of particle diameter. The impact of

particle-wall interaction is predicted using erosion modeling. A new design set of geometrical ratios is optimized to achieve the minimum pressure drop and to investigate the efficiency. Flow simulation in a cyclones has been operated using CFD commercial package FLUENT v18.5. The following methodology in FLUENT is to divide the solution domain into a large number of control volumes and to transfer the partial differential equations by integrating over the control volumes into their algebraic equivalents.

CFD simulations depend on Reynolds stress model are used in the cyclone investigation. The flows of Fluid have been numerically described by using the Navier–Stokes equations. With the current technology, it cannot possible to solve the Navier–Stokes equations for turbulent flow to the appropriate accuracy. Another way to simulate fluid flows in engineering applications by using turbulence, models and solve for mean fluid pressure and velocity. However to close the equations above, different turbulence models are derived varying from the simple k–ε model to the more complicated Reynolds stress model (RSM). In the cyclone flow simulation, a number of simulations was indicated that a simple k–ε model and its modification fail to predict accurately the flow structures inside a cyclone , On the other hand, the RSM is able to reproduce the notable flow features in the cyclones . However, the Reynolds stress model have been used for turbulence modeling in current suday. The RSM obtains calculation of the Reynolds stress components individually, $\overline{\dot{u_\iota} \quad \dot{u_J}}$, use differential transport equations.

The result of simultaneous algebraic equations are solved using iterative methods to give the distribution field of such dependent factors like pressures and components velocity, subject to the suitable boundary conditions specifying the problem individually. The computational domain employed for cyclone simulation contains from around 460218 cells hexahedral cells for 20cm and 299858 hexahedral cells for 10cm, with respect to the cyclone height. The grids hexahedral computational have been created by dividing the all cyclone geometry to the number of blocks and apply meshing for each single block separately. At the cyclone inlet a "velocity inlet" is used in boundary condition, that means the velocity will be normal to the inlet was defined. For

a boundary condition in the cyclone exit gas used the "outflow" condition in the FLUENT. Grid refinement test was applied to make sure that solution is not grid dependent. It is necessary to compare the simulation result with the available measurement data, to obtain the confidence about the simulation, The measurement data were indicated from the experiments .Take into consideration complexity of gas flow in the cyclone, the agreement between measurement and simulation is regarded as reasonable. Same agreement can be found for the distribution of axial velocity.

3.2.1.1. Concept of CFD

Using the finite volume method for numerical solution of conservation equations FLUENT v17.2 software is used. a commercially Fluent is available CFD software . The following steps are should be followed in the handling of a problem with the CFD method as shown in Figure 3.10., below.
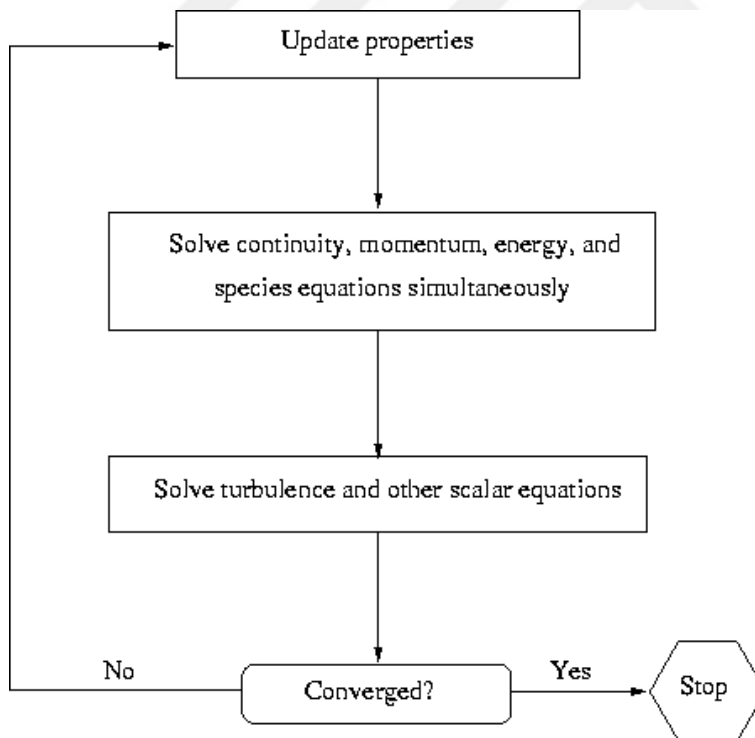
Figure 3.10. Overview of the Density-Based Solution Method (Swanson, April 2009).

3.2.1.2. Finite volume method

The finite volume method can be used to construct conservative equations in small cell-solving by separating them into algebraic equations by integrating them over their volumes Method. The finite volume method have been first used by (MCDONALD, 1971) and (MACCORMACK, R. W., PAULLAY.A. J. , 1972) have shown that Euler's equations are two-dimensional and time (RIZZI, A. W., INUOYE. M., 1973) in a 3D solution was performed.

(a) Account volume   (b) control volume
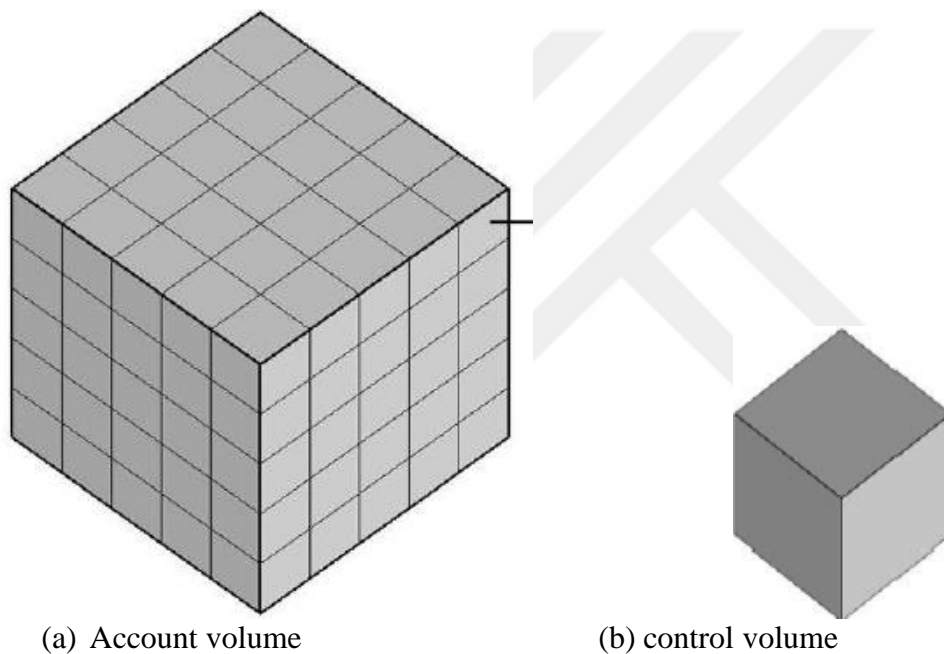
Figure 3.11. Show a control volume through account volume

In this method, the area of flow is dissolved and divided into the final number of control volumes Figure 3.11. The conservation equations (mass, momentum) are then decomposed into algebraic equations. Discrete equations are solved numerically. Governing equations discretization could be indicated easily by taking the unsteady conservation equation into considering for transport of the scalar quantity ϕ. This is can be clearly shown by following equation obtained in integral form forthe arbitrary control volume V as follows:

$$\int_{V} \frac{\partial \rho \phi}{\partial t} dV + \oint \rho \phi \, \vec{v} \cdot d\vec{A} = \oint \Gamma_{\phi} \nabla \phi \cdot d\vec{A} + \int_{V} S_{\phi} \, dV \qquad (4.1)$$

ρ = density

$\vec{u}$ = velocity vector ($= \overline{u_j} + v_j$ in 2D)

$\vec{A}$ = surface area vector

Γ_{ϕ} = diffusion coefficient for ϕ

$\nabla_{\phi} = gradient\ of\ \phi \left(= \frac{\partial \phi}{\partial x} \right) i + \frac{\partial \phi}{\partial y}) j$ in 2D

$S_{\phi} = source\ of\ \phi\ per\ unit\ volume$
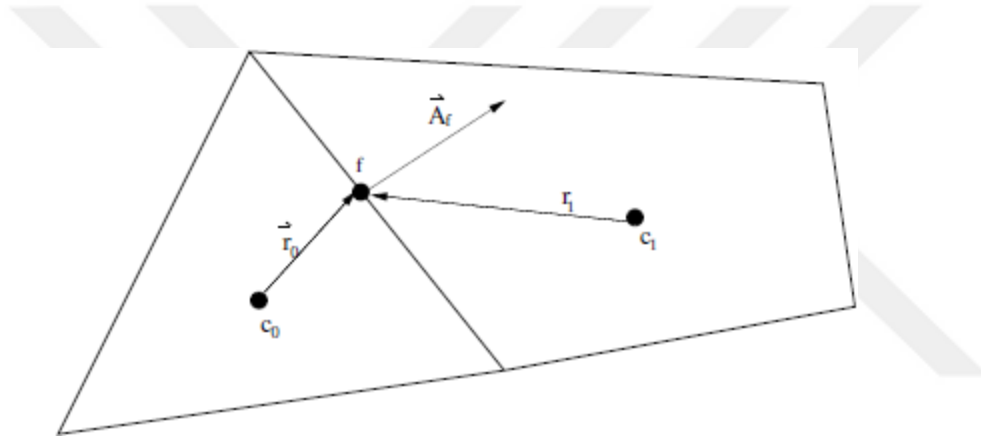
Figure 3. 12. Control Volume Used to indicate Scalar Transport Equation discretization

As shown in Figure 3.12., N is the number of surfaces on the calculated control volume, Φ_f f convection term from surface f, $\rho \, \vec{v}f$,$\vec{A}f$ f mass flow from surface, $\vec{A}f$ surface area, $\Delta \Phi_f$ is the gradient of "n" for surface f and V for control volume. discrete values for scale (C_0 and C_1). To be able to find "in each cell" Φ the convective term needs Φ_f to be solved. Using an appropriate decomposition scheme has done. The transport equation written in discrete form (2.28) is used in each cell center and contains unknown scales Φ at the center of other cells surrounding the cell. This linear (2.28) can be written in linearized form as follows:

$$a_p \phi = \sum_{nb} a_{nb} \phi_{nb} + b \qquad (4.2)$$

In Equation 3.2, nb is the neighboring cell, and the linear coefficients are b and the source (PATANKAR, 1980.). The number of neighboring cells depends on grid structure, but typical the number of surfaces surrounding a cell equals the number of neighboring cells at the same time. Similar equations are written in every cell in the grid. Then the coefficients generated in this way the matrix is solved by Fluent using the Gauss-Seidel method.

3.2.1.3. Solver options

ANSYS FLUENT allows you to choose one of the two numerical methods:
• density-based solver
• pressure-based solver
The density-based approach is mainly used for high-speed compressible flow, however The pressure-based approach is developed for low-speed incompressible flows. While, both methods was reformulated and extended to operate for a different range of flow conditions above their traditional intent. For both of methods the velocity field was obtained from the momentum equations. For the density-based approach, the continuity equation was used to derive the density field however the pressure field is obtained from the equation of state., while in pressure-based approach, the pressure field is given by solving a pressure or pressure correction equation that is derived by manipulating continuity and momentum equations. In the pressure based solver, pressure and momentum can be considered as primary variables.

After calculating the pressure and velocity fields, energy, turbulence and other transport then if any equations will be solved. In density-based solvent, pressure, energy and momentum are primary solved at the same time. Next, turbulence and other transport equations will be solved. In addition, PBS can be handled in two different ways within itself.

❖ Pressure based coupled solver (PBC)
❖ Pressure based segregated solver (PBS)

The PBS solvent can be compressed at high speed from low speed incompressible flow regimes flow regimes (Swanson, April 2009). Also need less memory requirement The PBC solvent is preferred over the steady-state flows while the memory requirement is 1.5-2 times more. Also it cannot be used in multi-phase flows (Eulerian). Density based (DB) the solver should be preferred if there is a strong interaction between in tensely, momentum and energy. This method should be selected, for example, if it is desired to combine combustion with compressible flow. Because of the less memory requirements and the use of a large field PBS solvent was used.

3.3. Decomposition (Interpolation methods)

The variables held in the cell centers interpolate to a surfaces of control volumes $\sum_{f}^{N} \rho \, \phi_f \, \vec{v}_f \, \vec{A}_f$ the interpolation schemes that can be used for convection are given below.

3.3.1 First-Order Upwind scheme

This method calculates the average value of calculated variable at the center of cell by using this value at other points of the cell. The convergence is very fast This method is not very sensitive If there is a swirling flow like cyclone applications do not give satisfactory results. However, with the first degree upwind method a good starting condition is created. Then the high-grade methods convergent and sensitive results are obtained. In this study, first degree upwind method was used to create the initial condition for the analyses. When accurate first-order is required, quantities at cell faces are obtained by assuming the cell-center values for each field variable that appears a cell-average value and hold throughout the entire cell; the face quantities are same to cell quantities. However the first-order up winding was selected, the value face Φ_f is set equal to cell-center value of Φ_f in upstream cell.

3.3.2. Second -Order Upwind scheme

This Second degree method may be preferred when sensitivity is required from the root. In this method the cell surface values are used when the calculated variable is not constant throughout the cell. Equation 2.30 is used to calculate for the surface variable.

$$\phi_{f,sou} = \phi + \nabla \phi . \vec{r} \tag{4.3}$$

Here; ϕ represent value at the cell center, $\nabla \phi$ is a gradient of the value at the cell center, $\vec{r}$ is the vector displacement. This method is generally preferred when triangular elements are used. When accurate second-order is required, quantities at the cell faces were derived using a multidimensional linear reconstruction approach . For such approach, higher-order accuracy can be carried out at the cell faces through a Taylor series expansion of cell-centered solution about cell centroid.

3.3.3. QUICK scheme

In this method, the weighted average of the variable and second order upwind method are calculated using the central interpolation of the variable. . QUICK-type schemes based on a weighted average of the second-order-upwind and the central interpolations of variable. The QUICK scheme is more accurate on structured meshes range with flow direction. For hexahedral and quadrilateral meshes, where unique downstream and upstream faces and cells are identified, ANSYS FLUENT also gives the QUICK scheme to compute a higher-order value of convicted variable ϕ For the face e in Figure 3.13., if flow is from left to right, such a value is written as EQN 3.4

$$\phi = \theta \left[\frac{S_d}{S_c + S_d} \phi P + \frac{S_c}{S_c + S_d} \phi E \right] + (1 - \theta) \left[\frac{S_u + 2 S_c}{S_c + S_u} \phi P - \frac{S_c}{S_u + S_c} \phi w \right] \tag{4.4}$$
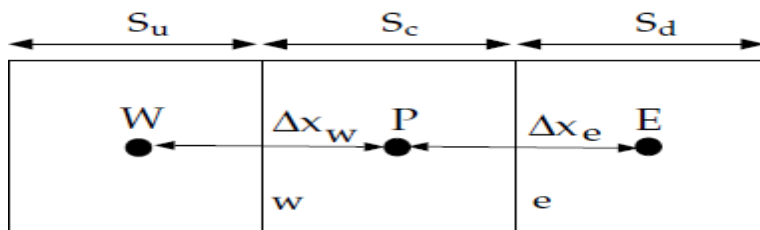
Figure 3.13. One-Dimensional Control Volume.

in above equation θ = 1   results in the central second-order interpolation while in the second-order upwind value yields θ = 0. The QUICK scheme is given by setting θ = 1/8. The application in ANSYS FLUENT using variable, the solution dependent value of θ, chosen to avoid the introducing of new solution extreme.

Taking into a consideration that the ANSYS FLUENT permit the use of QUICK scheme for hybrid meshes or unstructured as well; in such cases The second-order upwind scheme is used at the partition boundaries while parallel solver is used. And also the usual second-order upwind discretization scheme is used at faces of non-hexahedral (or non-quadrilateral, in 2D) cells.

3.3.4 PRESTO (Pressure staggering option scheme) method

Presto's algorithm ,calculate the pressure value in the surface using the cell center values It provides the stability of the cross-control volume in the vicinity of the cell due to High Reynolds numbers; pressure values can be predicted and due to viscous at high pressure gradients in the regions along with higher order upwind methods velocity profile can be also predicted.

3.4. Numerical Simulation

3.4.1. Tow tested cyclones configurations

The numerical simulations are applied for two cyclones with different height (10cm, 20cm) many studies have been carried and investigate the influences of different geometrical parameter such as the cyclone length , pressure drop and cyclone efficiency were investigated for 10 cm, then 20 cm was cut from cyclone length to investigate the influences of cyclone under different length taking into account different inlet velocities was applied (18.5,27.8,37.04,46.3,55.5,and 64.8 m/s) in addition to that various particles diameter was applied to check the behavior of cyclone under different particles diameter (0.2,0.4,0.6,0.8,1,3,4,5,6,7,8,9,10,15,20,25,35 μm).

As has been shown Figure 3.14., give the cyclone dimension that is used to carry out the pressure drop and cyclone efficiency using CFD comparing to the result of the same cyclone dimension used in the experimental.
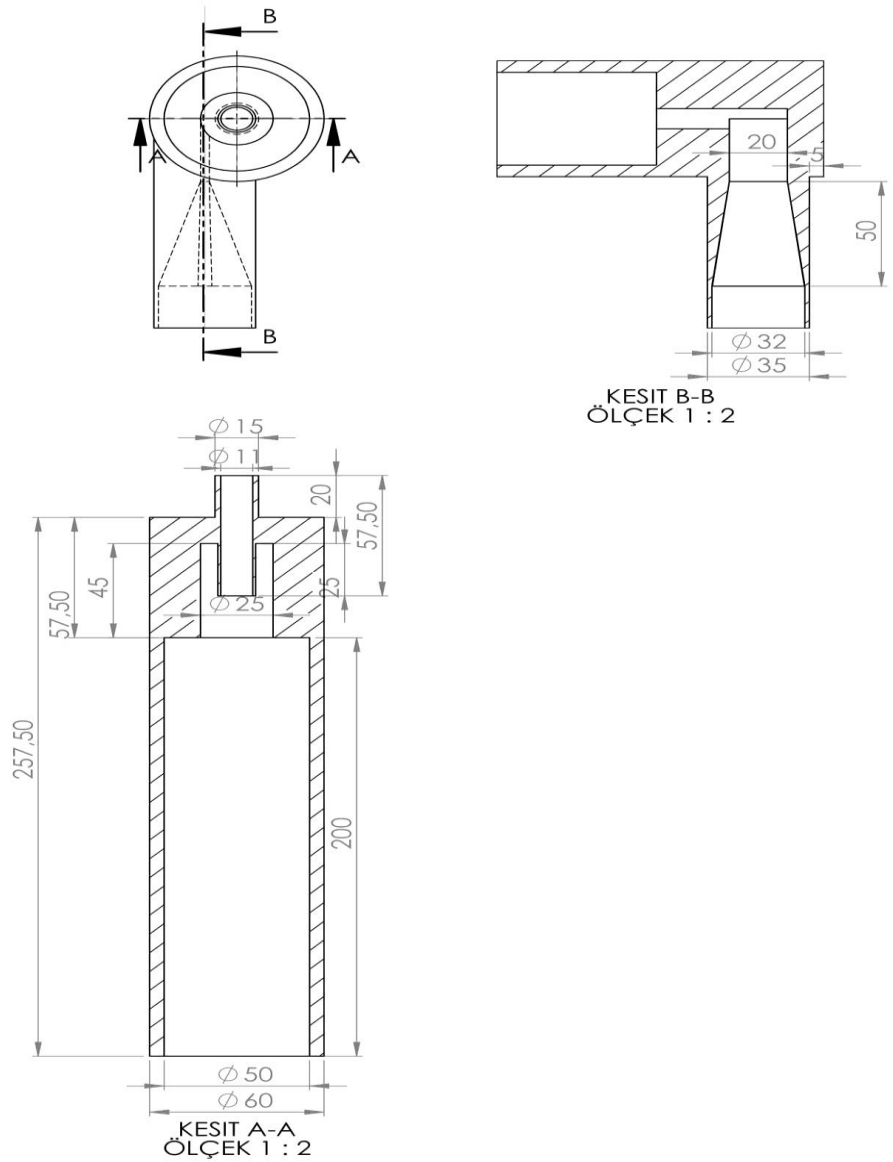
Figure 3.14. Sketch the dimension of cyclone used in the numerical solution.

3.4.2 Computational mesh

The simulated cyclone has a rectangular entry, so that it has seven basic geometry parameters was sized in function of its body diameter, Dc, as shown in Figure3.6:. The inlet has a height(a), and width (b). The outlet of air is a cylinder with diameter De and a depth of S, while The outlet of particle matter has a diameter B. The high of the device is divided in H_T, corresponding to its total high, and h_c, corresponding to the cylindrical part. The cyclone design was based on a high efficiency model. So, the computational domain was generated in software Design Modeler, available on ANSYS 17.2 packages. Flow volume have been divided into a number of computational cells using Icem CFD software, as shown in Figure 3.15. The cyclone geometry and computational mesh were used in the numerical solutions the standard wall function is used in turbulence model, fine mesh structure have been used in the core region where strong gradients in the flow parameters were present. However, very fine mesh didn't need near the cyclone walls. The complex geometry of the cyclone was subdivided into simple bodies, such as cylinders divided into four parts, in order to match with the rectangle that guides the O-grid generated. By using this method, generation of well-structured meshes got simpler when software Meshing is used, also available on ANSYS 17.2packages, with exclusive elements hexahedral, so the simulation cyclone could become easier to converge, by reducing its process time and machine efforts, is favored.

The characteristic of grid mesh where measurements of experimental have been taken are given in Fig.3.15. a & b and Table 3.3., 3.4. Number of tests were performed to obtain grid independent solutions. It was noted that Total elements : 485420 cells provide sufficient grid independency for 20cm cyclone mesh and Total elements : 322020 cells provided to 10 cm cyclone height .Geometry and ICEM CFD 17.2 was used to create achieve grid independent solutions.

61

(a)   (b)
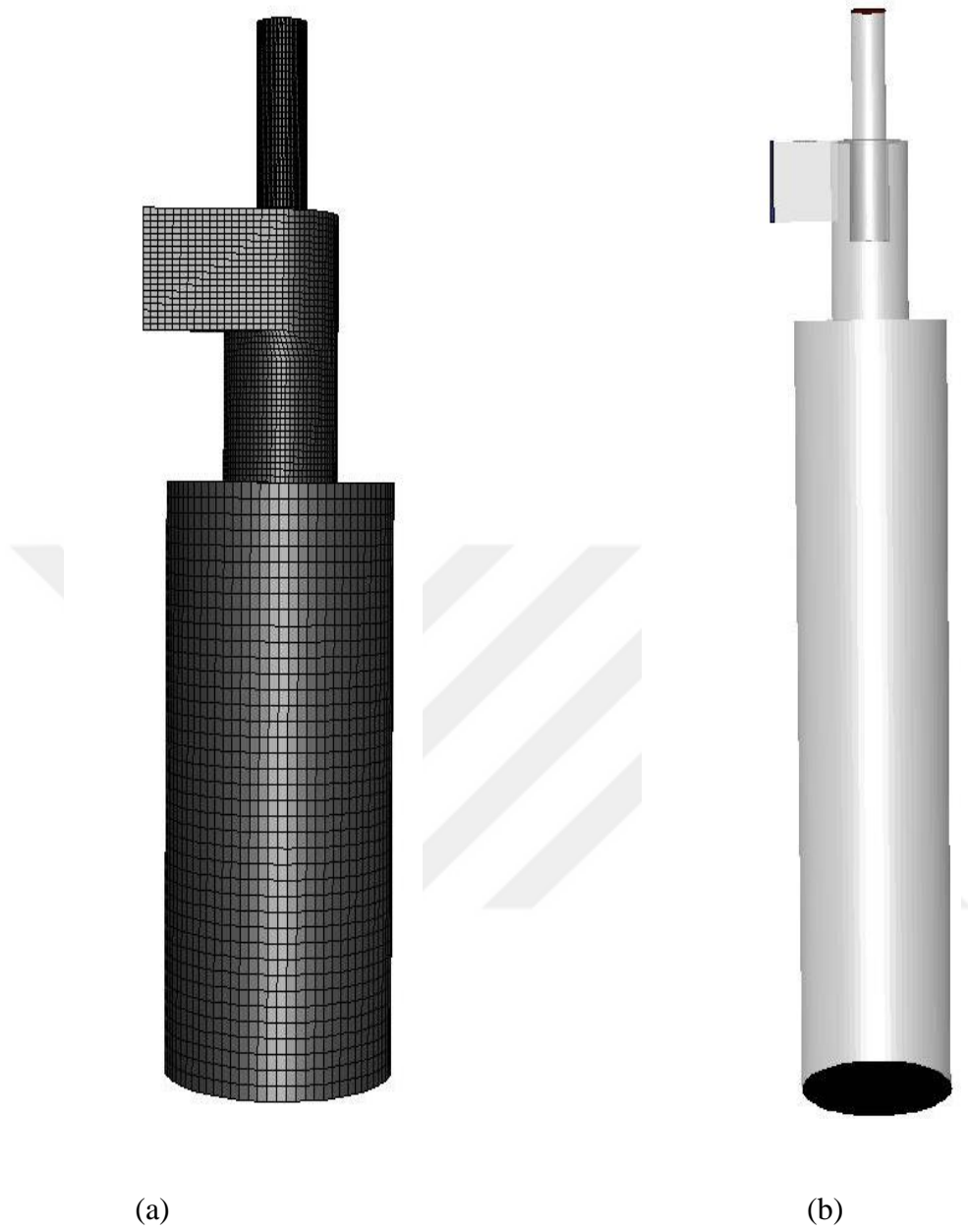
Figure 3.15. Geometry of the cyclone and computational mesh used in the numerical solution

Table 3.3 Geometry and ICEM CFD 17.2 mesh details for 20cm cyclone height.

Geometry Info Units are meters	
surfaces	17
curves	44
prescribed points	34
parts	6
Mesh Info Element types	
NODE	8
LINE_2	912
HEXA_8	460218
QUAD_4	24282
Total elements	485420
Total nodes	472568
Min	-0.0249784 0 -0.03
Max	0.0249779 0.2775 0.0249835
Blocking Info Number of blocks	
All blocks:	54
Mapped blocks	54
Element parts	
BOTTOM	1
INLET	14
OUTLET	1
Element parts	
BOTTOM	4009
FLUID	460218
INLET	441
OUTLET	1197
WALL	19555

Table 3.4. Geometry and ICEM CFD 17.2 mesh details for 10cm cyclone height.

Geometry Info Units are meters	
surfaces	17
curves	42
prescribed points	31
parts	6
Mesh Info Element types	
NODE	8
LINE_2	912
HEXA_8	299858
QUAD_4	21242
Total elements	322020
Total nodes	310648
Min	- 0.024979 0.1 -0.03
Max	0.0249783 0.2775 0.024985
Blocking Info Number of blocks	
All blocks:	54
Mapped blocks	54
Element parts	
BOTTOM	7
INLET	14
OUTLET	1
Element parts	
BOTTOM	4085
FLUID	299858
INLET	441
OUTLET	1197
WALL	16439

3.4.3 Boundary conditions

Air is supposed to enter the cyclone by regular inlet velocity. Bu assuming No slip boundary conditions have been applied at the walls of cyclone and outflow boundary condition is used at the exit as shown in Table 3.5.

Table 3.5. Summarizes the cyclone boundary conditions

Boundary conditions	Values
Air density (kg/m3)	1.225
Air viscosity	1.7894E-5
Inlet velocity (U_{in}) (m/s)	18.5,27.8,37.04,46.3,55.5,64.8
Inlet Hydraulic diameter (m)	0.005
Pressure outlet Hydraulic diameter (m)	0.011
Walls	No slip condition
Roughness height μm	100
Backflow Turbulent intensity	5
Mass flow rate Kg/s	0.00413059

3.4.4 Set up solution

At numerical part of cyclone the first step is reading the mesh by clicking on read mesh file then through solution steps the gravity of cyclone was adjusted in general set up at Z direction by -9.81, then move to model step and activate turbulent – model in case of cyclone we have really complex flow fluid so we need to use Reynolds stress model any other of Reynolds averaged Navier Stokes (RANS) turbulence model will give results which is close to reality then in Near – wall treatment , Standard Wall Function has been chosen then Linear Pressure Strain is chosen in Reynolds stress model, in model setting very important setup should be carefully identify which is Discrete Phase Models by clicking in editing new window opens then Interaction with continuous phase and update DPM source every flow iteration should be checked then min

50000000Max. number of step is set with 5 step length Factor in (Tracking) by moving to (numeric) a trapezoidal is defined for Tracking Scheme with 1e-07 tolerance and 20 Max. Refinements to make solution as simple as possible no more advance setting is added to simulate trap in cyclone bottom or reflect in wall or velocity inlet a very important setting should be created which is create (Injection) by setting injection properties starting from (Surface) in injection type then as the particles inters from inlet so (inlet) is chosen for Release from surface and (anthracite) (uniform) is defined for both Material and Diameter Distribution respectively, the precious point is to set point properties which is include Diameter of particles a different diameter of particles is sent in numerical solution inside cyclone to check the response of pressure drop and collection efficiency of the cyclone at different length starting from very small Dim (0.2,0.4,0.6,0.8,1 μm) up to (1.3.4.5.6.7.8.10.5.30,35 μm) also to verify pressure drop and efficiency numerically another essential parameter should be taken in account which is inlet velocity so different kind of velocity is adjusted in (velocity Magnitude) staring from (18.5, 27.8 ,37.04, 46.3, 55.5 and 64.8 m/s) that shows great change in results which will discuss later, to define number limitation of particles a (number of tries) is adjusted 5 for 20 cm that gives 1045 no of particles that is sent to cyclone a part of trapped particles to that is sent will be used to calculate the collection efficiency and 7 for 10cm which gives 1463 no of particles that is sent to cyclone a part of trapped particles will be used to calculate the collection efficiency also but small changed in separation efficiency has been observed with respect to the different inlet velocities this due to the limit number of particle that has been released so the limitation number of particles a (number of tries) is adjusted to 15 that is eventually shows great difference in efficiency for different velocities, which is approved good results particularly for small particles diameter. In material step don't need to change anything except air as fluid is need ,obviously some information was changed in boundary condition.

Starting from velocity inlet now as specification method for turbulence, Intensity and Hydraulic Diameter should be specified, however from test condition the inlet velocity magnitude was defined, staring from (18.5, 27.8, 37.04, 46.3, 55.5 and 64.8 m/s) then 5% and 0.005 m for turbulence intensity and Hydraulic Diameter is chosen respectively,

it has to define the Discrete Phase Model in Bc type to (reflect), since only turbulence model was used we don't have worry about any other boundary condition, pressure outlet was defined changing specification method for the turbulence Intensity and the Hydraulic Diameter so 5% and 0.011 m was applied for back turbulence intensity and back Hydraulic Diameter is defined respectively, we shouldn't forget to define the Discrete Phase Model in Bc type to (escape). In wall function setup (no slip) was set up in shear condition and keep roughness constant at 0.5 with stationary wall in wall motion with type (reflect) at Discrete Phase Model in Bc, same setup has been done for bottom except (trap) at Discrete Phase Model in Bc, is defined to ensure the that trapped particles is collected in the bottom of cyclone. Before Running calculation a (Standart Initialization) is pointed for Solution Initialization then not less 5000 number of iteration with 10 Reporting interval is adjusted for solution that will take a time depending on type of machine is used till we get a Convergent solution in that time we don't worry about reversed flow and pressure outlet message because that is exactly what we want from cyclone event sometimes after 5000 we could not find a convergent for solution that is fluctuate in several values.

3.5. Solution Algorithm.

3.5.1. Computational setup

The key to choose the perfect solution of CFD lies with the description of the turbulent behavior accuracy for a flow (Boysan, W., Griffiths D., 1996). For the turbulent flow in cyclones. There is a number of turbulence models are available in FLUENT to model, the swirling turbulent flow in the cyclone separator, These vary from the standard k-Ɛ model to the more sophisticated Reynolds stress model (RSM). The standard k Ɛ, RNG k Ɛ and Realizable k Ɛ models have not simulated for the swirling flows strongly founding cyclones (Chuah, 2006). Also Large eddy simulation(LES) available as the alternative to the Reynolds averaged Navier–Stokes approach. Reynolds stress turbulence model(RSM) require solution of the transport equations for the Reynolds stress in each components. It yield an good prediction on axial velocity, swirl flow

pattern, pressure drop, and tangential velocity in cyclone simulations (Slack, M. D. R., Prasad, O., Bakker, A., Boysan, F., 2000).

Refer to the study of (Karagoz, I., Fuat, K., 2008), RSM turbulence equations and the governing equations of the three-dimensional, incompressible flow inside the cyclone have been discretized over a computational cells and iteratively was solved using the Fluent software. Hence it is straight forward and is successfully applied in numerous CFD process ,SIMPLEC algorithm have been used for pressure velocity coupling in this study. One of the lack of SIMPLEC and SIMPLE algorithms is the new velocities and corresponding fluxes cannot satisfy the momentum equilibrium after pressure-correction equations were solved. As a result, the calculation must be repeated until the balance is satisfied.

 The PRESTO (Pressure Staggering Option) scheme using discrete continuity balance toa "staggered" control volume about the face to compute the "staggered" (i.e., face) pressure. PRESTO (Pressure Staggering Option) scheme was chosen for the pressure interpolation as it has been shown to be well convenient for the steep pressure gradients involved in the complex swirling flows This procedure is same to staggered-grid schemes that has been used with structured meshes. However for triangular, tetrahedral, hybrid, and polyhedral meshes, comparable accuracy was given by using the same algorithm. The PRESTO! scheme is available for all meshes. Quick was chosen to momentum, Second order upwind differencing discretization scheme have been applied for turbulent kinetic energy, Second order upwind differencing discretization scheme was chosen for turbulent dissipation rate and the first order upwind scheme was chosen for turbulence stresses, and 0.0001 s was defined as time step. However For more advance setting monitor was set to give pressure and static pressure graphic this by integral in Report type at inlet velocity was specified this will help to investigate the stability of ideal solution that will be chosen beside residual lines which is include (velocity pressure).

3.5.2. Discrete phase models & boundary conditions setup

The three-dimensional Governing equations of incompressible flow in the cyclone and RSM turbulence equations have been applied over the computational cells and solved iteratively by using the Fluent software 17.2Pakcage . Since it is straight forward relatively and was successfully applied in numerous CFD procedures, the Table 3.6,3.7., show boundary conditions of CFD setup

Table 3.6. Summarizes the discrete Phase Models & boundary conditions setup

Boundary Condition Type	Continuity and Momentum Equation	Discrete Phase Model
Inlet	Inlet velocity /hydraulic diameter /turbulent intensity	Reflect
Outflow	Outlet condition	Escape
Wall	No sliding	Reflect
Bottom (Dustbin)	No sliding	Trap

Table 3.7. Summarizes the discrete Phase Models & boundary conditions values

Properties	value
Air viscosity	**1.7894E-5**
Inlet velocity (U_{in}) (m/s)	18.5,27.8,37.04,46.3,55.5,64.8
Inlet Hydraulic diameter (m)	0.005
Pressure outlet Hydraulic diameter (m)	0.011
Walls	No slip condition
Roughness height μm	100
Backflow Turbulent intensity	5

Table 3.8. Summarizes the discrete Phase Models

Max No of step	50000000	Injection type	surface
Step Length Factor	5	Diameter distribution	uniform
Numeric	Trapezoidal	Diameter	0.2 μm to 35 μm
Pressure outlet Hydraulic diameter (m)	0.011	Inlet velocity magnitude	18.5m/s to 64.8m/s

Different type of solution method was applied to get best result in efficiency and analysis due to the flow complexity in the cyclone and the high precision of solution the Analysis wasn't completed in one step so the solution is reached by repeating and first (presto) solution algorithms is accurate solution then velocity and pressure fields at input.

Table 3.9 Use of different Algorithm Solutions

Properties	1. Analaysis RSM	2. Analaysis k- w	Analaysis RSM	Analaysis RSM
Pressure	Presto	Second order	Presto 3.	Presto 1.
Momentum	Quick	Second order	Quick	Quick
Turbulent kinetic energy	Second order	Second order	First Order	Second order
Turbulent dissipation rate	Second order	Second order	First Order	Second order
Reynolds stresses	First order	Second order	First Order	First order

3.5.3. Particle-wall interaction

The collected particles are allowed to exit out underflow pipe however the gas phase return its axial direction flow and exits out through the finder vortex. The flow enters near the cyclone top through tangential inlet, which gives rise to axially spiral downward of the gas and the centrifugal force field that let the incoming particles to spiral down, and collect along, the inner walls of the cyclone separator. Let's start by considering a simple swirling flow of the annular fluid element for differential thickness, change with time is Set in its moment-of-momentum, $\partial/\partial t$ ($mv\theta r$), equal to the sum of moments of a forces acting on it, can be called the shear forces on the inside and outside of the element.
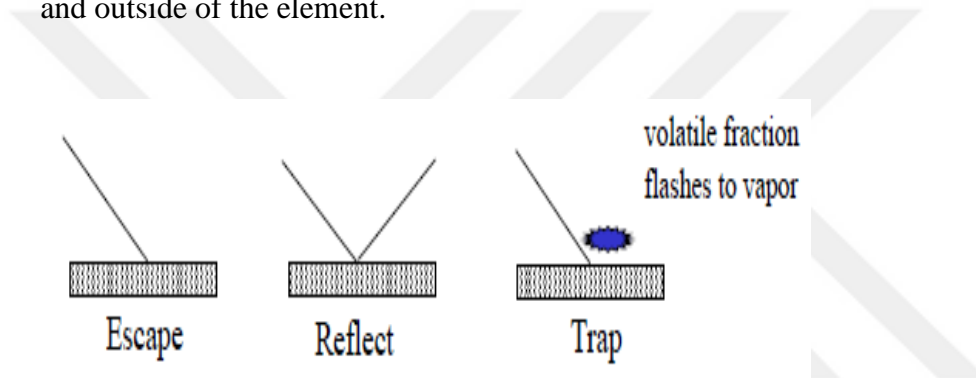
Figure 3.16. Particle-wall interactions used for boundary conditions is given in (Swanson, April 2009)

As shown in Figure 3.16. in the "Reflective" boundary condition, the particle come to wall with Θ1 angle continue to reflect on the wall with angle Θ2. We noticed the wall friction effect of on the rotating fluid is viewed in this way: the frictional force moment could be seen as a moment-of-momentum flow in the fluid, just shear force can be treated as the flow of momentum in Cartesian coordinates. The tangential and normal velocity of the particle impact velocity of the normal and tangential components of the particle reflection rate Particle-wall interactions can be used for boundary conditions for wall we set as no sliding and reflect and for Discrete Phase Model at inlet governing the condition by escape then for Outlet condition Discrete Phase Model has set by escape to let particle escape out of cyclone finally setting trap for the bottom of cyclone trap is bordered, the particle is trapped by the bumpy wall Digressing for a moment.

4. RESULT AND DISCUSSION

The flow field characteristic was studied in the cyclones and the effect of varying cyclone length and inlet velocity are observed so result has been done by define the height of cyclone from 10 cm to 20 cm, inlet velocity 18.5, 27.8, 37.04 , 46.3 , 55.5 and 64.8 m/s and 0.004131 Kg/s of has been added as mass flow rate. Analyses of results and CFD predictions shown that an increase in cyclone length lead to decrease of cyclone efficiency and pressure drop in addition to the tangential velocity decreases with increasing cyclone height which is responsible for the lower separation efficiency observed in long cyclones. Tangential velocity profiles, cut-off diameter, pressure losses and cyclone efficiency are investigated under the influence of different length height of a cyclone separator. It is observed that different geometries, also different inlet velocities, roughness and different particle diameter could effect on the pressure drop and fractional separation efficiency in addition to cut-of diameter and tangential velocity . Collection efficiency and flow patterns obtained numerically were compared with the experimental data and reasonable agreement was observed. Four cyclone of different height were simulated using Reynolds Stress Model (RSM) to investigate the effect of the cyclone height on the performance of cyclone. The following results have been reported.

4.1. Cyclone Collection Efficiency

The efficiency is the measure the capacity of cyclone to collect the particles and its define as fraction of the particles for a given size that is retained in the cyclone (John Dirgo & David Leith, 1985).

4.1.1. Efficiency investigated by CFD

The following table shows the effect of different inlet velocity and particles diameter over cyclone efficiency for 10 cm cyclone length.

Table 4.1. Separation efficiency value for 18.5 & 27.8 inlet velocity and particles diameter over cyclone efficiency for 10 cm cyclone length.

Particles diameter	No of track	18.5			27.8		
		Trapped	Efficiency	Escaped	Trapped	Efficiency	Escaped
0.2	3135	994	31.70654	2141	1097	34.99203	2038
0.4	3135	964	30.7496	2171	986	31.45136	2149
0.6	3135	1198	38.21372	1937	1289	41.11643	1846
0.8	3135	1382	44.08293	1753	1468	46.82616	1667
1	3135	1491	47.55981	1644	1526	48.67624	1609
3	3135	1535	48.96332	1600	2267	72.3126	868
4	3135	2487	79.33014	648	2746	87.59171	389
5	3135	2894	92.3126	241	3018	96.26794	117
6	3135	2969	94.70494	166	3128	99.77671	7
7	3135	3083	98.34131	52	3118	100	17
8	3135	3135	100	0	3135	100	0
9	3135	3135	100	0	3135	100	0
10	3135	3135	100	0	3135	100	0
15	3135	3135	100	0	3135	100	0
20	3135	3135	100	0	3135	100	0
25	3135	3135	100	0	3135	100	0
30	3135	3135	100	0	3135	100	0
35	3135	3135	100	0	3135	100	0
			78.10916			**81.05618**	

Table 4.2. Separation efficiency value for 37.04 & 46.3 inlet velocity and particles diameter over cyclone efficiency for 10 cm cyclone length.

Particles diameter	No of track		37.04 m/s			46.3 m/s		
		Trapped	Efficiency	Escaped	Trapped	Efficiency	Escaped	
0.2	3135	1148	36.61882	1987	1241	39.58533	1894	
0.4	3135	1059	33.7799	2076	1193	38.05423	1942	
0.6	3135	1462	46.63477	1673	1556	49.63317	1579	
0.8	3135	1527	48.70813	1608	2079	66.31579	1056	
1	3135	2168	69.1547	967	2493	79.52153	642	
3	3135	2572	82.04147	563	2768	88.29346	367	
4	3135	2869	91.51515	266	2967	94.64115	168	
5	3135	3089	98.5327	46	3120	99.52153	15	
6	3135	3130	99.84051	5	3132	99.90431	3	
7	3135	3135	100	0	3131	100	4	
8	3135	3135	100	0	3135	100	0	
9	3135	3135	100	0	3135	100	0	
10	3135	3135	100	0	3135	100	0	
15	3135	3135	100	0	3135	100	0	
20	3135	3135	100	0	3135	100	0	
25	3135	3135	100	0	3135	100	0	
30	3135	3135	100	0	3135	100	0	
35	3135	3135	100	0	3135	100	0	
			83.71256			**86.41503**		

Table 4.3. Separation efficiency value for 55.5 & 64.8 inlet velocity and particles diameter over cyclone efficiency for 10 cm cyclone length.

Particles diameter	No of track	55.5 m/s			64.8 m/s		
		Trapped	Efficiency	Escaped	Trapped	Efficiency	Escaped
0.2	3135	1462	46.63477	1673	1538	49.05901	1597
0.4	3135	1358	43.31738	1777	1841	58.72408	1294
0.6	3135	1784	56.9059	1351	2186	69.72887	949
0.8	3135	2189	69.82456	946	2684	85.61404	451
1	3135	2764	88.16587	371	2867	91.45136	268
3	3135	2937	93.68421	198	3028	96.58692	107
4	3135	3057	97.51196	78	3098	98.81978	37
5	3135	3131	99.87241	4	3135	100	0
6	3135	3134	100	1	3135	100	0
7	3135	3135	100	0	3135	100	0
8	3135	3135	100	0	3135	100	0
9	3135	3135	100	0	3135	100	0
10	3135	3135	100	0	3135	100	0
15	3135	3135	100	0	3135	100	0
20	3135	3135	100	0	3135	100	0
25	3135	3135	100	0	3135	100	0
30	3135	3135	100	0	3135	100	0
35	3135	3135	100	0	3135	100	0
			88.66206			**91.66578**	

According to the inlet velocity affects, radial distance traveled by the rebounded particles .Accelerating the inlet velocity build up the centrifugal forces that act on small particles and increases their separation efficiency as it has been shown in Figure 4.1. and Figure 4.2. below which illustrated the variation efficiency of 10cm and 20cm cyclone length according to the different particles diameter and inlet velocity.
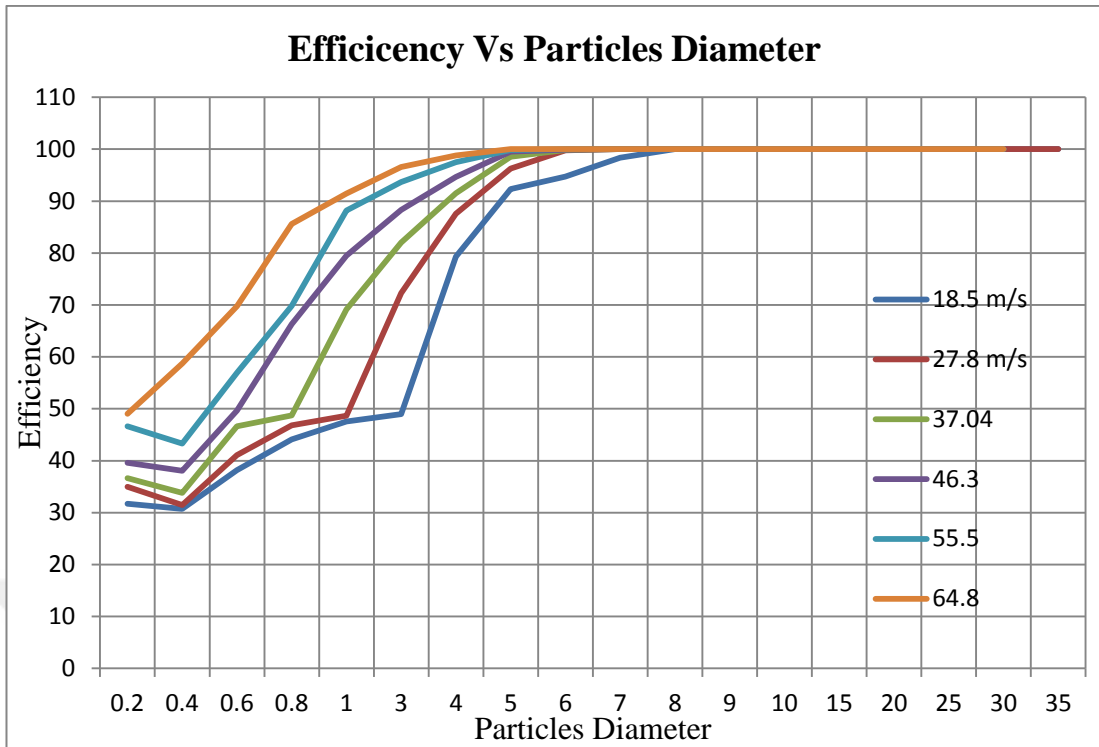
Figure 4.1. Variation of separation efficiency based on particles diameter and inlet velocity for 10cm cyclone length.
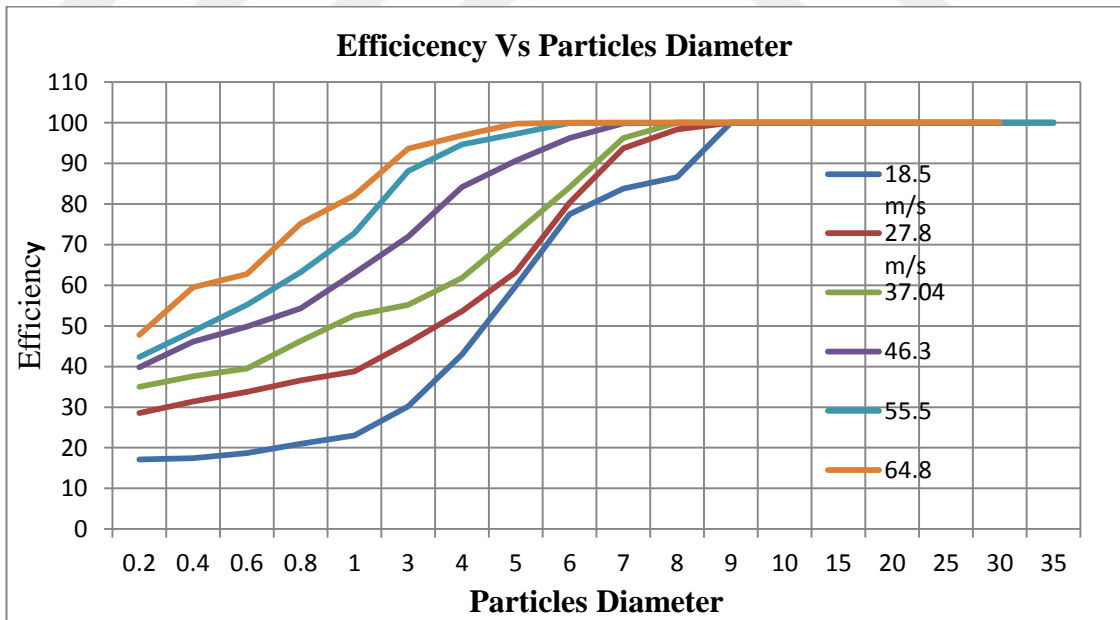
Figure 4.2. Variation of separation efficiency based on particles diameter and inlet velocity for 20cm cyclone length.

Because of lower inlet velocity, the rebounded particles has less kinetic energy. Therefore, radial distance move by given rebounded particle is shorter than the width of downward gas flow. Accordingly, the particles travel towards the wall again as result of centrifugal force. The energy loss due to the collision decreases the velocity particle. In the next rebound process, the radial distance of particles will shorten. Thus, particles that didn't escape from the cyclone after first collision is barely rebound into the upward gas flow in the following motion and will be completely captured (Yang, J., Sun, G., Zhanb, M., 2015). Instead, at the higher inlet velocity obtains rebounded particles and more kinetic energy. As a result of, the radial distance travelled by a rebounded particle is longer than the width of the downward gas flow. Finally, rebounded particles move back into upward gas flow. Within the fast upward gas flow, the particles will move towards the vortex finder instantaneously with little separation. Hence, the particles rebounded out of downward gas flow escape from the cyclone separator and not be captured so that why some times trapped particles reported as incomplete in CFD result.

It has been clearly shown that from Table 4.1., of 10 cm cyclone height the significant effect of the inlet velocity on cyclone efficiency when the inlet velocity increase eventually cyclone collection efficiency increase starting from 18.5 m/s minimum inlet velocity the value of average cyclone efficiency (78.10916) has been found up to maximum inlet velocity 64.8m/s which shows highest value of cyclone average efficiency (91.66578). On the other hand less efficiency can be seen in Figure 4.2., for 20cm cyclone length with same inlet velocity 18 m/s and 64.8 m/s that generate (65.45277) and (89.2823) minimum and maximum Average efficiency respectively.

The effect of cyclone length its properly achieved and investigated also in four different cyclone length staring from 6cm, 10, 15 and 20cm so it's obviously shows that increase the cyclone length lead to decrease of cyclone collection efficiency as shown in Table 4.4. , 4.5., 4.6., and Figure 4.3. below.

Table 4.4. Separation efficiency value for 6cm cyclone length and particles diameter over cyclone efficiency at constant inlet velocity.

Particles diameter	Governing Equation for 6 cm cyclone length and inlet velocity 18 m/s			
	No of track	Trapped	Efficiency	Escaped
0.03	3135	1127	35.94896	2008
0.05	3135	1059	33.7799	2076
0.1	3135	1026	32.72727	2109
0.2	3135	1074	34.25837	2061
0.4	3135	1026	32.72727	2109
0.6	3135	1287	41.05263	1848
0.8	3135	1528	48.74003	1607
1	3135	1625	51.83413	1510
3	3135	1761	56.17225	1374
4	3135	2736	87.27273	399
5	3135	2983	95.15152	152
6	3135	3058	97.54386	77
7	3135	3109	99.17065	26
8	3135	3135	100	0
9	3135	3135	100	0
10	3135	3135	100	0
15	3135	3135	100	0
20	3135	3135	100	0
25	3135	3135	100	0
30	3135	3135	100	0
35	3135	3135	100	0
			75.52153	

Table 4.5. Separation efficiency value for 10 cm cyclone length and particles diameter

Particles diameter	Governing Equation for 10 cm cyclone length and 18 m/s			
	No of track	Trapped	Efficiency	Escaped
0.03	3135	1008	32.15311	2127
0.05	3135	1012	32.2807	2123
0.1	3135	967	30.8453	2168
0.2	3135	994	31.70654	2141
0.4	3135	964	30.7496	2171
0.6	3135	1198	38.21372	1937
0.8	3135	1382	44.08293	1753
1	3135	1491	47.55981	1644
3	3135	1535	48.96332	1600
4	3135	2487	79.33014	648
5	3135	2894	92.3126	241
6	3135	2969	94.70494	166
7	3135	3083	98.34131	52
8	3135	3135	100	0
9	3135	3135	100	0
10	3135	3135	100	0
15	3135	3135	100	0
20	3135	3135	100	0
25	3135	3135	100	0
30	3135	3135	100	0
35	3135	3135	100	0
			73.45455	

Table 4.6. Separation efficiency value for 15 cm cyclone length and particles diameter

Governing Equation for 15 cm cyclone length and 18 m/s				
Particles diameter	**No of track**	**Trapped**	**Efficiency**	Escaped
0.03	3135	629	20.0638	2506
0.05	3135	637	20.0638	2506
0.1	3135	618	20.31898	2498
0.2	3135	647	19.71292	2517
0.4	3135	715	20.63796	2488
0.6	3135	742	22.80702	2420
0.8	3135	784	23.66826	2393
1	3135	869	25.00797	2351
3	3135	1124	27.7193	2266
4	3135	1496	35.85327	2011
5	3135	1952	47.7193	1639
6	3135	2449	62.26475	1183
7	3135	2721	78.11802	686
8	3135	3024	86.79426	414
9	3135	3135	96.45933	111
10	3135	3135	100	0
15	3135	3135	100	0
20	3135	3135	100	0
25	3135	3135	100	0
30	3135	3135	100	0
35	3135	3135	100	0
			100	0
			61.29263	

Table 4.7. Separation efficiency value for 20 cm cyclone length and particles

Particles diameter	Governing Equation for 20 cm cyclone length and 18 cm			
	No of track	Trapped	Efficiency	Escaped
0.03	3135	580	18.5008	2555
0.05	3135	584	18.62839	2551
0.1	3135	504	16.07656	2631
0.2	3135	537	17.12919	2598
0.4	3135	546	17.41627	2589
0.6	3135	586	18.69219	2549
0.8	3135	658	20.98884	2477
1	3135	722	23.0303	2413
3	3135	946	30.17544	2189
4	3135	1348	42.99841	1787
5	3135	1876	59.84051	1259
6	3135	2429	77.48006	706
7	3135	2627	83.79585	508
8	3135	2715	86.60287	420
9	3135	3135	100	0
10	3135	3135	100	0
15	3135	3135	100	0
20	3135	3135	100	0
25	3135	3135	100	0
30	3135	3135	100	0
35	3135	3135	100	0
			58.63598	
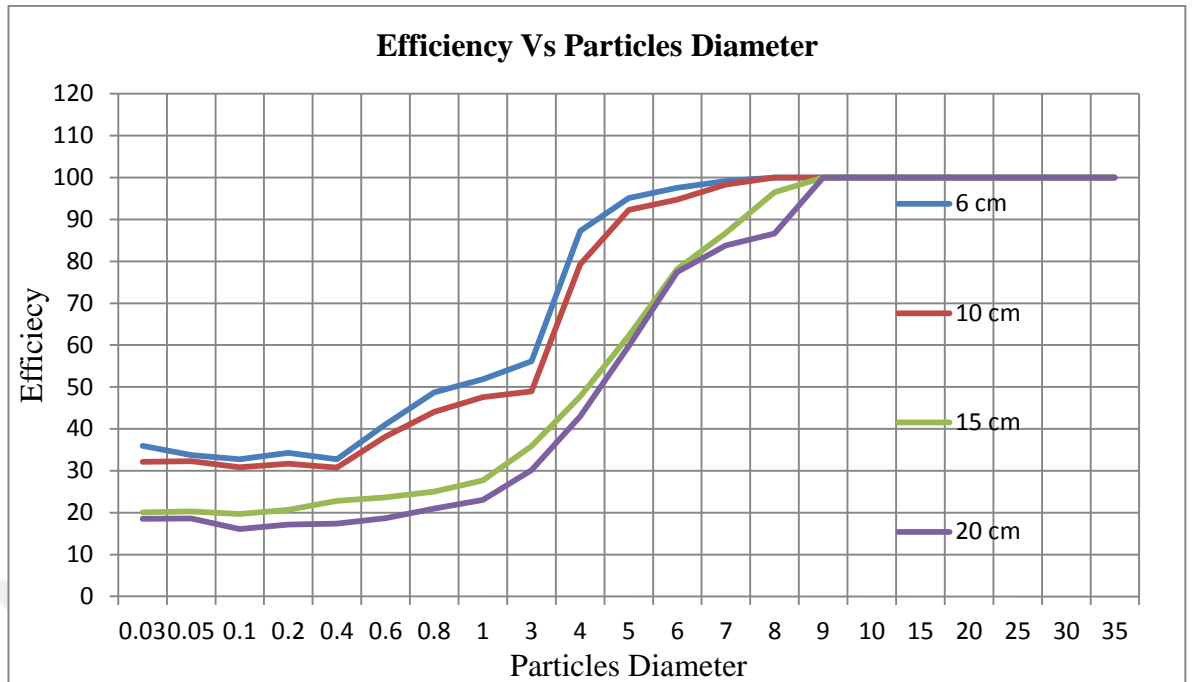
Figure 4.3. Variation of separation efficiency with different cyclone length and constant inlet velocity

In order to demonstrate the cyclone efficiency increase when the length of cyclone decrease and vice versa, (Zhu, Y., Lee, K. 1999.), Reported that, when the height of cyclone increase then less gas will migrate down to the bottom of cyclone section where it accelerate due to decreased cross-section area. Actually many flow field experiments have been reported the tangential velocity more or less independent of cyclone height (Peng, W., Hoffmann, A. C., Boot, P. J. A. J., Udding, A., Dries, H.W. A., Ekker, A., Kater, J., 2002), (Solero, G., Coghe, A. 2002.) and (Gorton, A., Woisetschl, J., Wigley, G., Staudinger, G., 2000).

Obviously the cyclone tangential velocity increase readily when cyclone height decrease from 20cm to 6 cm, however in larger centrifugal force higher tangential velocity is results so it leads to separation efficiency increment, this explain definitely why the separation efficiency increase monotonically from 20cm cyclone to 6 cm cyclone.

4.1.2. Efficiency investigated by experiment

As CDF predictions showed an increase in cyclone length lead to decrease in cyclone efficiency, pressure drop and tangential velocity. The CFD results compare with experiments results and showed good agreement between them as obtained in Table 4.8. and Table 4.9.

Table 4.8. Efficiency and static pressure of 20cm length of cyclone for 50g for

Q (m3/s)	Injected particle (g)	Trapped	Efficiency	Static pressure (pa) EXP	Static pressure by CFD (pa)
4	50	42.5	85	401	384.26
6	50	43.75	87.5	679	694.54
8	50	45.75	91.5	1065	1130.6
10	50	47.3	94.6	1690	1704.32
12	50	48	96	2615	2620.8
14	50	48.95	97.9	3370	3378.04

Table 4.9. Efficiency and static pressure of 10cm length of cyclone for 50g for 1h

Q (m3/s)	Injected particle (g)	Trapped	Efficiency	Static pressure (pa) EXP	Static pressure by CFD (pa)
4	50	46	92	469	422.651
6	50	46.7	93.4	919	942.6774
8	50	47.6	95.2	1290	1328.64
10	50	48.7	97.4	1902	1829.51
12	50	49.6	99.2	2886	2968.681
14	50	49.75	99.5	3385	3481.728

The Separation efficiency and pressure drop can be calculated for different inlet velocity, analyses of experiment results shown that the cyclone separation efficiency increase with increasing the inlet velocity and decrease with increasing cyclone height.

To find cyclone separation efficiency of particles the equation below as used.

fractional separation efficiency$= \dfrac{\eta p\ trapped}{\eta p\ injeceted}$

fractional separation efficiency for 10cm length, 18.5 m/s for 15 $(\mu m)dim = \dfrac{46}{50} = 92\%$

fractional separation efficiency for 20cm length, 18.5 m/s for 15 $(\mu m)di = \dfrac{42.5}{50} = 85\%$.

4.1.3. Fluid sample with CFD fractional separation efficiency

To evaluate the effectiveness of cyclone model, the prediction of fractional separation efficiency and pressure drop results from experiment were compared to the numerical solution with sample fractional efficiency a good consistency between the data was obtained from experimental and numerical solution as shown in tables below. For 10 cm and 18.5 m/s inlet velocity the fraction efficiency with CFD was obtained in Table 4.10.

Table 4.10. The fraction efficiency of CFD for 10 cm and 18.5 m/s inlet velocity

18.5 m/s		Roughness = 0		Roughness =100	
Particle DIM	Efficiency	Sample	Efficiency * Sample	Efficiency	Efficiency * Sample
0.2	58.92	0.4	23.568	31.4	12.56
0.4	52.565	1.93	101.4505	30.8	59.444
0.6	65.1	0.59	38.409	38.2	22.538
0.8	79.2	1.95	154.44	44.2	86.19
1	86.1	0.71	61.131	47.8	33.938
3	93.1	12.13	1129.303	49.02	594.6126
4	96.3	2.4	231.12	79.3	190.32
5	98.8	5.42	535.496	92.3	500.266
6	99.5	3	298.5	94.94	284.82
7	100	3.21	321	98.5	316.185
8	100	3.46	346	100	346
9	100	3.76	376	100	376
10	100	4.12	412	100	412
15	100	20.81	2081	100	2081
20	100	6.05	605	100	605
25	100	11.87	1187	100	1187
30	100	5.81	581	100	581
35	100	15.68	1568	100	1568
		103.3	10050.42	78.13667	9256.874
			97.29349		89.61155
			CFD Efficiency without roughness	CFD Efficiency for 100 roughness	Experimental efficiency
			97.29349	**89.11097**	**92**

From the previous table its clearly shows that the efficiency value obtained from experiment is (92) close the value given by CFD (89.11097) this difference result due to the particles average diameter has been used in experiment, in contract a define particle diameter was injected to the cyclone but for higher inlet velocity the difference between two values get close to each other as can be shown in the following Tables 4.11, 4.12, 4.13., of different inlet velocity for 10 cm and 20 cm cyclone length .

Table 4.11. The fraction efficiency of CFD for 10 cm and 27.8 m/s

Inlet Velocity = 27.04 m/s, Roughness =100			
Particle DIM	**Efficiency**	**Sample**	**Efficiency * Sample**
0.2	0.4	34.99	13.996
0.4	1.93	31.5	60.795
0.6	0.59	41.112	24.25608
0.8	1.95	46.83	91.3185
1	0.71	48.7	34.577
3	12.13	72.3	876.999
4	2.4	87.6	210.24
5	5.42	96.3	521.946
6	3	99.77	299.31
7	3.21	100	321
8	3.46	100	346
9	3.76	100	376
10	4.12	100	412
15	20.81	100	2081
20	6.05	100	605
25	11.87	100	1187
30	5.81	100	581
35	15.68	100	1568
	103.3		9610.438
			93.03425
	CFD efficiency for 100 roughness		**Experimental** efficiency
	93.03425		**93.4**

Table 4.12. The fraction efficiency of CFD for 10 cm and 37.8 m/s

Inlet velocity = 37.04 m/s, Roughness =100			
Particle DIM	**Efficiency**	**Sample**	**Efficiency *Sample**
0.2	0.4	36.62	65.234
0.4	1.93	33.8	27.494
0.6	0.59	46.6	95.1795
0.8	1.95	48.81	49.132
1	0.71	69.2	995.1452
3	12.13	82.04	219.648
4	2.4	91.52	534.0326
5	5.42	98.53	299.4
6	3	99.8	321
7	3.21	100	346
8	3.46	100	376
9	3.76	100	412
10	4.12	100	2081
15	20.81	100	605
20	6.05	100	1187
25	11.87	100	581
30	5.81	100	1568
35	15.68	100	9776.913
			94.64582
CFD efficiency for 100 roughness			**Experimental efficiency**
	94.64582		**95.2**

Table 4.13. The fraction efficiency of CFD for 10 cm and 46.3 m/s

Inlet velocity = 46.3 m/s, Roughness =100			
Particle DIM	**Efficiency**	**Sample**	**Efficiency * Sample**
0.2	0.4	39.6	15.84
0.4	1.93	38.1	73.533
0.6	0.59	49.6	29.264
0.8	1.95	66.3	129.285
1	0.71	79.5	56.445
3	12.13	88.3	1071.079
4	2.4	94.64	227.136
5	5.42	99.52	539.3984
6	3	99.9	299.7
7	3.21	100	321
8	3.46	100	346
9	3.76	100	376
10	4.12	100	412
15	20.81	100	2081
20	6.05	100	605
25	11.87	100	1187
30	5.81	100	581
35	15.68	100	1568
			9918.68
			96.0182
CFD Efficiency with 100 roughness			Experimental efficiency
		96.0182	97.4

Table 4.14. The fraction efficiency of CFD for 10 cm and 55.5 m/s

Inlet velocity = **55.5 m/s,** Roughness = 100			
Particle DIM	**Efficiency**	**Sample**	**Efficiency * Sample**
0.2	0.4	46.64	18.656
0.4	1.93	43.3	83.569
0.6	0.59	56.91	33.5769
0.8	1.95	69.83	136.1685
1	0.71	88.2	62.622
3	12.13	93.7	1136.581
4	2.4	97.5	234
5	5.42	99.9	541.458
6	3	100	300
7	3.21	100	321
8	3.46	100	346
9	3.76	100	376
10	4.12	100	412
15	20.81	100	2081
20	6.05	100	605
25	11.87	100	1187
30	5.81	100	581
35	15.68	100	1568
	103.3		10023.63
			97.03419
CFD Efficiency for 100 roughness			Experimental efficiency
97.0342			**99.2**

Table 4.15. The fraction efficiency of CFD for 10 cm and 64.8 m/s

Particle DIM	Efficiency	Sample	Efficiency * Sample
Inlet velocity = 64.8 m/s **,** Roughness = 100			
0.2	0.4	49.1	19.64
0.4	1.93	58.7	113.291
0.6	0.59	69.72	41.1348
0.8	1.95	85.6	166.92
1	0.71	91.5	64.965
3	12.13	96.6	1171.758
4	2.4	98.82	237.168
5	5.42	100	542
6	3	100	300
7	3.21	100	321
8	3.46	100	346
9	3.76	100	376
10	4.12	100	412
15	20.81	100	2081
20	6.05	100	605
25	11.87	100	1187
30	5.81	100	581
35	15.68	100	1568
	103.3		10133.88
			98.10142
CFD efficiency with 100 roughness			**Experimental efficiency**
98.10142			99.5

As it mentioned above the fractional separation efficiency were carried out numerically and then compared with experiment, good agreement between the data was obtained from experimental and numerical solution as shown in previous tables for 10 cm

cyclone height. The same solution was done for 20 cm cyclone height to evaluate the working fluid sample fraction efficiency as can be shown in Table 4. 16..

Table 4.16. The fraction efficiency of CFD for 20 cm and different inlet velocity

Inlet velocity	CFD Efficiency with 100 roughness	Experimental efficiency	CFD efficiency without roughness
18.5	84.04021	85	95.00441
27.8	86.269	87.5	96.1825
37.04	90.583	91.5	97.514
46.3	93.096	94.6	98.3624
55.5	96.02889	96	99.24467
64.8	97.41758	97.9	99.54

As shown in above Table 4.16., the fractional separation efficiency were investigate numerically for different inlet velocity and then compared to the experimental efficiency, a perfect agreement between the results found from experimental and numerical solution as shown in previous tables for 20 cm cyclone height.

4.1.4. Cyclone average efficiency in different length

To understand the effect of change cyclone height on separation depending on the flow field details obtained from the Figure 4.4., below show that the average separation efficiency increase with inlet velocity and decrease with length of cyclone.
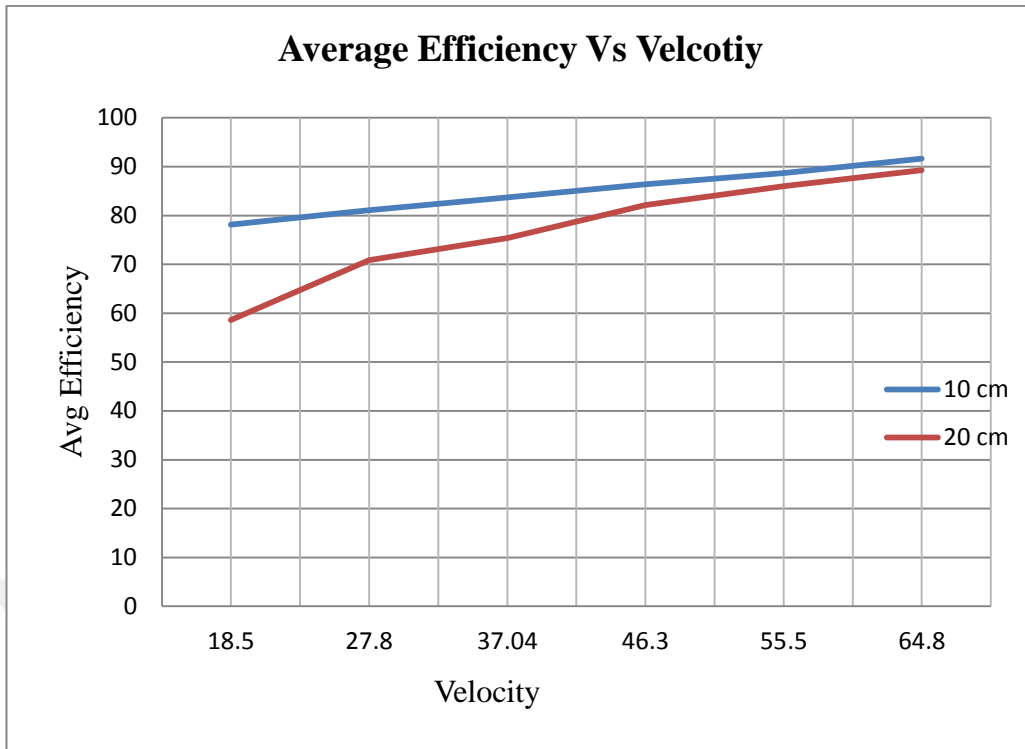
Figure 4.4. The effect of cyclone height on cyclone average efficiency

4.1.5. The effect of particles diameter on separation efficiency

Depending on many theoretical research that reported effect of the particles diameter on separation efficiency, due to the particles diameter increase eventually the separation efficiency increase as it has been shown in Figure 4.5 and Figure 4.6., its favorable for separation cyclone to work with large particles that could be normally separated, the fluid in the output contains only a particles smaller than critical diameter. It can be noticed from chart of efficiency and inlet velocity for 0.2, 1, 5 um that inclination of efficiency is become smaller and smaller with larger particles diameter till the defined large particle that all the efficiency is 100% despite the inlet velocity difference.
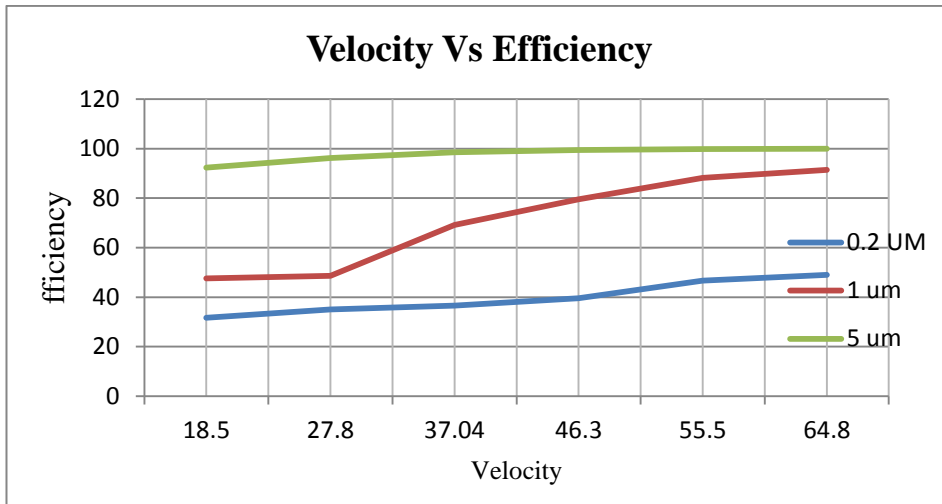
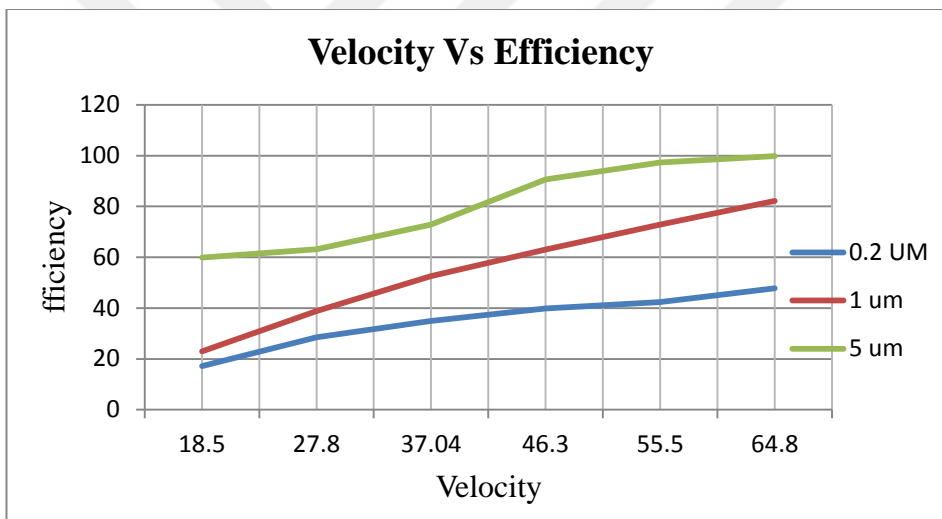**Figure 4.5.** The effect of cyclone height on cyclone average efficiency for 10 cm

Figure 4.6. The effect of cyclone height on cyclone average efficiency for 20 cm

4.2. Cut-off Diameter

In cyclone, the definition of cut diameter is a diameter of the particle for which efficiency curve has the value of 50%. The Cut-off diameter id the important factor for estimating dust performance in the cyclone separator. The smaller cut-off diameter in a cyclone separator, yields better dust performance. As shown in Figure 4.1. and Figure 4.2., an inverse relation between cut-off diameter and inlet velocity cyclone when the

inlet velocity increase cut off diameter decrease eventually, a decrease in the total efficiency and increase in cut-off diameter, respectively were carried out with increase in cyclone length, in 10cm cyclone length the cut off diameter range between 3, 4 um with (48.96 and 79.33) efficiency respectively, however in 20cm cyclone length the cut off diameter range between 4, 5 um with (42.998 and 59.84) efficiency respectively.

4.3. Pressure Drop

The definition of pressure drop through the cyclone is the difference between average static pressure values at inlet and outlet, and is related directly to the energy needed to run the cyclone unit (Lakhbir, S.B., Sharma, R.P., Elsayed, K., 2015). Table 4.8. & Table 4.9., indicates the relation of the pressure drop against the cyclone length increasing for a different inlet velocity. The pressure drop decrease non-linearly with increase the cyclone length and also with inlet velocity reduction as can be seen from Figure 4.7, below illustrates The effect of cyclone height on pressure drop for 10cm and 20 cm carried out by CFD.
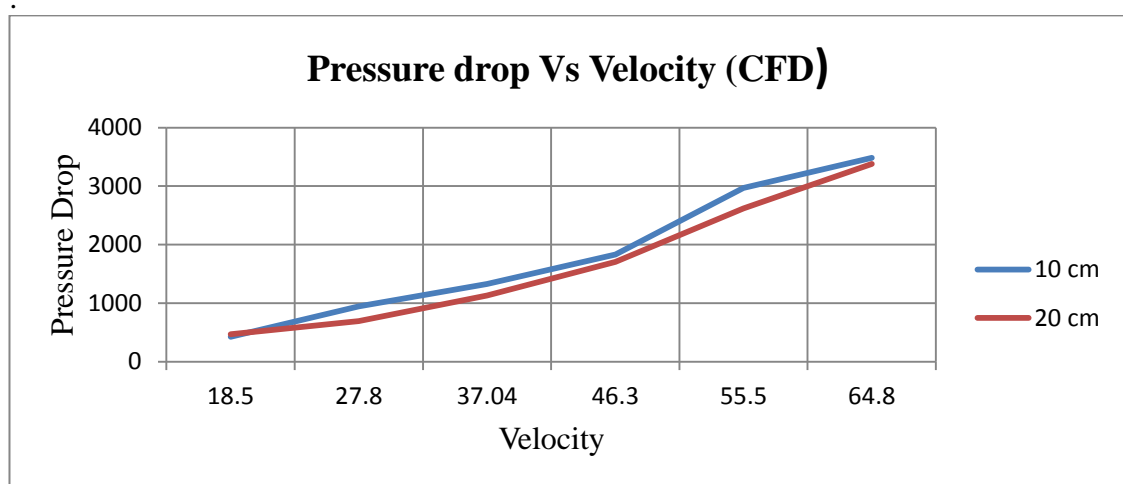
.

Figure 4.7. The effect of cyclone height on pressure drop for 10cm and 20 cm
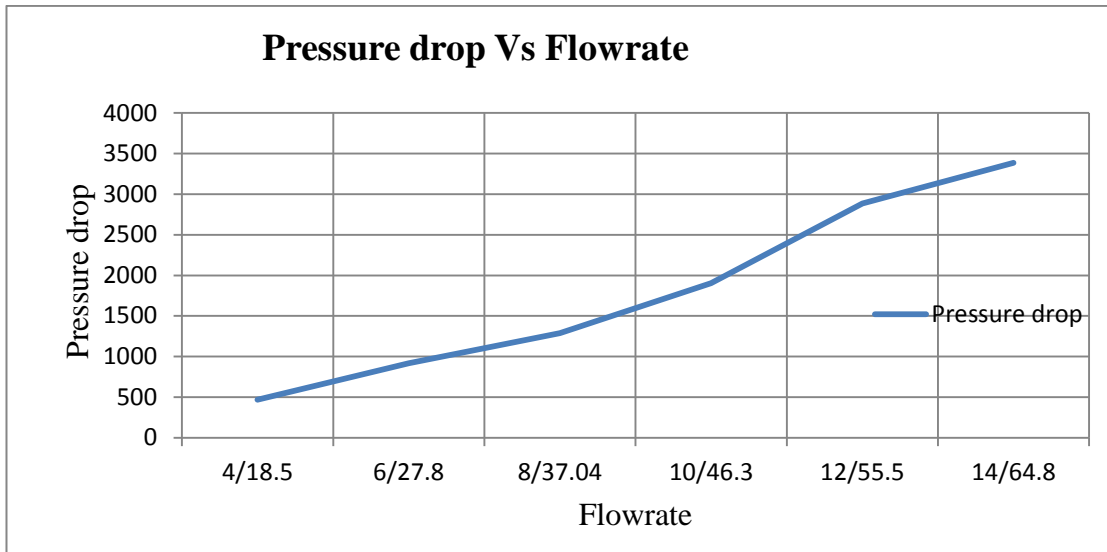
Figure 4.8. The effect of cyclone height on pressure drop for 10cm investigated by experiment

 Figure 4.9. The effect of cyclone height on pressure drop for 20cm investigated by experiment

Slope of the curve increase with inlet velocity and tend to be flat at lower inlet velocity values, which indicates at higher inlet velocity, pressure drop becomes more sensitive to the cyclone length, Figure 4.8 and Figure 4.9. shows the effect of cyclone inlet velocity to the pressure drop was carried out by cyclone model experiment.

95

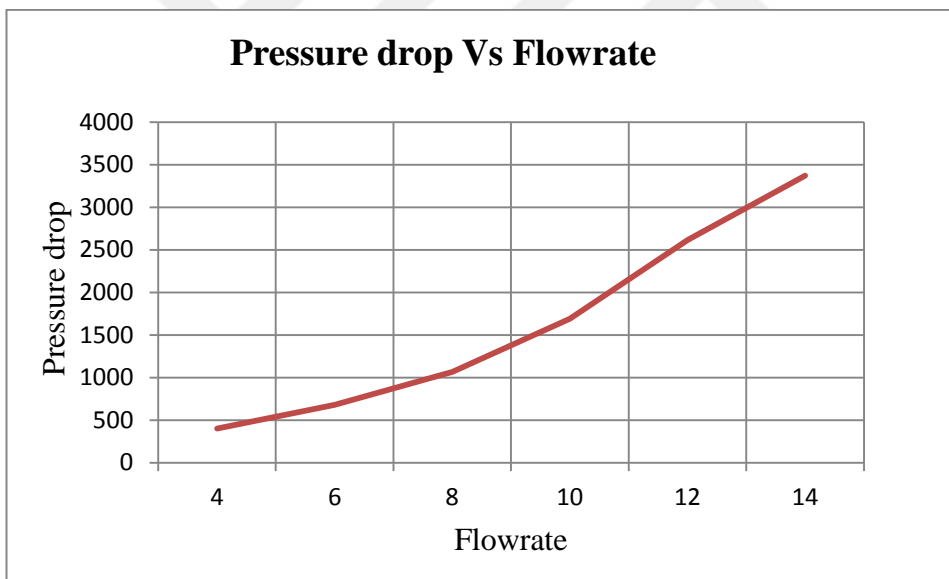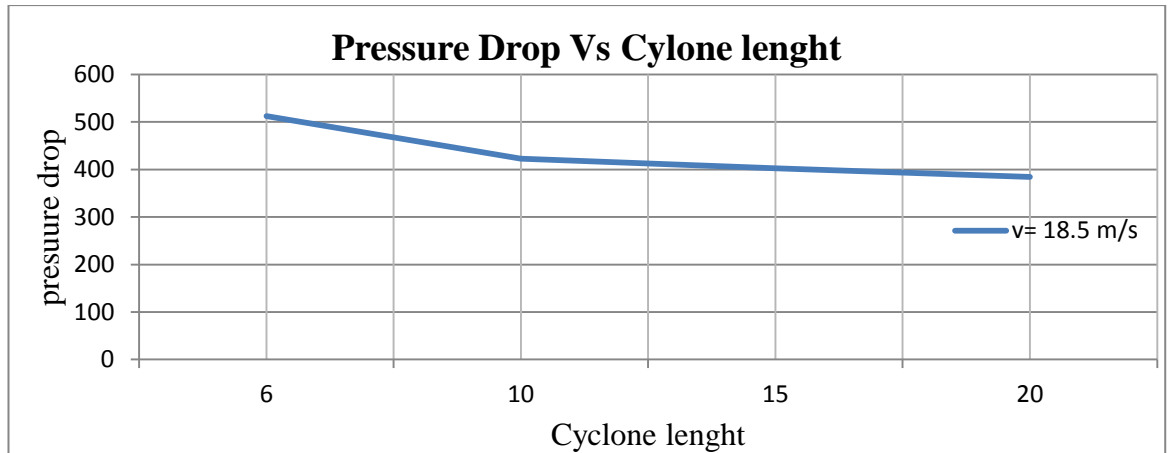**Figure 4.10.** The effect of different cyclone height on pressure drop at 18.5m/s investigated by CFD

Depending on the Slope of the curve at Figure 4.10, shows decrease of pressure drop with increase of cyclone height, pressure drop becomes more sensitive to the length of cyclone.

4.3. Roughness

The effect of cyclone wall roughness in has not been studied extensively so little articles and researches investigate the wall roughness act on cyclone performance (Kaya, F., Karagoz, I., Avci, A.2011), they carried out the effects of surface roughness on the flow field and cyclone performance. The result shows that the relative roughness increase due to wear, corrosion or accumulation of particles on the inner walls considerably effect the tangential velocity, the cyclone separation efficiency and pressure drop in cyclone especially for high inlet velocities. Decreasing the collection efficiency of the cyclone and pressure drop with the surface roughness increasing are found to be clearly for high values of relative roughness.

 The effect of wall roughness was carried out by CFD for different wall roughness 0, 30. And 100 um the result shows that an increase of roughness value lead to decrease the pressure drop and cyclone efficiency respectively as can be shown on Figure 4.11.
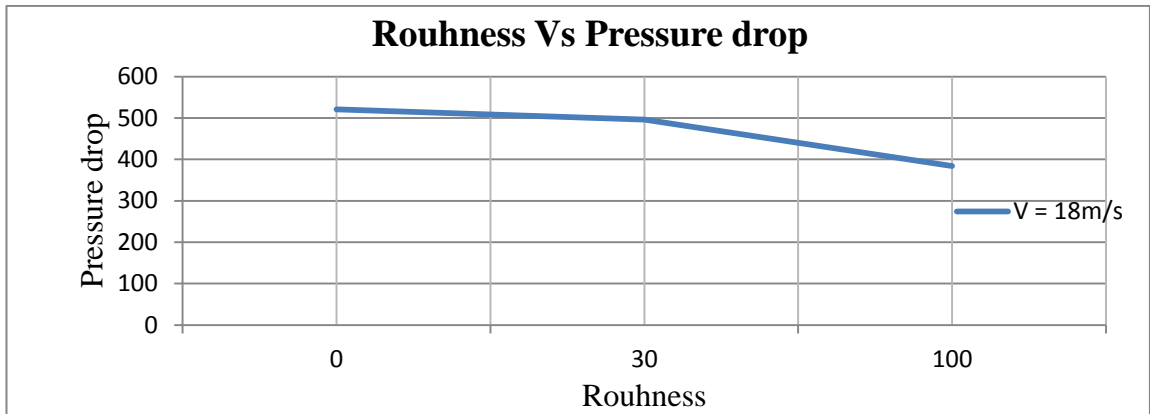
Figure 4.11. The effect of different roughness on pressure drop at 18.5m/s investigated by CFD

To set up the roughness effects of wall, they are two mainly roughness parameters: the Roughness Height (K_S), and the Roughness Constant (C_{K_S}) are specified in wall set up. The default roughness height (K_S) is zero, that corresponds to the smooth walls value . to carry out the effect of roughness, a non-zero value for K_S must be specified. As shown in following Table 4.17.

Table 4.17. The effect of roughness on separation efficiency by CFD for 20 cm and constant inlet velocity (18.5)

Particle DIM	Sample	Roughness=0 Efficiency	Roughness=0 Sample *Efficiency	Roughness =100 Efficiency	Roughness =100 Sample *Efficiency	Roughness =30 Efficiency	Roughness =30 Sample *Efficiency
0.2	0.4	48.7	19.48	17.1	6.84	37.8	15.12
0.4	1.93	36.6	70.638	17.4	33.582	39.77	76.7561
0.6	0.59	54.99	32.4441	18.7	11.033	48.07	28.3613
0.8	1.95	64.3	125.385	20.9	40.755	58.979	115.00905
1	0.71	80.03	56.8213	27.6	19.596	66.92	47.5132
3	12.13	85.5	1037.1115	39.6	480.348	79.55	964.9415
4	2.4	89.02	213.648	46.7	112.08	82.1	197.04
5	5.42	92.2	499.724	59.84	324.3328	85.5	463.41
6	3	96.6	289.8	77.48	232.44	91.73	275.19
7	3.21	98.37	315.7677	89.12	286.0752	95.15	305.4315
8	3.46	99.36	343.7856	93.72	324.2712	100	346
9	3.76	99.87	375.5112	100	376	100	376
10	4.12	99.96	411.8352	100	412	100	412
15	20.81	100	2081	100	2081	100	2081
20	6.05	100	605	100	605	100	605
25	11.87	100	1187	100	1187	100	1187
30	5.81	100	581	100	581	100	581
35	15.68	100	1568	100	1568	100	1568
	103.3		9813.955		8681.3532		9644.7727
		95.00441		84.0402052		93.366628	
	Experimental efficiency	**CFD efficiency of 100 roughness**		**CFD efficiency of 30 roughness**		**CFD efficiency without roughness**	
	85	**84.04021**		**93.36663**		**95.00441**	

98

Choosing a proper roughness constant (C_{K_S}) is depend mainly the type of the material that is used which has a specific roughness value. The default roughness constant (C_{K_S} is 0.5) was already determined (SAKİN, A., KARAGÖZ, I., 2014). However three wall roughness height was set up 0, 30 and 100 um to investigate the effect of roughness on cyclone separation efficiency at 18.5m/s inlet velocity as shown in Table 4.17., then compared to experimental efficiency, wall roughness with 100um has shown good agreement rather than other, for 20 cm cyclone height,18m/s inlet velocity the cyclone efficiency with roughness 100um has an efficiency 84.04021 compared to experimental efficiency 85, in contract for cyclone with 0 and 30 um has higher efficiency, the same process was carried out for other different inlet velocity as illustrated in Table 4.18 and for 10cm cyclone length in Table 4.19.

Table 4.18. The effect of roughness on separation efficiency by CFD for 20 cm with different inlet velocity

Inlet velocity	Experimental efficiency	CFD efficiency without roughness	CFD efficiency with 100 roughness
18.5	85	95.00441	84.04021
27.8	87.5	96.1825	86.269
37.04	91.5	97.514	90.583
46.3	94.6	98.3624	93.096
55.5	96	99.24467	96.02889
64.8	97.9	99.54	97.41758

Table 4.19. The effect of roughness on separation efficiency by CFD for 10 cm with different inlet velocity

Inlet velocity	Experimental efficiency	CFD efficiency without roughness	CFD efficiency with 100 roughness
18.5	92	97.293	89.612
27.8	93.4	98.18	93.03425
37.04	95.2	98.626	94.64582
46.3	97.4	98.97	96.0182
55.5	99.2	99.553	97.0342
64.8	99.5	99.665	98.10142

The numerical simulation results shows that, wall roughness has a great effect on cyclone flow field. If the wall roughness is increased, the vortex length is decreased and the tangential velocity is also reduced a lot (Cia, H., Suna, G. 2015.). This brings two-side effects on the performance of cyclone: on one side, the reduction in separation efficiency which is not preferred, on the other hand the pressure drop is reduced that is preferred, there must be a compromise condition between separation efficiency and pressure drop, For a particular cyclone under specific working load.

4.4. Tangential Velocity Profile

The effect of cyclone on the tangential velocity profile is carried out by using RSM with higher order scheme, however the tangential velocity decrease with increase cyclone height, in contract increase the inlet velocity will increase tangential velocity by (Zhu, Y., Lee, K. 1999.). this should be responsible for the lower separation efficiency observed in long cyclones as shown Figure 4.12. & Figure 4.13.
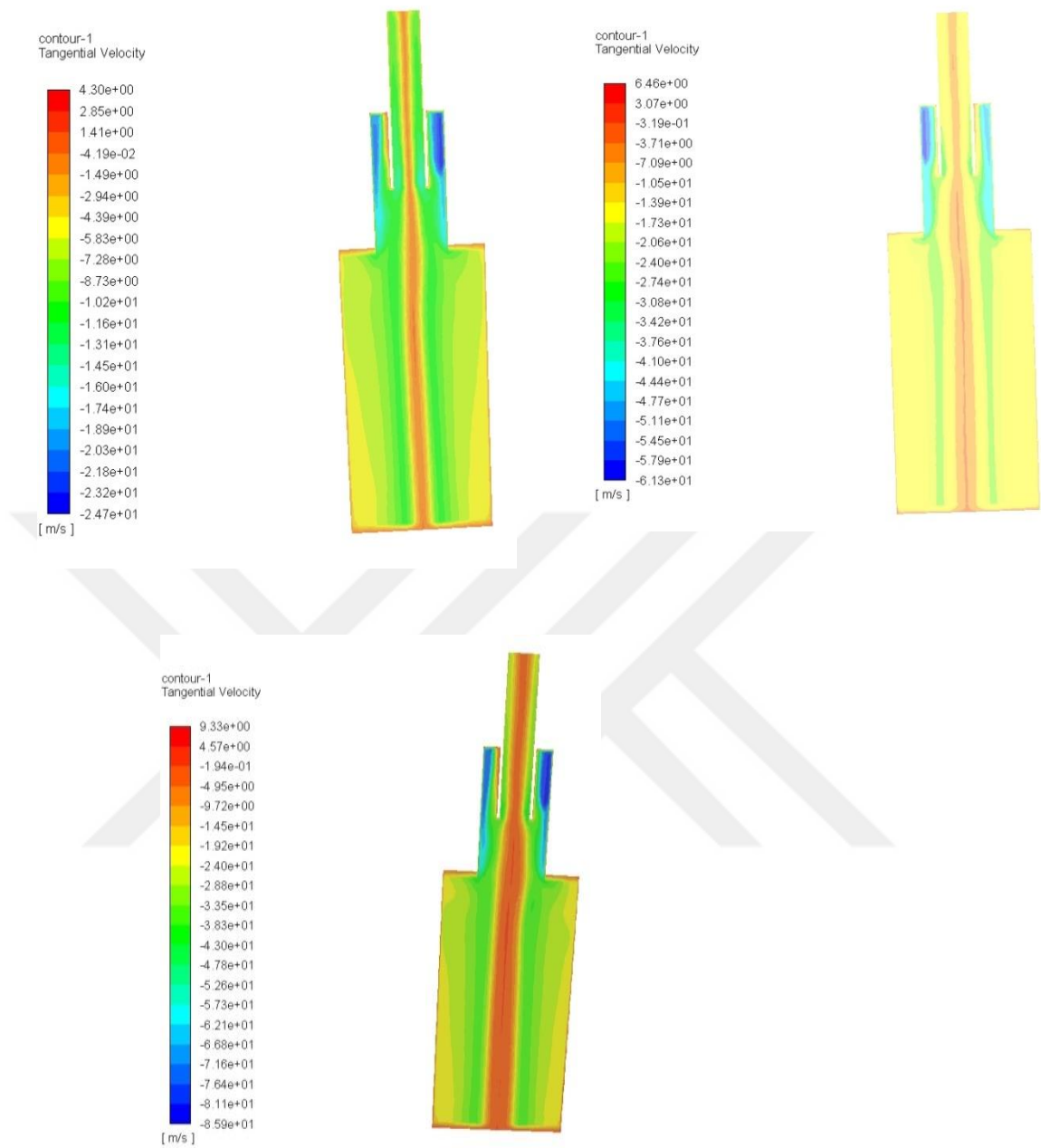
Figure 4.12. The contour plots for tangential velocity profile for time averaged flow in the sections Y=0 and throughout the inlet section for 10 cm cyclone length and (a)18.5 m/s, (b) 46.3m/s, (c) 64.8m/s
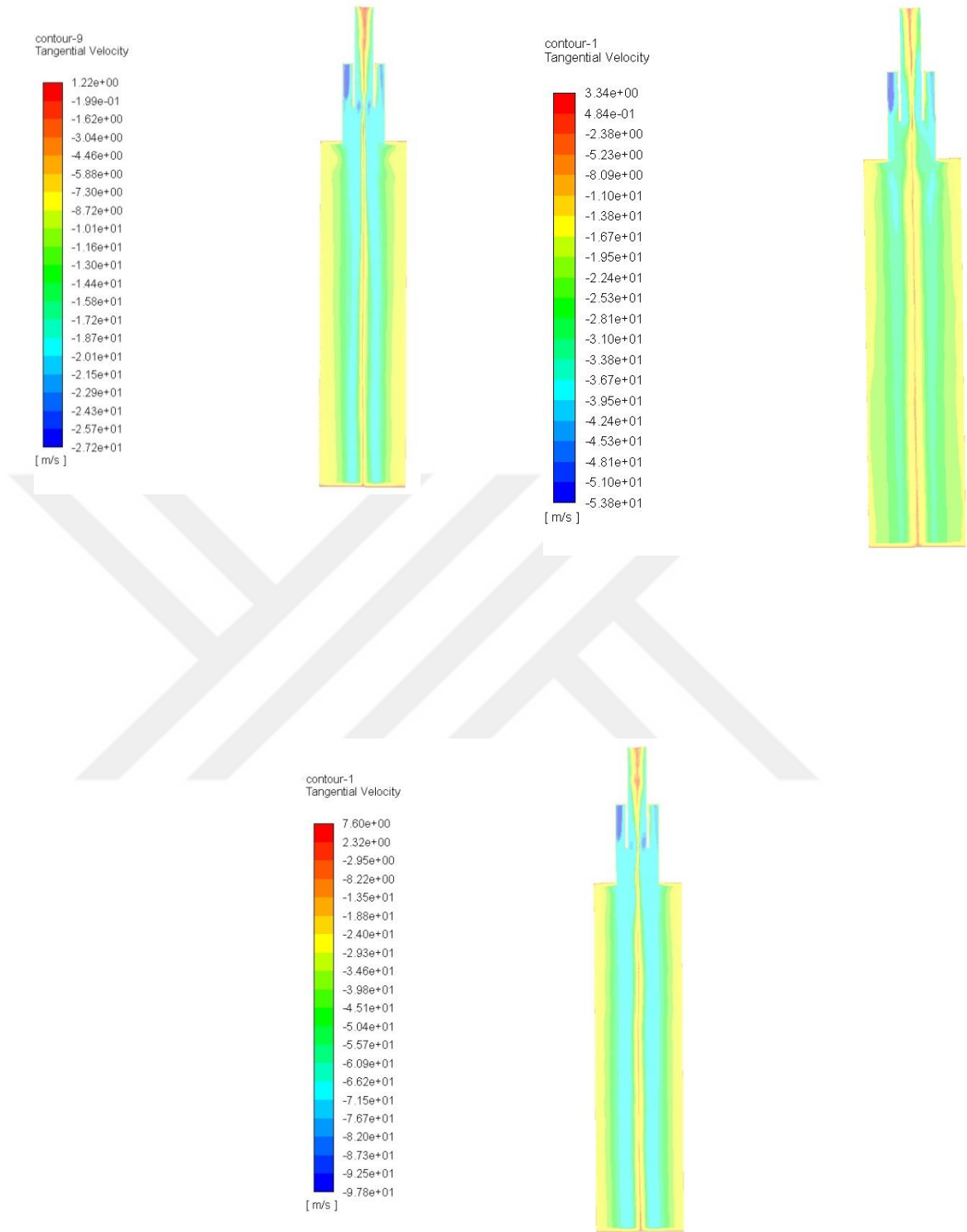
Figure 4.13. The contour plots for tangential velocity profile for time averaged flow in the sections Y=0 and throughout the inlet section for 20 cm cyclone length and (a)18.5 m/s, (b) 46.3m/s, (c) 64.8m/s

It has been observed from Figure 4.12. & Figure 4.13., the cyclone tangential velocity decreases readily when the cyclone length is increased from 10cm to 20cm. obviously higher tangential velocity will result in larger centrifugal force, according to that higher

separation efficiency is yield. This explains how the separation efficiency decreases constantly when the cyclone length is increasing from 10cm to 20cm.

5. CONCLUSION

This study carried out the effects of varying cyclone length, wall roughness, inlet velocity and different particle diameter on cyclone performance parameters. The behavior of the flow field were studied in the cyclones and the effect of different cyclone length and inlet velocity are observed so results have been given by define the height of cyclone from 10 cm to 20 cm, inlet velocity 18.5, 27.8, 37.04 , 46.3 , 55.5 and 64.8 m/s and 0.004131 Kg/s has been added as working fluid flow rate.. Flow field was calculated using 3D Reynolds-averaged Naveir–Stokes equations. Newton's second law was applied to study the particle trajectory with modeling gravity and drag forces effects on the particles. The Reynolds stress model (RSM) with linear pressure-strain and standard wall function is applied to simulate Reynolds stresses in viscous model. Eulerian–Lagrangian computational process is carried out to anticipate the particle trajectory in a cyclone. Green-gauss cell based was used for gradient, SIMPLE algorithm was chosen for pressure velocity coupling in this case. PRESTO(Pressure Staggering Option) scheme was used for pressure interpolation as it is shown to be convenient for the steep pressure gradients included in the complex swirling flows. Quick scheme was used for momentum, and second order upwind was applied for the turbulent kinetic energy also the second order upwind was used for the turbulent dissipation rate, finally first order upwind was used for Reynolds stresses and 0.0001s time step was taken. The cyclones was simulated at different height. The behavior of flow field was studied in the cyclones, and the effect of the different height is observed. Tangential velocity in addition to static pressure were carried out in cyclone different sections. Contour of tangential velocity, and static pressure were shown for different cyclones inlet velocities. It was realized that the different geometries, also different the inlet velocities, can effect on the collection pressure drop and efficiency. The collection efficiency and the flow patterns calculated numerically then were compared with the experimental data and good agreement is observed.

The cyclone models with increasing length were simulated and assessed successfully using RSM turbulence model with higher advection schemes. The Reynolds Stress Model turbulence successfully captured the flow physics inside the gas cyclones and

show accurate predictions of the grade separation efficiency pressure drop, and cut-off diameter. With according the standard cyclone model, the following conclusions have been obtained:

* The effect of cyclone length its properly achieved and investigated in four different cyclone length staring from 6,10, 15 and 20cm so it's obviously shown that increase the cyclone length lead to decrease of cyclone collection efficiency. The pressure drop decrease non-linearly with increase the cyclone length and also with inlet velocity reduction.

* According to the inlet velocity affects the radial distance traveled by the rebounded particles .Accelerating the inlet velocity enhances the centrifugal forces acting on small particles and increases their separation efficiency

* An inverse relation between the cut-off diameter and inlet velocity cyclone has been observed when the cyclone inlet velocity increase the cut off diameter decrease eventually, a decrease in total efficiency and increase in cut-off diameter ,respectively were observed with increase in cyclone length.

* The numerical simulation results proved that, the wall roughness has great effect on cyclone flow field. With an increasing wall roughness, the vortex length reduce and the tangential velocity is also reduced.

* The tangential velocity decrease with increase cyclone height this is responsible for the lower separation efficiency, in contract increase the inlet velocity will increase tangential velocity.

REFERENCES

Boysan, W., Griffiths D. 1996. Computational fluid dynamics (CFD) and empirical modelling of the performance of a number of cyclonesamplers. *Journal of Aerosol Science,* 24(3): 281–304.

Chen, M. 1999. Characteristics of the vortex structure in the outlet of a stairmand cyclone. Edmonton. University of Alberta,Department of Chemical and Material Engineering, Edmonton.

Chuah, T.G. 2006. A CFD study of the effect of cone dimensions on sampling aerocyclones performance and hydrodynamics. *Powder Technology,* 127(6): 126 – 132.

Cia, H., Suna, G. 2015. Effects of wall roughness on the flow field and vortex length of cyclone. The 7th World Congress on Particle Technology (WCPT7), 22-25 April, 2015, Beijing, China.

Çalişkan, E. 2017. Sanal gövdeli mini bir siklon ayırıcının tasarlanması ve deneysel incelenmesi. *Master Thesis*, School of Natural and Applied Science, Mechanical Engineering Department, Uludağ University, Bursa, Turkey

Elsayed, K. (2011). Analysis and Optimization of Cyclone Separators Geometry Using RANS and LES Methodologies. *Ph.D. Thesis*, Mehcnaical Engineering Department, Vrije University, Brussel,B

Gorton, A., Woisetschl, J., Wigley, G., Staudinger, G. (2000). Investigation of the flow field in the upper part of a cyclone withlaser and phase doppler anemometry. *Particle and Particle System characterization,* 17(1): 21–27.

Hoffmann, A.C., Stein, L.E. 2008. Gas Cyclones and Swirl Tubes: Principles,Design and Operation. Springer-Verlag, Berlin Heidelberg, 562 pp.

Dirgo, J., Leith, Dav. 1985. Cyclone Collection Efficiency: Comparison of Experimental Results with Theoretical Predictions. *Aerosol Science and Technology*, 22(3): 401-415.

Karagoz, I., Fuat, K. 2008. Performance analysis of numerical schemes in highly swirling turbulent flows in cyclones. *Current Science Association,* 36(3): , 1273-1278.

Kaya, F., Karagoz, I., Avci, A. 2011. Effects of Surface Roughness on the Performance of Tangential Inlet Cyclone Separator. *Aerosol Science and Technology,*26(3): 988-995.

Kolacz, J. 2002. Investigating flow conditions in dynamic air classification. *Minerals Engineering,* 15(3): 131-8.

Lakhbir, S.B., Sharma, R.P., Elsayed, K. 2015. The effect of the cyclone length on the performance of Stairmand high-efficiency cyclone. *Powder Technology,* 34(6): 668–677.

Maccormack, R. W., paullay.A. J. 1972. Computational Efficiency Achieved by Time Splitting of Finite Difference Operators. *AMA,* 15(4): 72-96.

Mcdonald, P. 1971. The Computation of Transonic Flow through Two-Dimensional Gas Turbine Cascades. Gas Turbine Conference and Products Show, Houston, Texas.

Meier, J., Klein, G.M., Crossflow, K.V. 2002. filtration as a new method of wet classification of ultrafine particles. *Separation and Purification Technology,* 26(1): 43-50.

Nied, R. 19996. Fine classification with vaned rotors: at the outer edge of the vanes or in the interior vane free area. *International Journal of Mineral Processing,* 44(5): 23-31.

Patankar, S. 1980. Numerical Heat Transfer and Fluid Flow. *Hemisphere Publishing Corp,* 18(2): 197-229.

Peng, W., Hoffmann, A.C., Boot, P.J., Udding, A., Dries, H.W., Ekker, A., Kater, J. 2002. Flow pattern in reverse-flow centrifugal separators. *Powder Technology, 127(4):* 212–222.

Peng, W.O., Hoffmann, A.C., Boot, P.J. 2002. Flow pattern in reverse flow centrifugal separators. *Powder Technology, 38(3):* 212–222.

Pisarev, G.I., Gjerde, V.I., Hoffmann, A.C., Peng, W., Balakin, B. V., Dijkstra, H.A. 2011. Experimental and computational study of the 'end of vortex' phenomenon in reverse-flow centrifugal separators. *AIChE Journal,* 1002(10): 33-58.

Pisarev, G.I., Gjerde, V.I., Hoffmann, A.C., Peng, W., Balakin, B.V., Dijkstra, H.A. 2011. Experimental and computational study of the 'end of vortex' phenomenon in reverse-flow centrifugal separators. *AIChE Journal, 28(4):*, 23-45.

Rizzi, A.W., Inuoye, M. 1973. Time Split Finite Volume Method for 3D Blunt Body Flows. *AIAA J,* 11(2): 1478-1485.

Sakin, A., Karagöz, I. 2014. Numerical investigation of surface roughness effects on the flow field in a swirl flow. *Journal of Engineering Faculty Uludağ University*, 19(2): 10-28.

Shih, T.H., Liou, W. W., Shabbir, A., Yang, Z., Zhu, A. k. 1995. Eddy Viscosity Model for High Reynolds Number Turbulent Flows - Model Development and Validation. *Computers Fluids,* 24(5): 227–238.

Skorve, T. 2011. Experimental and Theoretical Study on the Effect of Wall Roughness on the phenomenon "End of the Vortex" in Swirl Tubes. University of Bergen, Department of Physics and Technology. Norway, 351pp.

Slack, M. D., Prasad, O., Bakker, A., Boysan, F. 2000). Advances in cyclone modeling using unstructured grids. *Trans IChemE,* 45(2): 78-115.

Solero, G., Coghe, A. 2002. Experimental fluid dynamic characterization of a cyclone chamber. *Exp. Thermal Fluid Sci,* 27(2): 87–96.

Stein., A.C., Hoffmann, L.E. 2008. Gas cyclones and swirl tubes: princpel, Design and Operation. Springer, Berlin, Germany.

Swanson, J. (April 2009). *Ansys FLUENT Guide12.* ANSYS, washinton-USA, 816.

Teke, M. (2010). GAZ-PARTİKÜL İKİ FAZLI GİRDAPLI AKIŞLARIN MATEMATİK MODELLENMESİ VE SAYISAL ÇÖZÜMÜ. *Master Thesis*, School of Natural and Applied Science, Mechanical Engineering Department, Uludağ University, Bursa, Turkey

Xiang, R. 2005. Numerical study of flow field in cyclones of different height. *Chemical Engineering and Processing,* 15(2): 44, 877-883.

Yang, J., Sun, G., Zhanb, M. 2015. Prediction of the maximum-efficiency inlet velocity in cyclones. *Powder Technology,* 286(5): 124–131.

Yoshida, H.U., Takashina, T.A., Fukui, K.L. 2004. Effect of inlet shape and slurry temperature on the classification performance of hydro-cyclones. *Powder Technology,* 40(2): 1-9.

Zhu, Y., Lee, K. 1999. Experimental study on small cyclones operating at high flowrates. *J. Aerosol Sci,* 24(2): 1303-1315.

CURRICULUM VITAE

Name and surname   : Ammar Mohammed Ali Fdlelseed
Date and place of birth : Saudi Arabia., 5-7-1988
Languages   : Arabic, English, Turkish, Italian

Education
   Secondary   : Alhalfaiya Modern Secondary School   2005
   Bachelor   : Juba University   2011
   Master   : Uludag University   2018
                     : Bahri University   2014
Work and experiences
Contact (e-posta   : ammarkrc@gmail.com